Amphiphilic Glycopolymers and Glycopeptides: Properties and Applications

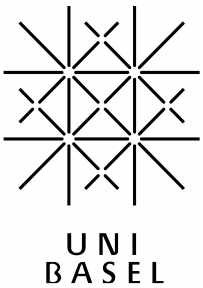

Inauguraldissertation zur Erlangung der Würde eines Doktors der Philosophie, vorgelegt der Philosophisch-Naturwissenschaftlichen Fakultät der Universität Basel

Von
Diana Sebök

aus
Sempach (LU) und Pozsony (SK)

Basel, 2008

Genehmigt von der Philosophisch-Naturwissenschaftlichen Fakultät auf Antrag von Prof. Dr. Wolfgang Meier (Universität Basel)

und

Prof. Dr. Andreas Taubert (Universität Potsdam & MPI für Kolloid- und Grenzflächenforschung)

Basel, den 24. Juni 2008

Prof. Dr. Hans-Peter Hauri
Dekan

TO MY FAMILY

Summary

In this thesis, the properties and potential application fields of saccharide-based block copolymers are explored.
The anionic polysaccharide heparin was coupled to hydrophobic blocks – poly(dimethyl siloxane) (PDMS) and poly (ethyl ethylene) (PEE) – using different synthetic methods, and investigated in terms of self-assembly behavior and insertion into polymeric membranes. We studied whether heparin's intrinsic anticoagulant activity is persistent upon chemical transformation and insertion into polymer membranes. We observed that coupling does not influence the anticoagulant activity, whereas methods involving degradation of heparin led to an almost complete loss of activity.

We also coupled heparin to the hydrophilic polymer poly(ehtylene glycol) (PEG), which produced a bis-hydrophilic block copolymer. Self-assembly of this anionic material in association with gadolinium cations was investigated by transmission electron microscopy. Electron paramagnetic resonance (EPR) spectroscopy provided more details about the polymer – metal interactions. The choice of gadolinium was justified by the fact that it has good contrast properties for medical imaging. In combination with the polymer, toxicity of gadolinium could be decreased. In addition, its relaxivity was enhanced. This way we obtained a new type of contrast agent.
MRI experiments proved that the relaxivity of the polymer-bound gadolinium was significantly higher than of unbound gadolinium and of commercially available gadolinium-based contrast agents. To further lower toxicity of gadolinium, we added phosphate to form small insoluble $GdPO_4$ particles, which were in fact stabilized in solution by polymer aggregates. Their contrast properties only slightly decreased compared to polymer-bound gadolinium ions.

Apart from synthetic blocks, we also combined sugar units with peptides. Firstly, we established new synthetic routes towards such biohybrids, using monosaccharides and a short peptide (named *TRUNK*). The coupling of D-glucuronic acid to the *TRUNK* was successfully achieved on solid phase. The resulting glycopeptide was investigated in terms of its self-assembly behavior.

This thesis is structured in eight parts. The first chapter is an introduction, focusing on amphiphiles and copolymers based on biological blocks. Chapter two includes the motivation and the concept of this work. In the third chapter, the results are described and discussed in detail. This chapter is divided into four main sections, dealing with heparin-based copolymers with amphiphilic as well as bis-hydrophilic properties. The latter was explored as a matrix for MRI contrast agents. Additionally, the synthesis and self-assembly behavior of materials combining carbohydrate and peptide blocks are discussed.
In chapters four and five we draw the conclusions and present the outlook for prospective experiments. The experimental conditions are given in chapter six, as well as descriptions of methods and equipment. The thesis finalizes with the references in chapter seven and an appendix including a historical outline of heparin in chapter eight.

Acknowledgments

I would like to thank *Prof. Wolfgang Meier* for giving me the opportunity to accomplish my thesis in his group, for his helpful advices and discussions during the work process and for always being patient and motivating.

Special thanks also go to *Prof. Andreas Taubert* for his engagement as my second reviewer, for helpful discussions, encouragement and criticism.

I am grateful to *Prof.* Edwin Constable for presiding my thesis.

Dr. Alessandro Napoli and *Dr. Christian Dittrich* have been supervising my projects, sharing their broad experience and knowledge and being great and discerning discussion partners in every field.

I am deeply grateful to *Dr. Katarzyna Kita-Tokarczik* who has been a very engaged writing coach.

Francesco Santini and his supervisor *Prof. Klaus Scheffler* believed in my project and have been very friendly and motivated collaborators for the MRI measurements.

I am appreciative to *Prof. German Marbet* and his staff members for the blood-coagulation measurements, for being very cheerful and showing great skills in taking my blood.

I want to thank *Sven Kasper* for his friendship and patient support in the lab and in every other domain.

Many thanks to my former and actual office-colleagues *Dr. Thomas Haefele, Dr. Daniel Streich, Dirk deBruyn* (special thanks for introduction and support concerning peptide synthesis and purification) *Thomas Schuster and Stefan Egli* for their friendship, many precious fun moments and helpful and distractive discussions.

I also thank the former and actual post-docs and former colleagues *Dr. Per Rigler* (special thanks for the operation of the confocal microscope and for his

comprehendible explanations of FCS), *Dr. Cornelia Palivan* (special thanks for being a great support in the field of inorganic chemistry and accomplishing EPR measurements), *Dr. Marc Sauer, Dr. Alexandra Graff-Meyer, Dr. Corinne Vebert, Dr. Caroline Fraysse-Ailhasse, Dr. Samantha Benito Gaberthüel, Dr. Violeta Malinova, Dr. Roxana Timmermans-Stoenescu, Dr. Ramona Enea, Dr. Ozana Onaca, Dr. Michael Strobel, Dr. Sayed Mohammady, Dr. Sandrine Poux, Dr. Julie Grumelard, Dr. Chantal Schmitt, Dr. Almut Mecke* and *Dr. Susana Moreno-Flores* for introduction and operation of equipment and special techniques, for sharing their experience and knowledge and for their friendliness.

Special thanks go to *Lucy Kind* and *Serena Belegrinou*, for their serenity and kindness, for mind liberating sports and their cordial friendship.

I thank my colleagues *Olivier Casse (special thanks for LS support), Alex Senti, Ekaterina Rakhmatullina, Mariusz Grzelakowski, Fabian Axthelm (special thanks for graphic and IT support), Francisco Teixeira, Rainer Nehring, Sylvia Schweizer, Julia Razumovitch, Kelnner França, Etienne Cabane, Nicolas Cottenye, Vimalkumar Balasubramanian, Jörg Braun and Philip Graf* for all support and making my time at work very pleasant.

My students *Benjamin Bircher, Tobias Bandi,* and *Olivia Haupt* have been an invaluable help during their block-course.

I thank *all staff* for technical, organizational and culinary supply.

Holger Hammerich in memoriam, he was a great support and a great person.

I am deeply grateful to *my beloved family* for always believing in me, for being supportive and caring all my life.
And I thank my precious friends *Sabina Winiger, Kathrin Isch, Sarah Menoia, Lukas Hostettler, Lars von Riedmatten,* and *Virág Csukás* for being there for me.

1 INTRODUCTION

1.1 Amphiphilic self-assembly

Amphiphiles play a fundamental role in biology. Essential fatty acids are used in the human body as energy resources and are involved in the prevention and treatment of coronary artery disease, hypertension, diabetes and arthritis, other inflammatory and autoimmune disorders and cancer[1]. Another prominent class of amphiphiles is represented by lipids, particularly phospholipids, the main component of biological membranes. Cholesterol and glycolipids are also part of those structures, responsible for the membranes' physical and biological properties. Cholesterol is present in mammalian cell membranes, forming microdomains, commonly referred to as "rafts" that contain high concentrations of membrane proteins[2]. Glycolipids serve four general functions in membranes: stabilization, shape determination, recognition, and ion binding[3].

The common intrinsic feature of amphiphiles (from the Greek amphis: both; philia: love, friendship) is the covalent linkage of parts with different polarities, which hence favor different solvents but cannot separate at the macroscopic scale. Parts which favor unpolar solvents are called hydrophobic or lipophilic and conversely those parts which are well soluble in aqueous media are called hydrophilic or lipophobic.

When exposed to a solvent, amphiphiles can self-assemble spontaneously and reversibly into ordered structures as a result of opposing interaction preferences of the chemically different parts. Self-assembly in the case of amphiphiles is based on non-covalent, mainly hydrophobic interactions and is commonly defined as lyotropic behavior. The Greek root ("lyo-" = solvent, "-tropic" = induced by) hints that the phase diagram is typically based on the molecule and solvent properties and on the concentration[4]. Considering thermodynamics, the drive for amphiphiles to organize in aqueous media derives from opposing preferences of the blocks with different polarities[5]. Avoiding contact between the hydrophobic chain and water molecules by segregation leads to entropy gain, thus decreasing the total free energy of the system.

The degree of repulsion, block length, concentration, and solvent selectivity determine the morphology of the self-assembly, which ranges from lamellae to micelles, vesicles, and other more complex shapes. The concept of the critical

packing parameter (P_c) was introduced as a model to predict the morphology of amphiphiles self-assembling into superstructures[6]:

$(P_c) = V/a_0L$

V : hydrophobic chain volume
L : length of the hydrophobic chain
a_0: area occupied by the hydrophilic group

For small amphiphilic molecules with a $P_c < 0.5$, highly curved aggregates such as spherical and cylindrical micelles are predominant, while for $0.5 > P_c > 1$ smaller curvature is favored. When P_c is close to 1, planar bilayers are formed.
The same principle is true for amphiphilic macromolecules, both biological and synthetic polymers, but additional factors such as polydispersity and flexibility play a role.

1.2 Polymers

At the beginning of the 20th century, the successful quest for surrogates for ivory, natural fibers, and rubber emerged parallel with the process of understanding the structural features of polymers. In 1907, Baekeland was the first to present a fully synthetic polymer – Bakelite – with excellent electrical insulating features. By this time, the molecular architecture of polymers was still unknown and it was believed that micellar self-assembly of molecules accounted for polymer properties. In 1920, when Hermann Staudinger (1881-1965) discovered that polymers consist of covalently bound building blocks[7], he already presumed the immense potential arising from the variety of polymeric substances and opened the door for future development of functional and structural high-tech materials[8].
The term polymer describes a molecule that consists of repeating low molecular mass structural units (monomers). Addition or subtraction of a few monomers to or from a polymer has a negligible effect on its chemical and physical properties. Copolymers represent a special class of polymers; they are built by at least two different sorts of monomer units (co-monomers). Mainly, physical properties of copolymers depend not only on the chemical nature of the monomers but also on their arrangement within a macromolecule. They are classified by means of their structural composition:

Statistical copolymers are built up by statistically distributed co-monomers, as for the example of a statistical copolymer with two units A and B:

AABBAAABABAABBABAABBBABAABAAABA

Alternating copolymers consist of a regularly repeating pattern of monomer units:

ABABABABABABABABABABABABABABABA

Periodic copolymers, similar to alternating copolymers also are constructed by regular repeating units, but sequences instead of single monomers:

AABBBAABBBAABBBAABBBAABBBAABBB

Graft copolymers represent a class of branched polymers with side chains grafted to the backbone:

```
AAAAAAAAAAAAAAAAAAAAAAAAAAAAA
     B         B       B
     B         B       B
     B         B       B
     B         B       B
```

Linear block copolymers are formed by a linkage of chains consisting of one monomer type:
AAAAAAAAAAAAAAAABBBBBBBBBBBBB

Just like lipids, amphiphlic block copolymers self-assemble into superstructures. When exposed to water, the hydrophobic part is protected from the aqueous environment. All forces leading to self-assembly in polymer systems are similar to those of low molecular weight amphiphiles, although the resulting morphology is predicted by the weight fraction of of the hydrophilic block, unlike for small molecules, where P_c is applied. At constant concentration in solution, increasing the length of the hydrophobic block at constant hydrophilic block leads to a transition from spherical to worm-like micelles and finally to vesicular structures[9,10,11] (Figure 1).

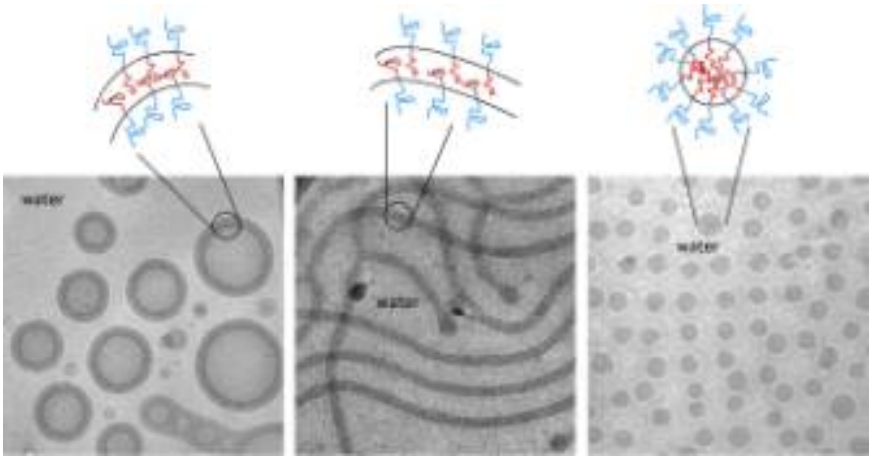

Figure 1: Three microstructures - vesicles, cylinders, and spheres - can be observed for aqueous dispersions of PB-PEO diblock copolymers by cryogenic transmission electron microscopy. The existence of these microstructures depends on the weight fraction of PEO[11].

The self-assembly process is driven by an unfavorable mixing enthalpy and a small mixing entropy, while covalent bonds between the blocks prevent macrophase separation[12]. However, not only thermodynamic control, but also kinetics of chain rearrangements can influence the phase behavior of amphiphilic systems. The resulting kinetically trapped structures are not perforce at the absolute free energy minimum state.

The first polymeric vesicles reported[13, 14] were from diblock dendrimers and copolymers made of poly(styrene) as hydrophobic block. Due to the high glass transition temperature (T_g) of poly(styrene), a higher energy barrier has to be overcome to achieve self-assembly and therefore the use of mixed solvents such as DMF or toluene in water is needed for the formation of colloidal structures. Hydrophobic blocks with lower T_g can accelerate the membrane formation by lowering the activation energy and thus make the use for cosolvents needless as for example with poly(butadiene), poly(ethyl ethylene), poly(dimethyl siloxane), poly(propylene sulfide), poly(butylene oxide), poly(propylene oxide).

Several amphiphilic multiblock copolymer architectures were synthesized and explored in terms of their self-assembly behavior. The control over other physical and chemical properties of self-assembled aggregates such as permeability or responsiveness was achieved by the right choice of building blocks.

1.3 Functional polymer membranes

Different approaches were used to tune the properties of amphiphilic block copolymers and polymer membranes for applications in biosciences as varied as diagnostics, drug delivery and sensor technology[15].

In contrary to lipids, polymer chemistry allows for various chemical modifications to introduce functionality and make polymers responsive to environmental stimuli. Unsaturation of the hydrophobic block[16] or introduction of a methacrylate end-functionality[17] were used to crosslink and thus stabilize membranes in water.

Many research groups investigated vesicle forming properties of block copolymers that can be degraded upon a change on pH by hydrolysis[18,19] or by exposure to oxidants[20, 21]. Degradability resulting in vesicle destabilization is an attractive feature for controlled release of e.g. drugs.

Another example of degradable superstructures are azobenzene-based block copolymers that were reported to form light-responsive vesicles, which reversibly disintegrate when exposed to UV light (360 nm) due to conformational changes in the azobenzene and rebuild upon illumination with visible light (440 nm)[22].

Insertion of membrane proteins provides additional functionalization possibilities, where the natural properties of the proteins are retained in synthetic membranes. Particularly, membranes formed by poly(methyloxazoline)-poly(dimethyl siloxane)-poly(methyl oxazoline) (PMOXA-PDMS-PMOXA) triblock copolymers were used for such a purpose. The bacterial porin OmpF proved to be consistently active in artificial membranes[23], allowing passive diffusion of small molecules up to 400 Da across the membrane. The enzyme β-lactamase was encapsulated into polymeric vesicles and ampicillin was added to the vesicle solution. Ampicillin can be hydrolyzed by β-lactamase to ampicillinoic acid after it reached the inside of the vesicle through the channels. Ampicillinoic acid is able to reduce iodine to iodide. Therefore, the activity of the enzyme could be monitored by iodometry (Figure 2).

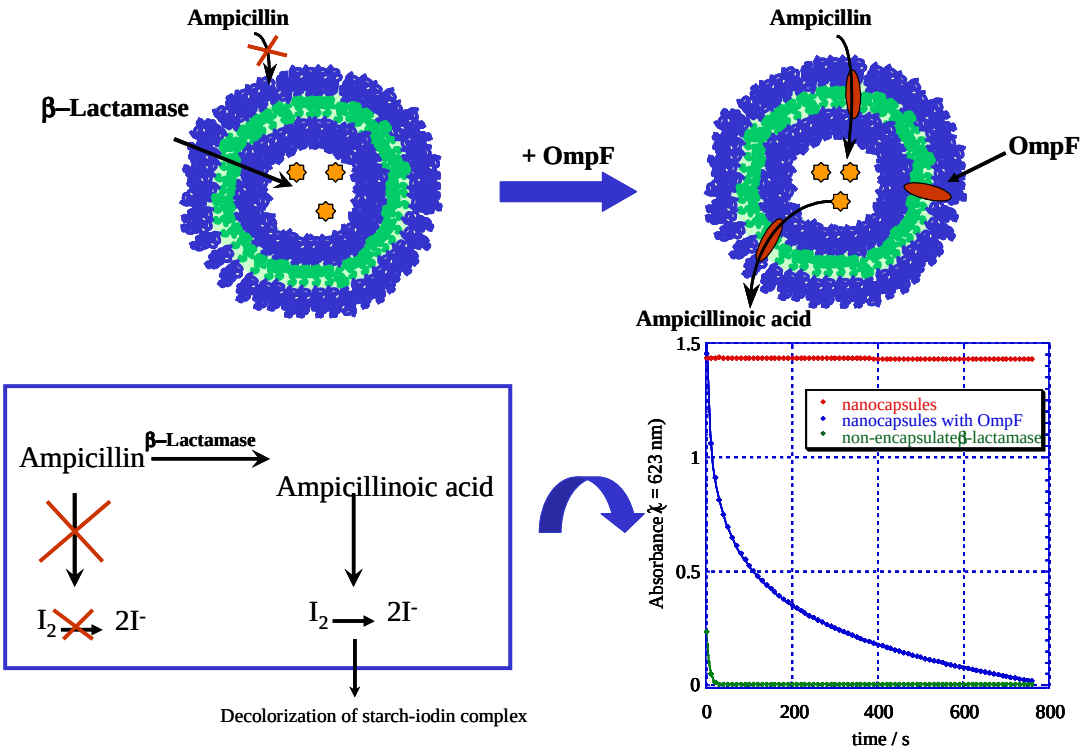

Figure 2: Vesicular nanoreactor by insertion of OmpF into a polymeric membrane. β-lactamase hydrolyzes amphicillin to ampicillinoic acid, that can be detected iodometrically[24].

Other attempts followed to prove functionality of channel-forming membrane proteins in artificial membranes using proteins with more specific permeabilities: The bacterial channel protein LamB, which serves also as receptor for λ phage to release its DNA, was inserted into polymeric membranes for virus-assisted loading of polymer nanocontainers[25]. The incorporation and release was monitored using the fluorescent dye YO-PRO-1, a label for the viral DNA.

Insertion of the specific water channel Aquaporin Z[26] into polymer membranes led to increased water permeability of the membranes, by orders of magnitude. Furthermore, the selectivity of the Aquaporin Z-polymer membrane for water over small solutes such as salt, glucose, urea and glycerol was demonstrated.

Polymeric vesicles have been used as a model for biomimetic mineralization such as what nature applies for production of inorganic composites like bones or teeth. Insertion of calcium transporting ionophores was achieved for controlled precipitation of calcium phosphate in giant polymer vesicles[27]. For medical application of polymeric vesicles, not only the control over permeability, but also programmability towards specific targets is a great challenge of biomaterial science. Vesicles from biotinylated PMOXA-PDMS-PMOXA block copolymers

attached to biotinylated ligands using streptavidin as coupling agent, thus demonstrating the applicability of polymer nanocontainers as injectable cell-targeting vehicles. The nanocontainers bound to the cell surface were rapidly taken up without observable cytotoxic effect[28].

A more direct approach to introduce biofunctionality is to tailor the polymer's properties at the stage of molecular engineering, one possibility being the use of biological building blocks, such as sugars and peptides. This way, new properties of the resulting materials can be expected, and improved biocompatibility may facilitate applications such as drug delivery or medical imaging. In the following sections, such bio-blocks will be discussed in more detail.

1.4 Biohybrid amphiphiles (I): Sugars as building blocks

In nature, carbohydrates represent a main building class of living matter, where they are usually associated to proteins, lipids (as glycolipids), making up a part of biological lipid membranes and are also parts of DNA and RNA[29].

Exploring functional carbohydrates as building blocks of amphiphilic block copolymers opens the possibility to investigate their biofunctionality as membrane-forming material and to design membranes that can interact specifically with proteins.

Sugar-based surfactants, such as Sorbitan esters, sucrose esters and alkyl polyglycosides are well established in industrial applications such as leather and textile auxiliaries, emulsifiers for food, cosmetics, dishwashing and detergent applications. For household applications, alkyl polyglycosides feature very good performance and mildness and are completely based on renewable resources; therefore they are the most successful sugar-based surfactants nowadays[30].

Out of all classes of sugars known, many are only used for very specific applications, depending on their activity spectrum determined by nature. As an example, a major component of the mammalian extracellular matrix is proteoglycans, proteins covalently linked to glycosaminoglycans (GAGs), which can interact with different proteins or enzymes to regulate their activity[31].

GAGs (or mucopolysaccharides) are linear polysaccharides consisting of partly sulfated alternating glucosamine and uronic acid units. The most prevalent GAGs are chondroitin sulfate, dermatan sulfate, keratin sulfate, hyaluronan, heparan sulfate and heparin with the highest negative charge density of any known biological molecule. The high charge density, its anticoagulant activity and ability

to interact with fibroblast growth factors make heparin an interesting candidate as bioactive building block for hybrid molecules such as glycopolymers.

Several attempts have been made to bind heparin covalently[32] or non-covalently[33] to solid supports in order to prepare blood compatible surfaces, chromatographic gels for affinity chromatography and to study heparin-protein interactions. Heparin-coated albumin microspheres were used as ion-exchanging drug delivery systems with controlled release[34]. Porous poly(D,L-lactic-co-glycolic acid) (PLGA) microspheres were coated with heparin for sustained release of basic fibroblast growth factor (bFGF) to induce angiogenesis[35].

The methods to covalently couple heparin (Figure 3) include the binding to functional groups, as for example peptide binding at the carboxylate present at every uronic acid moiety. The main drawback here is the unpredictable amount of coupled material. Although Bergman et al.[36] claim to be able to control the coupling ratio by varying the quantity of the coupling reagent, in the case of amphiphiles the determination by NMR fails due to the lack of a good solvent.

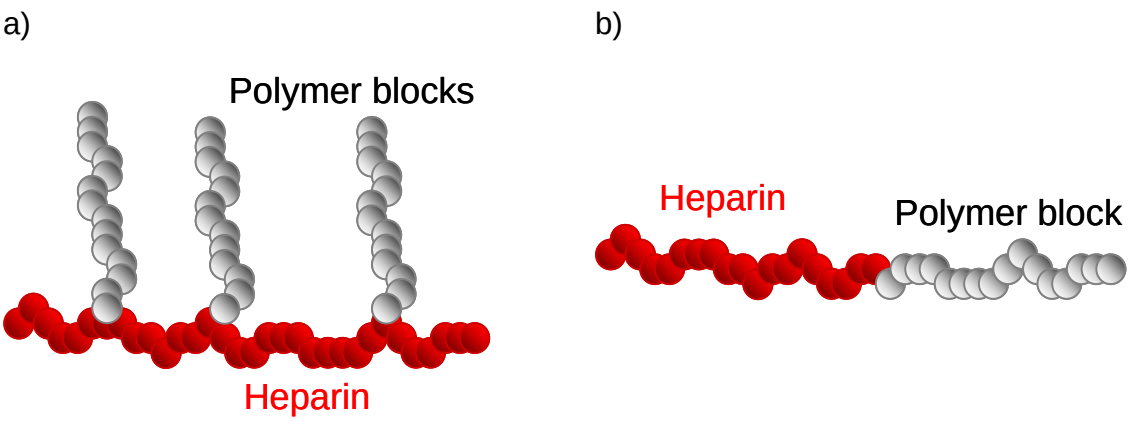

Figure 3: a) Polymer blocks grafted to heparin *via* peptide binding on the carboxylate functional group. b) Polymer blocks bound linearly after end functionalization of heparin

On the other hand, end-group functionalization of heparin allows highly predictable block proportions but includes degradation and therefore loss of heparin's anticoagulant activity. The purpose and potential application of the resulting material have to be well considered before choosing the coupling method.

1.4.1 Heparin

Structure and biological activity

Heparin is a linear polysaccharide composed of repeating units of iduronic acid, some containing an O-sulfate group at the C2 position and D-glucosamine, usually N-sulfated with an additional O-sulfate group at C6[37]. Heparin exists primarily as an extended helical structure and is not known to fold to any tertiary structure. The specific interactions of heparin with proteins depend on the exposure of the sulfo- and carboxyl groups on the surface. The conformational flexibility of L-iduronic acid is probably responsible for heparin's wide range of interaction partners.

Heparin has a very broad molecular mass distribution; however, the anticoagulant activity strongly depends on the chain length. The molecular weight (MW) of unfractionated heparin (UFH) ranges between 4000-40'000 Da, 15'000 Da being the most frequent MW. Low molecular weight heparin (LMWH) can be obtained by ultrafiltration or by cracking and has a less heterogeneous MW distribution, ranging between 4000 and 6000 Da.

The numerous negative charges are important for different reasons. They are key for the complex building with antithrombin III (ATIII) (Figure 4), which is the basis of heparin's anticoagulant activity[38].

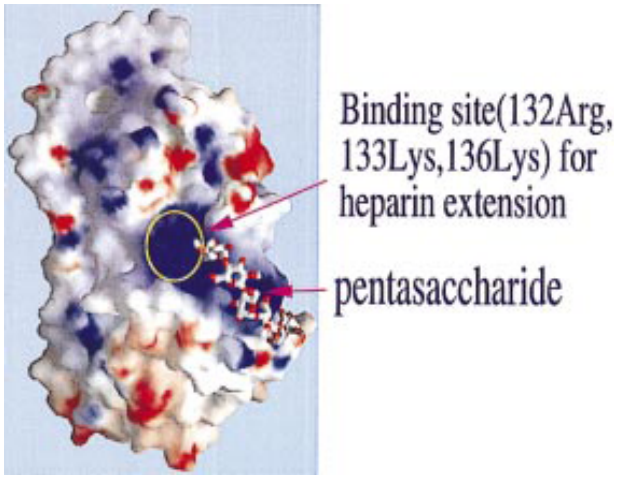

Figure 4: Heparin-ATIII complex[38]

They are also important for the interactions with the inactivator protamine, a polycationic protein. To be able to interact with ATIII and thus be biologically active, heparin needs a minimum of a particular pentasaccharide as binding site[39,40] (Figure 5)

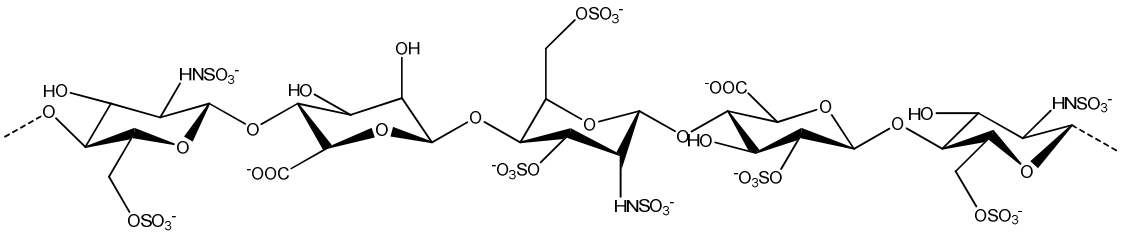

Figure 5: Active pentasaccharide moiety of heparin

Only ca. 22% of unfractionated heparin and ca. 16% of low molecular weight heparin consist of this bioactive pentasaccharide sequence, the remaining part consists also of alternating glucosamine-iduronic acid units, however, sulfate groups are distributed randomly.

The development of low molecular weight heparin began in the 1980s. To provide better regulation of blood coagulation a more specific compound than unfractionated heparin (UFH) had to be found, which might overcome the major pharmacokinetic, biophysical and biological limitations. Apart from complications common to all coagulants, such as bleeding, UFH can cause heparin-induced thrombocytopenia (HIT) and osteoporosis. Various research groups found out that chemical or enzymatic fractionation of heparin led to much more specific inhibition of factor Xa[41,42,43,44]. LMWH was introduced as new effective and improved antithrombotic agent with a chain length ranging from 4000 to 6000 Da. Major advantages of LMWH over UFH are its improved pharmacokinetic and biological properties resulting in longer biological half-lives and its enhanced subcutaneous bioavailability. As a result, LMWH can be administered in subcutaneous injections each day, permitting its clinical use on an out-patient basis. This has reduced the hospitalization costs normally associated with the intravenous use of heparin[45,46].

Recently, a scandal outraged the world concerning heparin products. Despite the awareness of all benefits of LMWH, UFH is still produced and used in medicine as cheaper anticoagulant alternative. Impurities in some UFH batches produced from porcine intestinal mucosa led to at least 19 death cases in the US in spring 2008. Allergic shocks of patients taking the same UFH medicament have been

reported in Europe. Production of LMWH includes more purification steps, thus such dramatic adverse effects from impurities could be avoided.
For a detailed historical outline of heparin development, see annex chapter 8.3.

Blood clotting

If an organism is injured, it needs the ability to control blood clotting. This means that there must be a regulatory mechanism that stops blood flow, starts clot formation, and finally terminates the process. The first step after injury is constriction of blood vessels, preventing massive bleeding. Next, platelets become activated by thrombin and aggregate at the site of injury, forming a temporary, loose platelet plug, and further release proteins important for the coagulation cascade. The last step of the cascade is the formation of a fibrin mesh which stabilizes the platelets resulting in the actual clot.
There are two pathways in the coagulation cascade (Figure 6), the intrinsic and the extrinsic one, which come together at the activation point of factor X to Xa[47]. The clot growth is controlled by specific inhibitors, the most important of them being antithrombin III (ATIII), which inhibits factor Xa among others.
The activity of ATIII is potentiated in the presence of heparin by the following means: heparin binds to a specific site on antithrombin III, altering the protein conformation, and the new conformation has a higher affinity to factor Xa. Thus blood coagulation is prevented[48] .

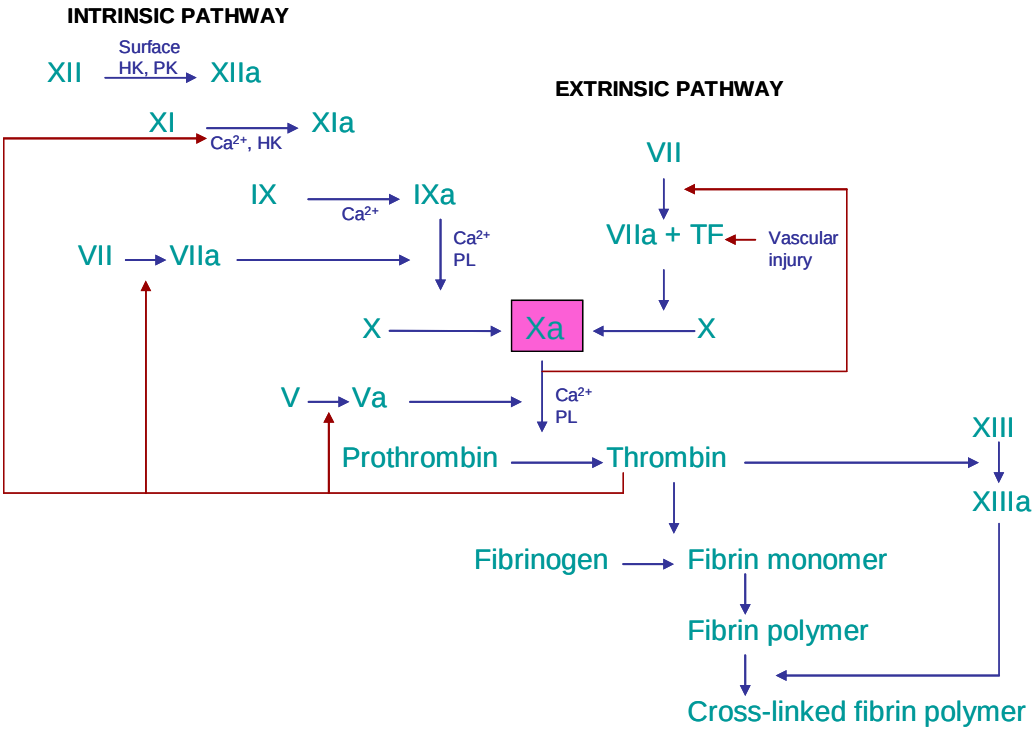

Figure 6: The intrinsic and the extrinsic pathway of the blood clotting cascade

Due to its biological properties and high density of negative charges, heparin can be exploited in studies of self-assembly, bioactivity and medical applications of materials based on this particular biological block.

1.5 Magnetic resonance imaging (MRI) and contrast agents

The vast building block diversity and stability of hybrid polymeric materials provides the opportunity to establish them in a wide range of applications, such as drug delivery systems, diagnostics and imaging. However, to be suitable for life science, biocompatibility is an essential feature.

Good biotolerance can be achieved by covering a surface with PEG to obtain a steric protection against opsonization and macrophage uptake and thus prolong the vascular retention time[49]. When PEG is covalently attached to a negatively charged polymer, for example an anionic saccharide, the block-copolymer can interact with a cation such as Gd^{3+} and form an aggregate.

Gadolinium is a well known positive contrast agent for MRI, that affects the longitudinal relaxivity of protons. They are associated to the relaxation time T_1, which is characterized by the longitudinal return of the magnetization to its

maximum. (Negative contrast agents affect T_2, the time needed to lose the transverse magnetization.)
MRI is an imaging technique that does not involve ionizing radiations and has been increasingly used over the years for its safety for the patients and its ability to discriminate between different tissues and between healthy and pathological structures.
MR images have excellent contrast, mainly because the magnetic relaxation time constants T_1 and T_2 differ markedly between tissues (Figure 7).

Figure 7: Example of an MRI section of my upper body without contrast agent. Areas with a high proton density like blood vessels and some organs are bright.

Nevertheless, certain diseases leave T_1 and T_2 unchanged and, as a result, allow no change in image intensity. Contrast agents facilitate the detection of certain abnormalities that would have otherwise the same intensity as surrounding tissues, and also help resolve ambiguity between possible diagnoses.
The parameter that describes the performance of an MRI contrast agent is the relaxivity, which is the ratio between the change in relaxation times of the imaged tissue and the concentration of the contrast agent in the tissue itself, according to the following formula:

$$\frac{1}{T_{1/2}} = \frac{1}{T_{1/2,0}} + r_{1/2}C$$

$T_{1/2}$ = T_1 or T_2 values of the tissue with contrast agent
$T_{1/2,0}$ = original T_1 and T_2 values of the tissue
$r_{1/2}$ = relaxivity values
C = concentration

Contrast agents (CA's) affect both - T_1 and T_2 - values, and for gadolinium-based compounds, r_1 and r_2 values are normally similar. When the value of r_2 is less than twice the value of r_1, the CA can be used as a positive enhancer, meaning that the pixel intensity is higher where the contrast agent is localized; otherwise, it can be used as a negative enhancement CA, which reduces the image intensity in the tissue.
Positive enhancers are generally preferred by clinicians, because high intensity spots are more visible on images and less mistakable for artifacts.
Gadolinium is a positive CA but as a plain ion it is toxic due to its interaction with phosphate in the cells and its accumulation in bone tissue. Therefore gadolinium ions have to be embedded into a matrix that meets the biocompatibility requirements. Moreover, coating results in contrast gain because of the retention of water molecules in close proximity to the gadolinium. The reduction of the translational and rotational mobility induces also an enhancement of the relaxivity. Many gadolinium-embedding CA products are already available on the market, such as MultiHance and ProHance® (Bracco) Magnevist® (Bayer), Omniscan® (GE Healthcare) and OptiMARK® (Covidien). However, there is still a wide range of research going on to further increase the relaxivity and thereby reduce the amount of required gadolinium. The majority of the proposed matrix materials are based on chelators such as diethylene triamine pentaacetic acid (DTPA) or the kinetically more stable tetraaza cyclododecane tetraacetic acid (DOTA)[50], more recent research focuses on dextran stabilized particles[51] or liposomes incorporating lipophilic gadolinium complexes such as Gd-DTPA[52]. Stabilization of gadolinium with anionic polysaccharides such as heparin has been patented[53] but not further investigated: no PEGylation of the polysaccharide and no addition of phosphate was explored.

1.6 Biohybrid amphiphiles (II): Peptides as building blocks

The countless possibilities towards the design of new amphiphilic compounds with a biological block are not limited by their linkage to synthetic units, but also include combinations among each other.
Not only the monomer sequence, but also specific intramolecular folding motifs and intermolecular interactions can control formation of superstructures[54]. Controllable specific interaction is a desirable feature of membrane constituents. Peptides and proteins organize into characteristic secondary and tertiary structure to be able to fulfill their biological tasks. This process involves formation of disulfide bonds and weaker nonbonding interactions such as Van der Waals-forces, π-π interactions and hydrogen bonds. Such specific attraction forces as part of the membrane formation process is an attractive approach towards precisely built superstructures[55].
For example, amphiphilic peptide sequences deriving from the antibiotic gramicidin were synthesized as model systems to investigate how self-assembly can depend on individual building blocks[55, 56].
Gramicidin is a short antibacterial peptide deriving from *Bacillus brevis* that consists of 15 amino acids[57]:

formyl-L-X-G-A-*d*L-A-*d*V-V-*d*V-W-*d*L-W-*d*L-W-*d*L-W-ethanolamine

The sequence is entirely hydrophobic and exhibits a β-sheet-like pattern of hydrogen bonds. The backbone folds into a $\beta^{6.3}$-helix, a secondary structure formed by the association of parallel beta strands in a helical pattern. The superscript indicates the number of units per turn in the helix. Gramicidin inserts into membranes to form channels specific for the transport of monovalent cations across membranes[58]. The high affinity of gramicidin channels to each other suggests this peptide a suitable candidate as hydrophobic block for self-assembling amphiphiles.
In fact, Kimura et al were among the first ones to report vesicular self-assembly of a gramicidin-polymer (PEG) conjugate[56].
A purely peptidic derivative of gramicidin and its reduced sequence, the seven C-terminal amino acids, was synthesized by Dittrich et al by N-terminal addition of oligo-lysine[55]. Dialysis of the peptide solubilized in ethanol led to the formation of rigid and monodisperse spherical structures, predominantly micelles. The

hydrophilic lysine with a pK_a of 10.2 can act as molecular switch. Removal of the charges by increasing the pH results in immediate but reversible precipitation[59].
The properties of this fully peptidic amphiphile can be changed in terms of functionality by amino acid point mutations or insertion of functional groups other than amino acids.
Combination of peptides with saccharides leads to glycopeptides. Not only the need for homogenous samples (single glycoforms) for the better understanding of glycoprotein formation and function, but also their exploitation in terms of self-assembly and applications has resulted in great effort in the synthesis development of glycopolymers over the past 15 years[60,61-64].
The vast majority of natural glycopeptide synthesis is based on *O*-glycosidic linkage via the hydroxyl groups of serine and threonine or *N*-glycosidically via the amide side chain of asparagines, resulting in a peptidic bond. Many synthetic routes have been exploited to achieve chemical or enzymatic glycosilation, as reviewed recently[65].
The need to synthesize glycopeptides in large quantities is not only based on the research need to understand how glycosilation affects the function and activity of proteins, but also on the current investigations for new vaccines. Cancer cells and viruses tend to express selective carbohydrate motifs in the form of glycoproteins or glycolipids. Utilization of those carbohydrates in a glycopeptide-based vaccine could potentially trigger immune recognition, generating a protective response against the disease. Since the isolation of carbohydrate antigens from natural sources is difficult and yields mostly minimal quantities, it is virtually impossible to obtain homogeneous starting materials for medical use. Therefore the purity and availability problem falls to organic chemists to be solved[66].
Although many elegant and rapid preparation methods for glycopeptides have been found, there is still a need to explore ways that require minimal protection and one-pot glycosylations towards complex constructs that can be used in clinical settings.

2 MOTIVATION AND CONCEPT

2.1 Motivation

Heparin is a hydrophilic linear polysaccharide, with high density of negative charges. Its main biological role is - among others - controlling blood coagulation, and therefore it finds medical applications as an anticoagulant agent.
When combined to different synthetic polymers or natural blocks like peptides, interesting material properties and aggregation behavior could be foreseen, due to amphiphilic or bis-hydrophilic self-assembly. In particular, the question whether heparin would retain its biological activity depending on the block copolymer synthesis and the self-assembly process was important for perspective applications.
Materials combining saccharide and peptide blocks would have novel characteristics, since the peptide's intrinsic secondary structure and the features of short amphiphilic peptides promise a well defined aggregation behavior. To explore feasibility and adaptability of such bio-inspired amphiphiles, it was interesting to establish new synthesis pathways to produce glycopeptides consisting of a gramicidin-derived sequence linked to a monosaccharide and to study aggregation properties of such hybrid materials under different experimental conditions.
The primary motivation of this work was to study the aggregation properties and potential applications of glycopolymers and glycopeptides, especially hybrid materials consisting of heparin or its monosaccharide units.
Additionally, given the heparin's charges, we assumed electrostatic interactions of heparin-PEG with metal ions and thus the formation of metal-encapsulating superstructures. A further goal of this study was the development a new type of contrast agent for medical imaging using gadolinium.

2.2 Concept

Carbohydrates such as heparin are promising candidates for the exploitation of the behavior of hybrid materials. Heparin as hydrophilic part of an amphiphilic block-copolymer may be used to functionalize the surface of colloidal nanoparticles such as vesicles or micelles. Key to any biomedical application is the retention of heparin's biological activity.
We will synthesize amphiphilic copolymers composed of a hydrophobic poly(dimethyl-siloxane) (PDMS) block and low molecular weight heparin (LMWH) as the hydrophilic one. Different approaches can be implemented to characterize the properties of heparin-PDMS, i.e. binding of heparin to protamine[67] used in medicine as heparin inhibitor and the anticoagulant activity of heparin-based materials.
As an example of a biomedical application for glycopolymers, a new type of MRI contrast agent using stabilized $GdPO_4$ can be introduced. In order to obtain a good CA it is necessary to decrease the mobility of the system and in this respect we propose to use heparin-PEG block copolymers which will trap the gadolinium ions inside their core.
This bis-hydrophilic material consisting of heparin and the non-toxic hydrophilic block PEG can be applied as matrix for gadolinium phosphate particles. This copolymer is a promising candidate due to its hydrophilic character which ensures retention of water molecules in proximity of the paramagnetic core giving a high relaxivity. The ensuing addition of phosphate results in formation of small and stable gadolinium-phosphate particles, which reduces the toxicity of gadolinium.

Another class of block copolymers containing bio blocks are glycopeptides: they consist of a peptide block and a sugar block. Peptides open a new interesting class of tectons for amphiphilic block copolymers to be investigated in terms of synthesis and self-assembly behavior.
The idea of this project is to couple the hydrophobic oligopeptide tryptophane-(D-leucine-tryptophane)$_3$ to the hydrophilic monosaccharide D-glucuronic acid by Fmoc-solid phase, resulting in an amphiphilic glycopeptide (W(DL-W)$_3$-GluAc). Furthermore, glucosamine could be coupled to the same peptide, but due to its amino functionality, the simple SPPS strategy is inapplicable. Therefore new strategies, such as a "backwards" coupling method – where the peptide is detached from the solid phase – in solution have to be explored. A coupling on

solid phase is conceivable by reductive amination. The already gained insights of purely peptidic materials based on gramicidin and its derivatives can be expanded by the insertion of a new class of molecules and investigated in terms of their applicability for e.g. vaccines. DLS, CLSM and TEM are promising methods to explore the self-assembly behavior of such hybrid materials in different solvents.

3 RESULTS

3.1 Heparin-PDMS

We applied various synthesis strategies to obtain heparin-PDMS block copolymers. The first attempt included nitrous acid degradation of heparin to obtain aldehyde end-functionalization, which, upon reductive amination was coupled to an amino end-functionalized PDMS-block via Schiff's base. Another similar synthesis pathway is iodine oxidation of heparin which results in the formation of a lacton end-functionality, which then can also be coupled to an amino end-functionalized PDMS by amide bond.
A different strategy without degradation of heparin is based on DCC/DMAP coupling of amino end-functionalized blocks to the carboxylate groups of heparin. Using DCC/DMAP coupling, we obtain better yields through a one-pot reaction; nevertheless, quantification of the PDMS bound to heparin turns out to be a major difficulty.

3.1.1 Heparin coupled to PDMS by nitrous acid degradation followed by reductive amination

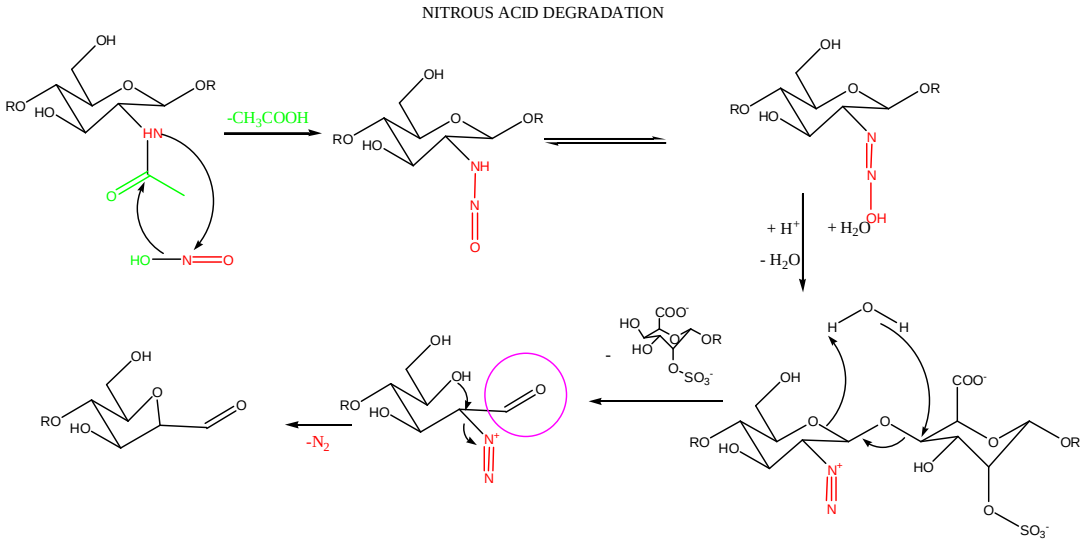

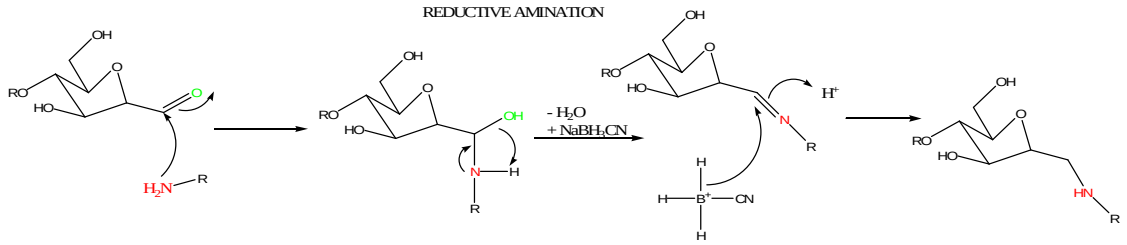

Figure 8: Synthesis pathway of nitrous acid degradation followed by reductive amination

The nitrous acid degradation of heparin seemed to be a reliable way to obtain reactive heparin with a desired end-functionality[68]. We coupled the functionalized heparin to a bi-funcional PDMS block by reductive amination and expected it to result in an ABA-triblock-copolymer.

FT-IR spectroscopy revealed the appearance of an aldehyde group at 1738 cm^{-1}, which means, that the end-functionalization took place. After the coupling step, the aldehyde band disappeared, showing, that the reduction of the aldehyde group and thus the coupling worked.

After washing the polymer with hexane, the product was dissolved in water, resulting in a turbid, slightly opalescent solution. This fact and the result from IR spectroscopy strongly indicate the formation of a covalent binding between heparin and PDMS.

To investigate, if the resulted amphiphiles are able to self-assemble in water, an aqueous solution of the polymer was dried on the rotary evaporator and redissolved in water. This rather unconventional variation of the film-rehydration method involves dissolution in water to form a thin film by evaporation, because the copolymer is insoluble in any other solvent. After extruding the turbid solution 6 times through a 0.2 µm Millipore filter, TEM images were taken. We observed spherical aggregates(Figure 9), but they could not be reproduced.

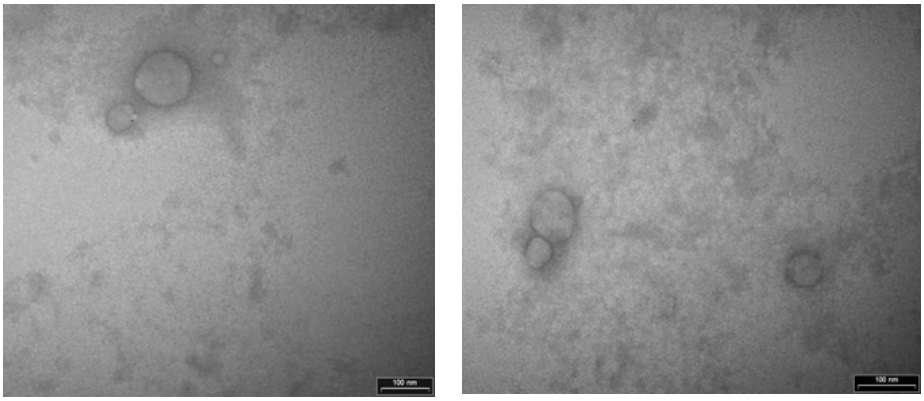

Figure 9: TEM images of heparin-PDMS aggregates.

NMR was performed in a 1:1 mixture of D_2O and acetone-D_6. The quantification was done by comparing the integral of the anomeric protons of the iduronate or the glucosamine as described in chapter 6.2.7. Those peaks were chosen, because the others overlap and are difficult to quantify. We assumed that a heparin molecule with a MW of 5000 Da is composed of approximately 20 repeating sugar units, which sum up from ten iduronate and ten glucosamine saccharides. Comparing the integrals with the ones of the coupled block could tell us the coupling ratio. However, PDMS is very poorly soluble in acetone, hence no quantification could be made, even though a peak at 0 ppm appeared and suggested that the reaction took place.

Gel electrophoresis revealed no difference between the educt and the product runtime. It can be hypothesized, that the stain toluidine blue is not able to interact with the degraded heparin due to changed chain length and charges.

The formation of an ABA triblock-copolymer could not be supported by NMR data or gel electrophoresis, however, a covalent binding can be presumed from the change in solubility and IR data. Very low yields and products which are very difficult to characterize by common analysis methods due to the intrinsic incompatible solubilities of the two building blocks, led to a provisional abandonment of this method.

We explored other methods to link heparin to polymer blocks. Formation of a lactone using iodine is another method to achieve end-functional coupling of heparin.

3.1.2 Heparin coupled to PDMS by iodine method

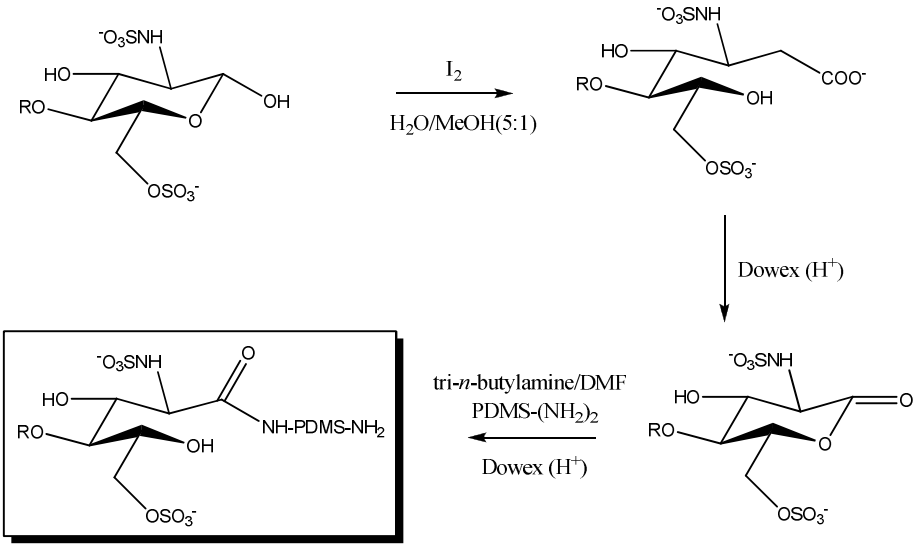

Figure 10: Synthesis pathway of lactone end-functionalization of heparin by iodine method

We attempted a second method reported by Matsuda et al.[69] which results in an end-functionalization of heparin but does not involve its degradation. Heparin gets oxidized by iodine, leading to a lactone end-functionality, which can be coupled to an amine-functionalized hydrophobic block by an amide bond. This strategy resulted in extremely low yields, though, and the characterization with NMR resulted in the same unsatisfactory quantification due to poor solubility of PDMS in acetone as in the method described in chapter 3.1.1. Heparin is soluble in water, poorly in formamide, but in no other solvent. PDMS is moderately soluble in DMF. A mixture of the deuterized forms of these two solvents would have been an alternative to the water-acetone mixture, but due to difficult availability and an insufficiently promising outcome, we abandoned this approach.

The characterization by NMR spectroscopy in a 1:1 mixture of D_2O and acetone-D_6 suggested the coexistence of PDMS and a residue of the sugar. It could not be evaluated if the product still contained heparin, its decomposition product or other impurities. Nevertheless aggregation studies were performed by TEM imaging.

TEM images were taken after producing a 1% solution through film rehydration method. Formation of spherical superstructures were observed, however, the nature of the superstructures could not be evaluated.

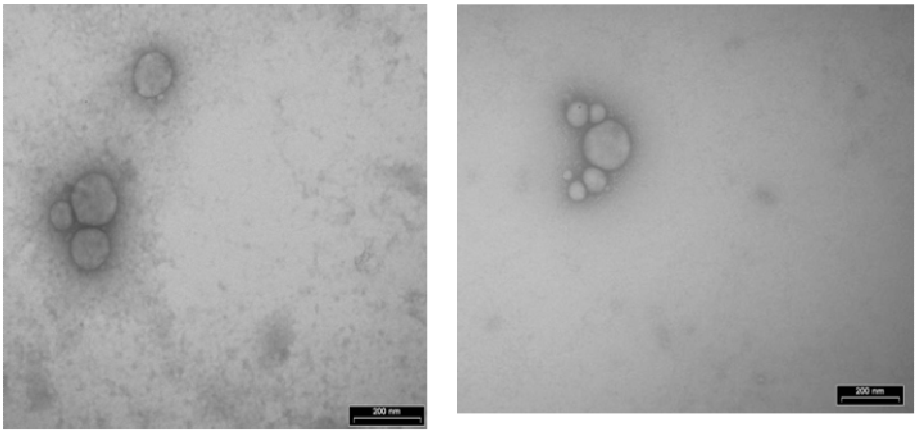

Figure 11: TEM images of heparin-PDMS aggregates

TEM does not reveal if the superstructures are hollow (vesicles) or full spheres, therefore we measured the hydrodynamic radius (R_h) by DLS and the radius of gyration (R_g) with SLS.
The DLS and SLS measurements were done on five solutions with a concentration gradient between 1 mg/mL and 0.1 mg/mL at angles between 30° and 150° (steps of 10°). For technical details and theory, see chapter 6.2.1.
We measured and calculated a hydrodynamic radius (R_h) of 208 nm from DLS.
SLS data were analyzed by Zimm plot, without (Figure 12a) and with (Figure 12b) considering a form factor. In the case where the form factor is not considered, the intensities, expressed by Kc/Rϴ are plotted against the angle, expressed by q^2 and extrapolated to 0°. The 0° intensities are then plotted against the different concentrations and extrapolated to zero concentration.
Figure 12a shows such a Zimm diagram. For clarity, only the values at zero scattering angles are plotted.
Form the slope (s) and the intercept of the extrapolated graph, the mass averaged weight (M_w) and the radius of gyration (R_g) of the particles can be calculated:

$$S = R_g^2 / 3M_W$$

Thereby, we obtained a molar mass of approx 41'000 kDa. The radius of gyration was calculated to be 180 nm.

In Figure 12b the extrapolations were done using the random coil form factor. The radius of gyration thereby was calculated to be 112 nm.

a)

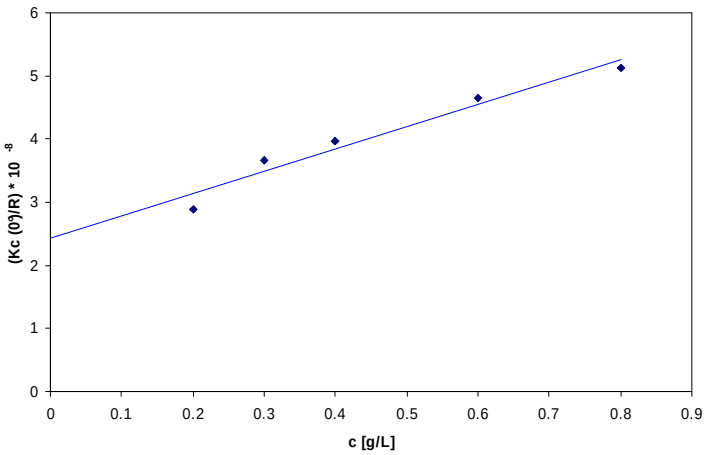

b)

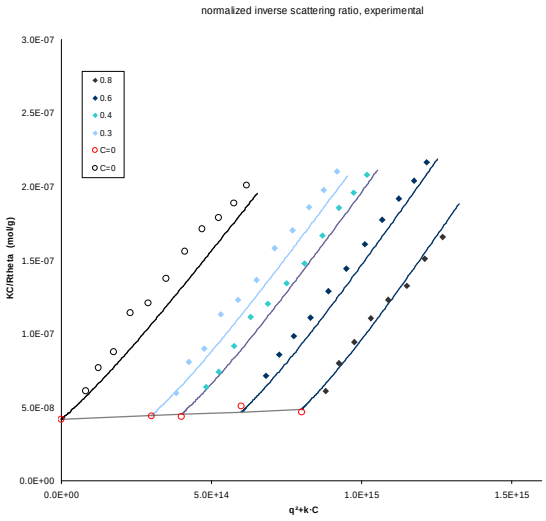

Figure 12: a) Static light scattering measurements of heparin-PDMS block-copolymer fitted without form factor. b) Fitted with random coil factor. The divergences of the fittings arise from high polydispersities, ranging from 0.15 to 0.25.

The theoretical quotient of R_g/R_h is 1 in case of vesicles and 0.78 in case of full spheres.

We obtained a quotient R_g/R_h of 0.87 without form factor and 0.54 with random coil form factor. Both results do not verify either – vesicle or full sphere – morphology. As we did not find any other than spherical shapes from this polymer by imaging techniques, we could not conclusively determine its aggregation behavior.

3.1.3 Heparin coupled to PDMS by DCC/DMAP method

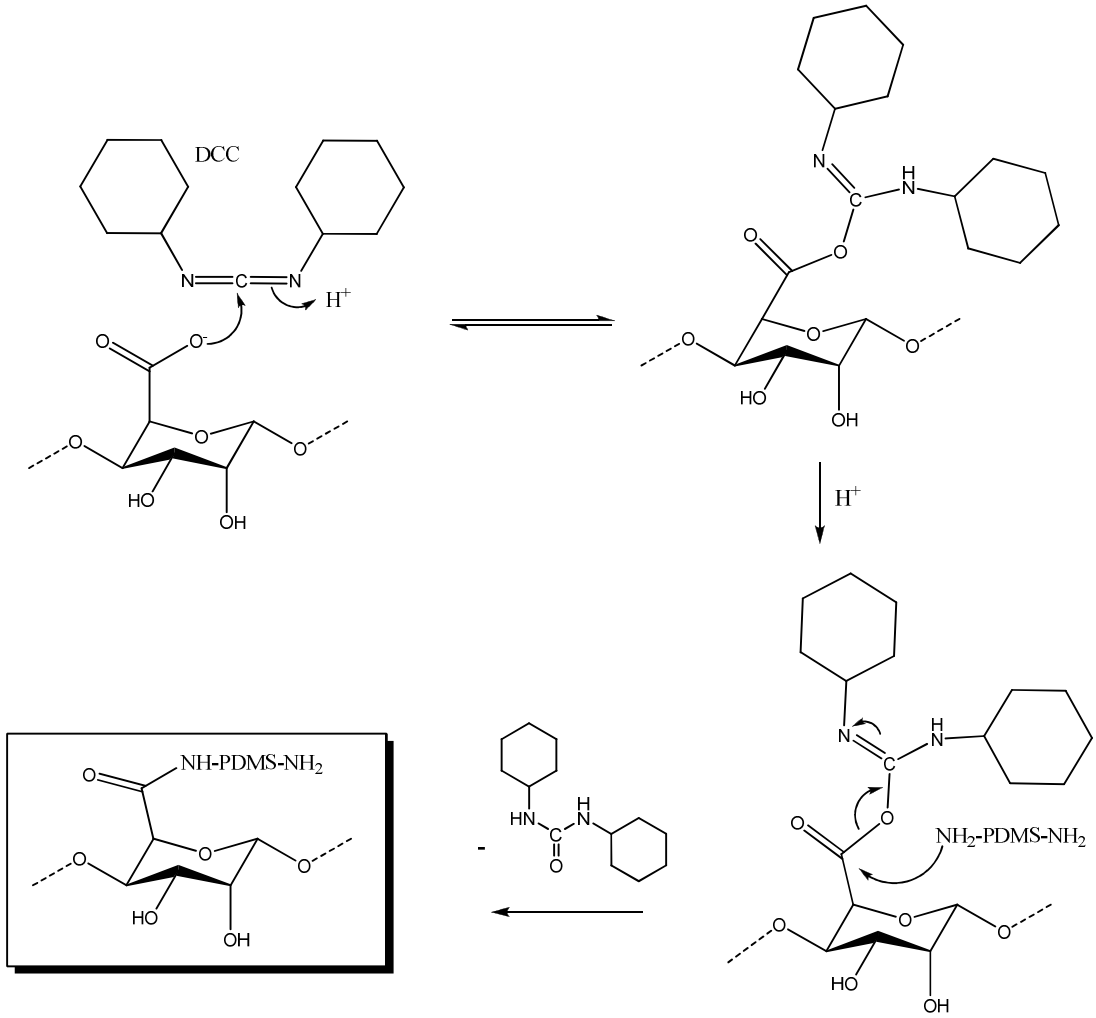

Figure 13: Synthesis pathway of PDMS grafted to heparin by DCC/DMAP method

The attempts described so far - involving end-functionalization - resulted in rather low yields, were time consuming and difficult to reproduce. Therefore we decided to use dicyclohexyl carbodiimide (DCC) / 4-dimethylaminopyridine (DMAP) to couple the carboxylate functional groups of heparin to amino end-functionalized blocks via amide bonds[70] (Figure 13). The DCC/DMAP coupling reaction is known from peptide synthesis. Being a one-pot reaction under mild conditions, it was a promising attempt to obtain higher yields and simpler purification, the drawback though being a more difficult quantification, considering that every second sugar unit is an iduronic acid possessing a carboxylate group, which is a

reacting group. The resulting amphiphile is best described as a graft block-copolymer.
The product was purified by UF and washed with hexane, resulting in poor water-solubility, which indicated the formation of covalent bonds. NMR spectra were acquired to quantify the amount of coupled PDMS. A mixture of D_2O and acetone-D_6 was used as solvent, but the poor solubility of PDMS in acetone precluded a correct quantification.
The formation of superstructures in water was observed by TEM imaging and measured by DLS, but the rather uncontrollable structures and sizes led to the idea to incorporate the polymers into the membrane of another polymer.

Probing heparin functionalization of polymer vesicles by specific peptide binding

Heparin-PDMS block copolymers are assumed to integrate into the membrane of vesicles formed by poly(ethylene glycol)-poly(propylene sulfide) (PEG-PPS) block copolymers, which were chosen because they are known to spontaneously form stable giant vesicles[71]. This polymer is an ideal candidate to be visualized by confocal microscopy. To verify the remaining bioactivity, we selected protamine because of its high affinity and specific binding to heparin leading to aggregation[72]. In medicine, it is used to inhibit the anticoagulant effect of heparin[73]. Protamines are small, highly positively charged peptides which bind to a variety of biological macromolecules, e.g. DNA. The used protamine, Salmine A1, consists of 32 amino acids, 21 of them are positively charged arginine residues which have a net charge of 21^+ at physiological pH[74]. These residues form very strong ionic interactions with the sulfo- and carboxyl groups of the heparin[75]. To visualize the binding procedure, we labeled the membrane and protamine fluorescently with two dyes which emit at different wavelengths.
To insert heparin-PDMS into a membrane made of PEG-PPS, three emulsions with different heparin-PDMS to PEG-PPS ratios were prepared. As a control experiment an emulsion with pure heparin and PEG-PPS was prepared. BODIPY was added to all solutions. Because of its high hydrophobicity, BODIPY incorporates into the polymer membrane labeling it (Figure 14).

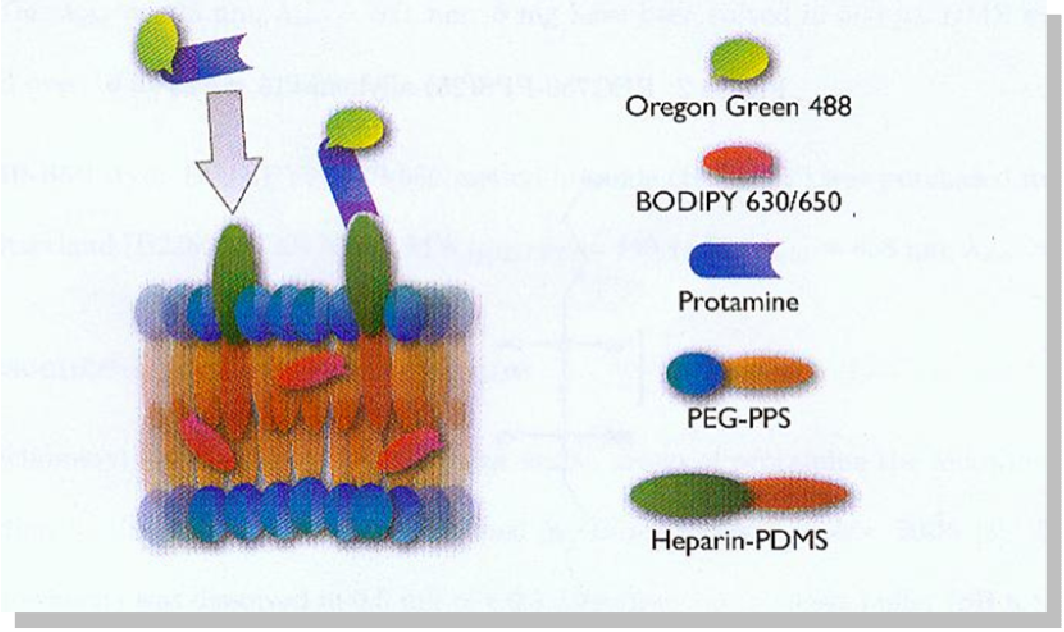

Figure 14: The two fluorescent dyes OG 488 and BODIPY 630/650 enable to locate the PEG-PPS membrane and the protamine. Heparin-PDMS diblock copolymers are integrated into the membrane

Immobilized giant vesicles with diameters between 10-100 µm were formed on glass fibers. To verify the binding, protamine labeled with OG488 was added, as discussed below.

Confocal Laser scanning microscopy - CLSM

After incubating with labeled protamine, several images were taken at different time intervals. Because the image just shows the emission intensity of the dye, no quantitative conclusion about the binding could be drawn. On average, there were no observable differences between the samples with PEG-PPS to heparin-PDMS ratios of 7, 30 and 76.
The solution for the negative control was dissolved in chloroform. Then an emulsion with an aqueous solution of pure heparin was produced, before the glass fibers were dipped in it. The sample solution was done in a similiar way by mixing PEG-PPS in chloroform with an aqueous solution of heparin-PDMS.
The fibers from both samples were dried in the drying oven over night and then immersed in 0.5 mL water[76]. Figure 15 a) and b) show the sample with heparin containing vesicles after 5 min and 20h. The negative control sample with pure PEG-PPS vesicles is shown in Figure 16 a) and b). The glass fibers which act as

a supporting medium for the polymer film are visible as green rods in the fluorescence images. The diagram next to the images shows the intensity development of both channels along the purple dart.

a) b)

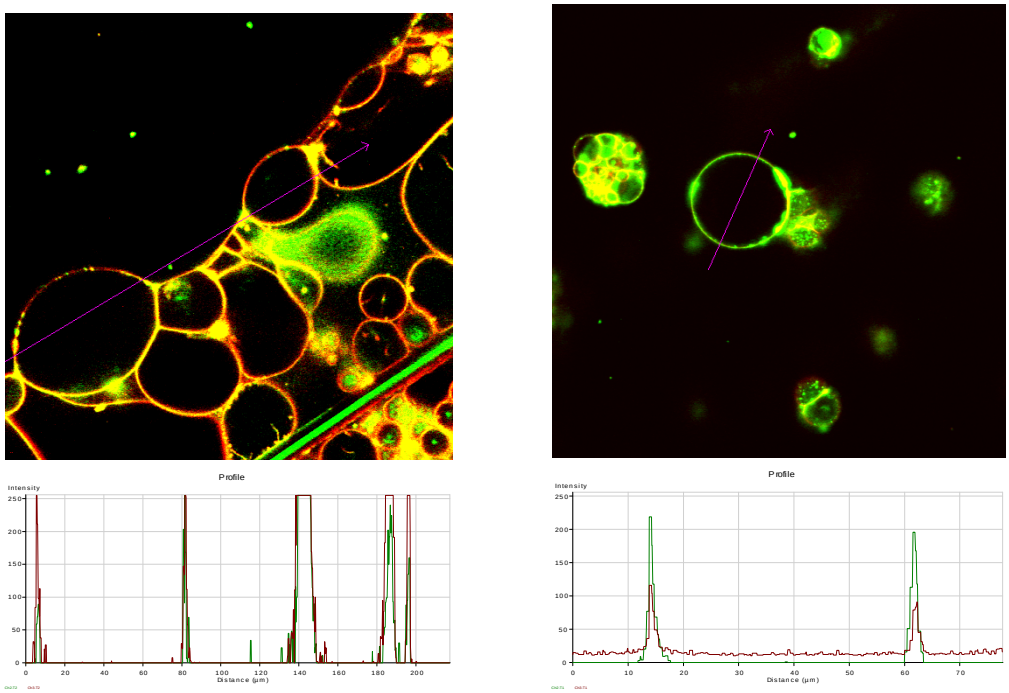

Figure 15: Heparin-PDMS and PEG-PPS, a) 5 minutes after incubation with protamine-OG488 and b) 20 hours after incubation. The bright green areas are aggregated vesicles.

The image dimensions are 230x230 µm.

a) b)

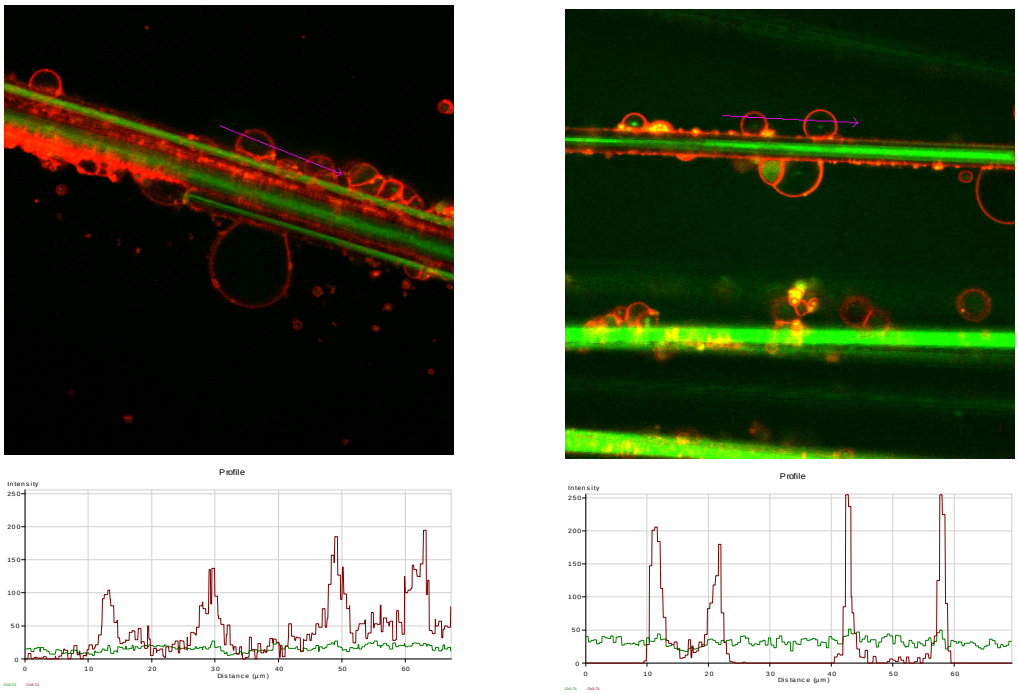

Figure 16: PEG-PPS negative control, a) 5 minutes after incubation with protamine-OG488 and b) 20 hours after incubation. The green rods are the glass fibres.

The image dimensions are 230x230 µm.

The red curve displays the intensity of the membrane marking BODIPY dye and the green one the intensity of the protamine-bound OG488 dye. In the positive control it can be observed that the peaks of both channels are nearly congruent, whereas the peaks in the negative control show no correlation. Therefore, we concluded that most of the protamine was bound to the membrane of heparin containing vesicles while it was freely diffusing in the solution with plain PEG-PPS vesicles.

FCS/FCCS measurements

Fluorescence correlation spectroscopy (FCS) and fluorescence cross correlation spectroscopy (FCCS) are powerful tools to determine the number, the diffusion properties and the molecular brightness of the species[77-79] and were performed to measure the interactions between fluorescently labeled protamine and heparin-PDMS decorated PEG-PPS vesicles labelled with BODIPY 630.
The samples were prepared by drying a solution of PEG-PPS in chloroform (control) or an emulsion of PEG-PPS in chloroform and heparin-PDMS in water

(samples) followed by rehydration. The solutions were extruded with a 0.2 µm Millipore filter.
FCS data of protamine showed a diffusion time of 102 µs. Control vesicles had a diffusion time of around 3 ms whereas heparin-containing vesicles had a diffusion time of 7 ms, i.e. they seem to be larger.
The binding was monitored by measuring FCCS of samples where the vesicles (both heparin- and control vesicles) were mixed with labeled protamine. The measurements suggested that there is some binding since the heparin-containing vesicles showed a high signal to noise ratio cross-correlation amplitude. The negative control vesicles did not, which indicates low binding. Also the diffusion times in the green channel were significantly higher in the positive control.
The concentrations of vesicles, protamine and vesicles labeled with protamine were calculated from the measured number of molecules (Table 1).

	Number molecules (N)	Confocal volume (V)	Concentration (c)
Red channel	$N_R = 0.52$	$V_R = 3.1*10^{-19}$ m^3	2.8 µM
Green channel	$N_G = 4.7$	$V_G = 1.4*10^{-19}$ m^3	55 µM
Cross correlation	$N_{GR} = 0.51$	$V_{GR} = 2.1*10^{-19}$ m^3	4 µM

Table 1: Concentrations of fluorescently labeled materials and their cross correlation calculated from the number of molecules

The concentration of vesicles bound to protamine calculated from the cross correlation is higher than the concentration of the pure vesicles (N_R). This peculiar quantification result has to be handled precautiously, because the vesicles have a size that approaches the size of the light beam. When this happens, the characteristic diffusion time and the particle number in the light beam are larger than those expected from theory[80]. In other words, the measured concentration exceeds the real amount of vesicles that are bound to labeled protamine. Another factor that leads to an excessive detection of concentration is the cross-talk. This effect is caused, when the emission wavelength of one fluorophore (in this case OG488) overlaps with the excitation wavelength of the other fluorophore (BODIPY).

3.2 Heparin-PEE

3.2.1 Heparin coupled to PEE by nitrous acid degradation followed by reductive amination

As an alternative hydrophobic block to PDMS we used monofunctionalized poly(ethyl ethylene) (PEE). It was produced by hydrogenation of amino monofunctionalized poly(butadiene)[81] on a palladium catalyst[82]. The coupling synthesis was carried out by degradation of heparin by nitrous acid, resulting in an aldehyde end-functionality of heparin, as described previously (chapter 3.1.1), and coupled to the amine end-functional PEE.
The product was purified by preparative RP-HPLC and characterized by IR spectroscopy. The product was verified by IR (Figure 17), but the yield was extremely low.

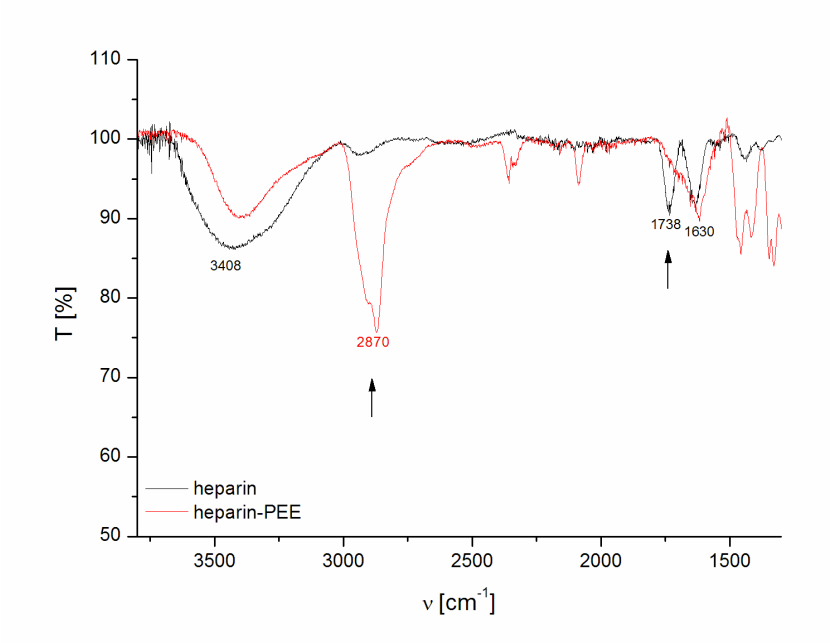

Figure 17: IR spectra of heparin-aldehyde (black curve) and heparin-PEE (red curve): The band at 1738 cm^{-1} of the aldehyde functional group disappeared, the typical OH and NH bands at >3000 cm^{-1} from heparin as well as the CH bands of PEE are visible in the spectrum.

Apart of its antifactor Xa activity (chapter 3.3.3), no further investigations were carried out with this copolymer.

3.3 Heparin-PEG

3.3.1 Heparin coupled to PEG by triazine method

The creation of a bis-hydrophilic compound, consisting of heparin as one and PEG as the other hydrophilic part, was supposed to be a model for the coupling of a hydrophobic block. The goal was to avoid handicaps caused by solubility differences between blocks, which lead to analysis problems. Furthermore, such bis-hydrophilic systems can also be considered amphiphilic due to their solubility differences in various solvents and may self-assemble in water, as for example the thermo-responsive micelles formed by poly(acrylic acid)-*block*-poly(*N,N*-diethylacrylamide) block copolymers[83]. Self-assembly in dilute aqueous slolution into highly dynamic and rather well-defined spherical aggregates was also observed for poly(ethylene oxide)-block-poly(2-methyl-2-oxazoline) diblock copolymers. They can be viewed as swollen water micelles or as "nanogels"[84].
As reported earlier[85], ionic self-assembly (ISA) bases on Coulombic interactions and heparin being a highly negatively charged polyelectrolyte is a promising candidate for the investigation of ISA.
One possible method for coupling was using triazine as coupling reagent[36] which was used by Bergman to control the amount of amino-functionalized polymers to hyaluronan. 2-Chloro-4,6-dimethoxy-1,3,5-triazine (CDMT), which is commercially available, can be used successfully for synthesizing esters, amides, and acid anhydrides from carboxylic acids[86].
The coupling of PEG was accomplished by the formation of amide-bonds between the carboxylic acid groups of heparin and the amine end-functionality of PEG 5000. One sample was synthesized with an equimolar amount of triazine to heparin. In the second sample, two equivalents of triazine were used. The amount of coupled PEG in the sample with excess triazine was supposed to be higher than in the sample with the equimolar amount of coupling agent. The NMR spectra of the products were evaluated by comparison of the anomeric protons of the idouronate and the glucosamine residues with the integral of the PEG peak. The sample with the excess triazine showed a ratio of average 1.7 PEG units per heparin, whereas the equimolar sample averages at 4.3 PEG units per heparin.
The method did not result in the expected controllability. The amount of reacted PEG did not agree with the amount of applied CDMT.

The triazine method was supposed to be a good way to control the amount of PEG bound to heparin; however we did not really manage to achieve this controllability.

3.3.2 Heparin coupled to PEG by nitrous acid degradation followed by reductive amination

The unpredictable heparin to PEG ratio that resulted from the triazine-method, motivated another experiment based on nitrous acid degradation followed by reductive amination. The procedure is described in chapter 3.1.1.
If heparin has one end-functionality, the aldehyde, to be coupled to a mono-functionalized PEG block, we expected that the product would result in a 1:1 heparin to PEG ratio (Figure 18).

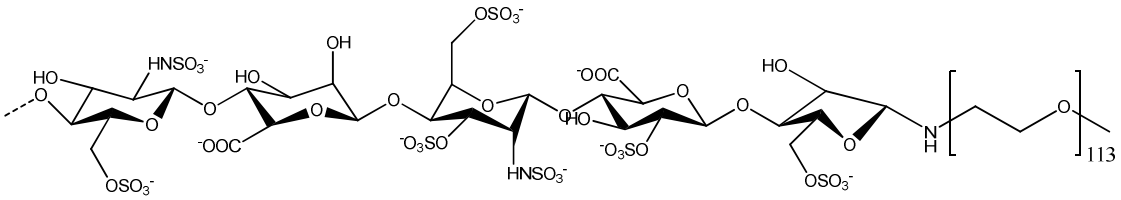

Figure 18: End-functionalized heparin coupled to monofunctional PEG

The product was purified by UF, a method that resulted in an unsastisfactory removal of all unreacted blocks. HPLC purification was not accomplishable due to the insufficient separation of the products.
The formation of a covalent bond between heparin and PEG was observed by IR. A peak at 1742 cm^{-1} appeared upon formation of heparin's aldehyde end-functionality and disappeared after the coupling step (Figure 19). We performed NMR measurements, to compare the amount of bound and unbound PEG by end-group analysis. It showed that ca. 60% of the PEG molecules are coupled, the rest is present as free molecules. We assumed the same amount of heparin to be coupled and calculated the average length of the heparin molecules after the degradation reaction. We found a length of four remaining sugar residues. Considering, that a pentasaccharide is the bio-active fragment of heparin, we expect that the anticoagulant activity of the degraded heparin will drop to a minimum. This is confirmed by activity measurements in chapter 3.3.3.

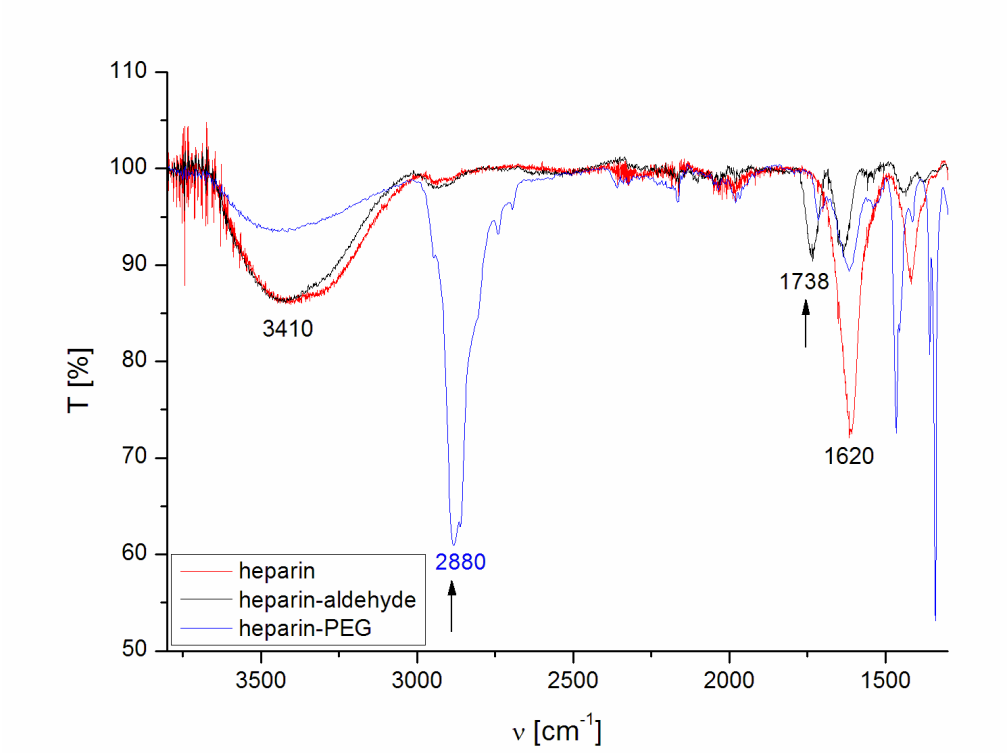

Figure 19: IR spectra of heparin (red curve) with N-H and O-H bands at >3000 cm^{-1} heparin-aldehyde (black curve), the aldehyde band appears at 1738 cm^{-1} and heparin-PEG (blue curve), the aldehyde band almost disappeared, the other typical bands are present

As already mentioned, bis-hydrophilic copolymers are able to form superstructures in water. Heparin-PEG seemed to be an interesting candidate to investigate if the different polarities of the two blocks result in the formation of ordered structures.

Heparin-PEG was dissolved in water and TEM-images were taken of highly concentrated solutions (30 mg/mL, Figure 20). The structures found indicated the formation of weakly bound superstructures, which coalesce upon drying.

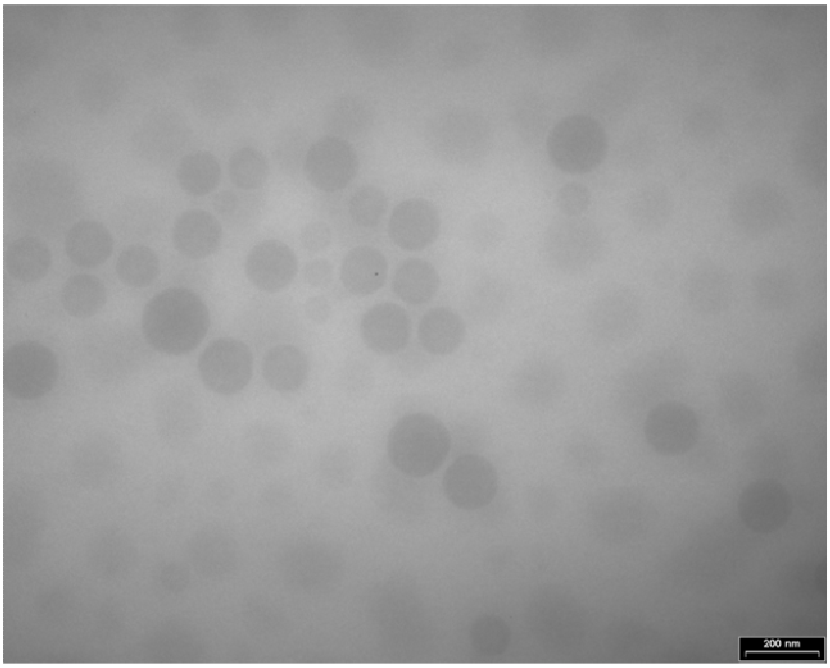

Figure 20: TEM image of 30 mg/mL heparin-PEG. The formation of superstructures is presumably induced by drying effects

DLS measurements - on the other hand - revealed that the superstructure formation was not detectable in solution. It can be speculated, that due to the hydrophilicity of both blocks the refractive index change and therefore the contrast for light scattering is too low to obtain a signal. The superstructures could also be too dynamic and thus the polymers can be considered dissolved in water, only interacting when the sample dries out.
Formation of an ionic self-assembly was done by the addition of a multivalent metal-ion, which intereacts with the heparin parts, leaving the PEG-blocks to the interface. This way, a stabilized network was produced by mixing $GdCl_3$ with heparin-PEG. The formation of such networks and also the salt's aggregation behavior upon addition of phosphate was investigated by TEM and SEM/EDX. The purpose and applicability of such an aggregate will be discussed in paragraph 3.3.4.

3.3.3 Antifactor Xa activity test

As it has been stated above, a particular pentasaccharide sequence is necessary to maintain heparin's anticoagulant activity. To see, what impact the performed

synthetic modifications as well as integration into a block-copolymer have, we compared blood coagulation activities for all heparin-hybrid materials.
Heparin's anticoagulant activity is mainly based on its ability to build a complex with antithrombin III (ATIII). The common point in both, the intrinsic and the extrinsic pathway of the blood coagulation cascade is the activation of factor X to factor Xa. Factor Xa gets inactivated by ATIII, when the coagulation process has ended and a clot forms. This inactivation gets potentiated 1000fold, when ATIII is bound to heparin. Therefore, a useful way of measuring heparin activity is to determine the amount of inactivated factor Xa in blood. Such a determination is a routine method in a haemostatic laboratory of a hospital.
Blood is primarily mixed with a citrate-solution in order to complex calcium to prevent immediate coagulation. Then thrombocytes are removed by centrifugation, the leftover yellow solution is called citrate-plasma (Figure 21), naturally containing ATIII.

Figure 21: Citrate plasma, obtained through centrifugation of my blood.

A solution of heparin is prepared in the citrate plasma and a chromogenic substrate (S-2222) is added to the solutions. S-2222 is a tripeptide, bound to p-nitroanilin, which can be degraded by factor Xa. P-nitroanilin gets detached from the tripeptide and, as free molecule, absorbs light at 405nm.
Figure 22 illustrates the citrate plasma solution after the addition of the chromogenic substrate, heparin and factor Xa. According to heparin's activity, a certain amount of ATIII gets complexed. When a well-known amount of factor Xa is added to the solution, one part gets deactivated by binding the heparin-ATIII complex and the rest detaches p-nitroanilin from the chromogenic substrate. Photometric determination of the free p-nitroanilin concentration leads to the amount of left-over anti-factor Xa and thus heparin-activity can be calculated.

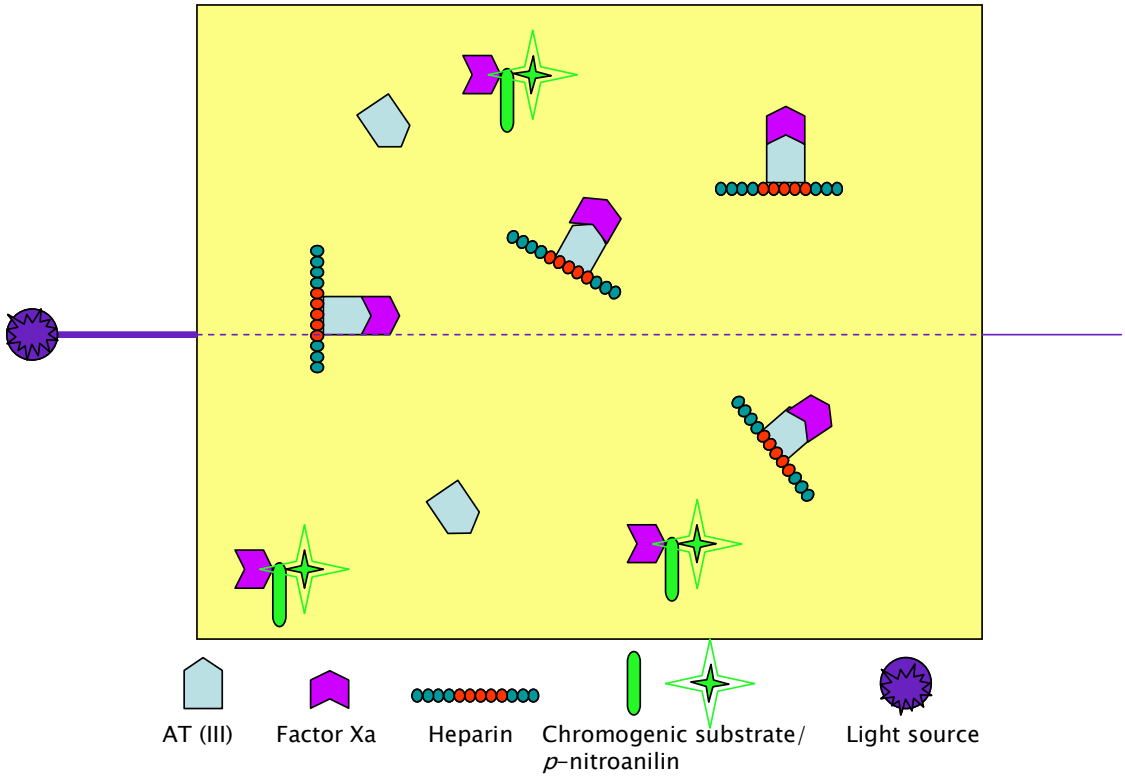

Figure 22: Antifactor Xa activity test in citrate plasma.

To prove the preserved biological activity of heparin and its derivatives, the following substances were subjected to antifactor Xa activity test:

Substance	Abbreviation	Conc. stock solution
LMWH (MW: 4000-6000 Da)	(LMWH)	1 mg/mL
(PDMS-(C_3H_6-NH_2)$_2$) (MW: 5000 Da)	(PDMS)	2 mg/mL
Heparin-PDMS (by DCC/DMAP)	(H-PDMS)	1 mg/mL
PEG-NH_2 (MW: 5000 Da)	(PEG5000)	1 mg/mL
Heparin-Aldehyde	(Hep-ALD)	1 mg/mL
Heparin-PEG	(H-PEG5000)	3.5 mg/mL

Table 2 shows the concentrations of active heparin in UI depending on the samples' heparin concentrations.

LMWH		H-PDMS		Hep-ald		H-PEG		H-PEE		PDMS	
c[mg/L]	UI	c[mg/L]	UI	c[mg/L]	UI	c[mg/L]	UI	c[mg/L]	UI	c[mg/L]	UI
15	>2	15	>2	500	0.48	300	1.26	15	0.00	15	0.00
7.5	1.59	7.5	1.53	250	0.24	200	0.86	100	0.00		
5	1.38	5	1.12	100	0.07	100	0.42			PEG	
2.5	0.71	2.5	0.58	50	0.01	50	0.22			c[mg/L]	UI
1	0.28	1	0.2			15	0.05			15	0.00
0.5	0.13	0.5	0.08								

Table 2: UI is the concentration of active heparin. It was measured at different sample concentrations. Pure LMWH was compared to varying heparin-hybrid molecules.

LMWH was measured as bought and compared to heparin-PDMS (Figure 23). The activity of heparin-PDMS dropped by a factor of nearly two compared to pure heparin. This can be explained by the fact that half of the weighed material is inactive PDMS.

As a control, we also measured pure amino-functionalized PDMS, which showed no activity, as expected.

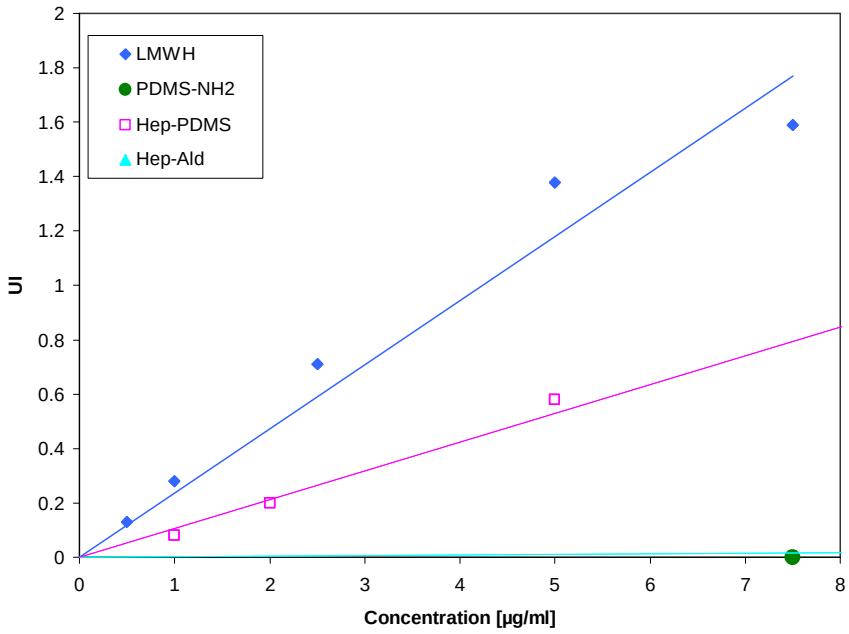

Figure 23: Concentrations versus activity of pure heparin sample, heparin-PDMS (produced by DCC/DMAP method) and pure PDMS as control. To compare pure heparin with its aldehyde derivative, it is added in bright blue.

Heparin-aldehyde, on the other hand, shows a dramatic drop of anticoagulant activity. The reason is the segmentation of the polysaccharide where a major part of the bioactive pentasaccharide moiety is destroyed. In the case of heparin-PEG the activity was expected to drop to at least half of the original heparin-aldehyde activity, because of the PEG attached to the sugar. However, the drop was smaller than expected. The reason could be that the purification by UF was not sufficient and there are still unreacted heparin fragments present.
As a control, we measured pure PEG-NH_2, which showed no activity, as expected.
We also compared the results to heparin-poly(butadiene), that was synthesized by nitrous acid degradation/reductive amination method as described above.

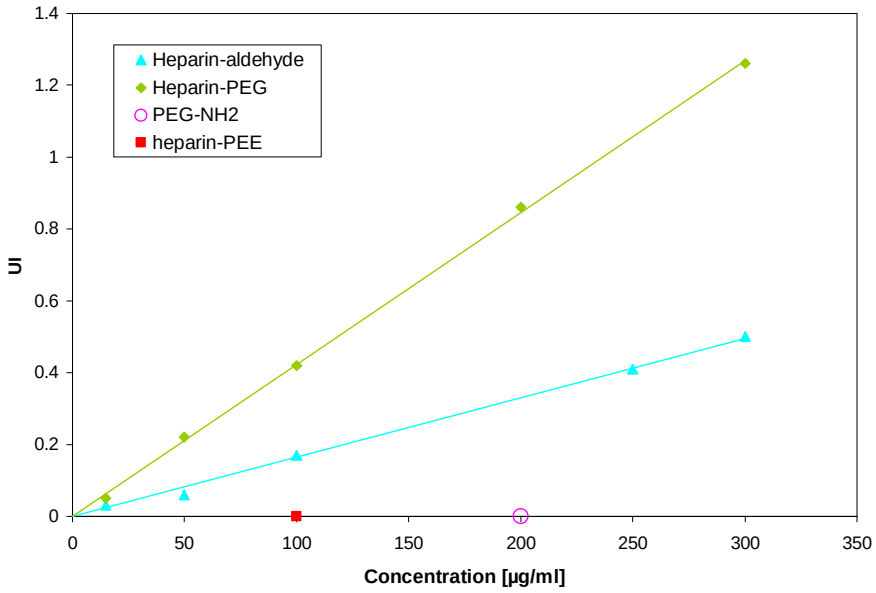

Figure 24: Concentration vs. activity of heparin-aldehyde (produced by nitrous acid degradation), heparin-PEG (PEG coupled to heparin-aldehyde by reductive amination) and as control: pure PEG. Note that the x-axis scale in Figure 23 differs from Figure 24.

The aldehyde functionalized heparin that was used for coupling was from the same batch as used for the coupling to PEG, therefore we expected, that the anticoagulant activity would be the same. Yet the activity of PEE bound heparin was zero. It can be speculated, that the poor solubility of the block copolymer in the aqueous solution (blood plasma) could be one reason. Since the amphiphile was purified by HPLC and thus more thoroughly than the heparin-PEG, it has

also to be considered, that the heparin-PEG activity derives from unbound heparin, which was not removed by UF.

3.3.4 Heparin-PEG for medical imaging

Gadolinium is a well-known positive contrast agent (CA). It is highly paramagnetic due to its 7 unpaired electrons in the f-shell. As a CA it allows the surrounding protons (usually deriving from water) to relax faster, increasing the contrast and that way the quality of an MRI image. Gadolinium can not be applied in its pure ionic form because of toxic effects. It has to be protected by a stable, water-soluble and biocompatible shell. The commercially available positive CA's are based on chelator-complexed ionic gadolinium. A new approach is to coat gadolinium by ionic interaction with a polyanion, such as heparin and form stabilized particles by adding phosphate, creating an insoluble gadolinium phosphate salt.
The heparin-PEG polymer prepared by nitrous acid degradation followed by reductive amination was used as a matrix to trap positively charged metal ions. As an example of a biomedical application for glycopolymers, we studied a new type of MRI CA using stabilized $GdPO_4$. In order to obtain a good CA it is necessary to decrease the mobility of the system[87] and in this respect we used heparin-PEG block copolymers which trap the gadolinium nuclei inside their core. Figure 25 shows such a trapping system for stabilized $GdPO_4$, however the dimensions and the exact shape are not assured.

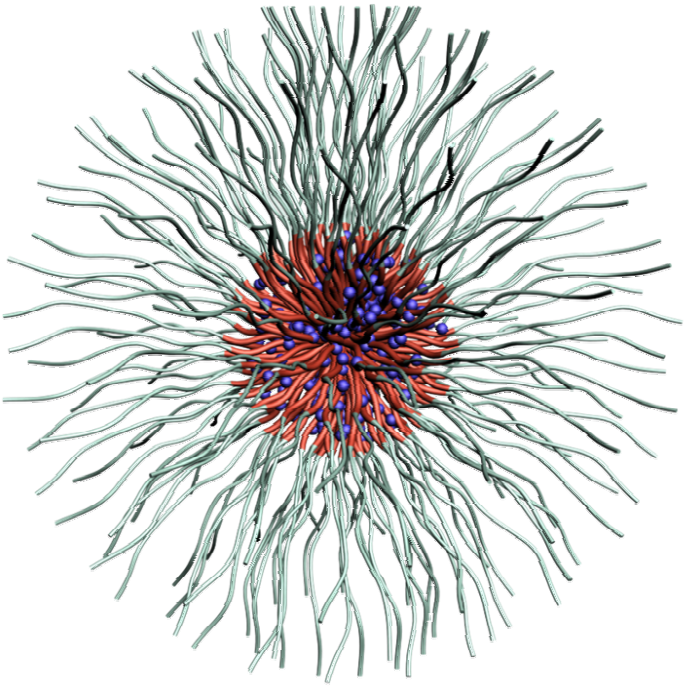

Figure 25: $GdPO_4$ stabilized by heparin-PEG diblock copolymer in water

The general principle of magnetic resonance imaging (MRI) and CA's was explained in the introduction. We will now introduce the heparin-PEG system with gadolinium ions and gadolinium phosphate as a potential new contrast agent.
Before starting in vitro measurements with the copolymer/gadolinium system, we wanted to investigate how the polymer interacts with gadolinium ions and how gadolinium phosphate salt forms in the presence of the copolymer. Therefore we took TEM images of heparin-PEG with gadolinium (Figure 26) and gadolinium phosphate trapped in it (Figure 27).

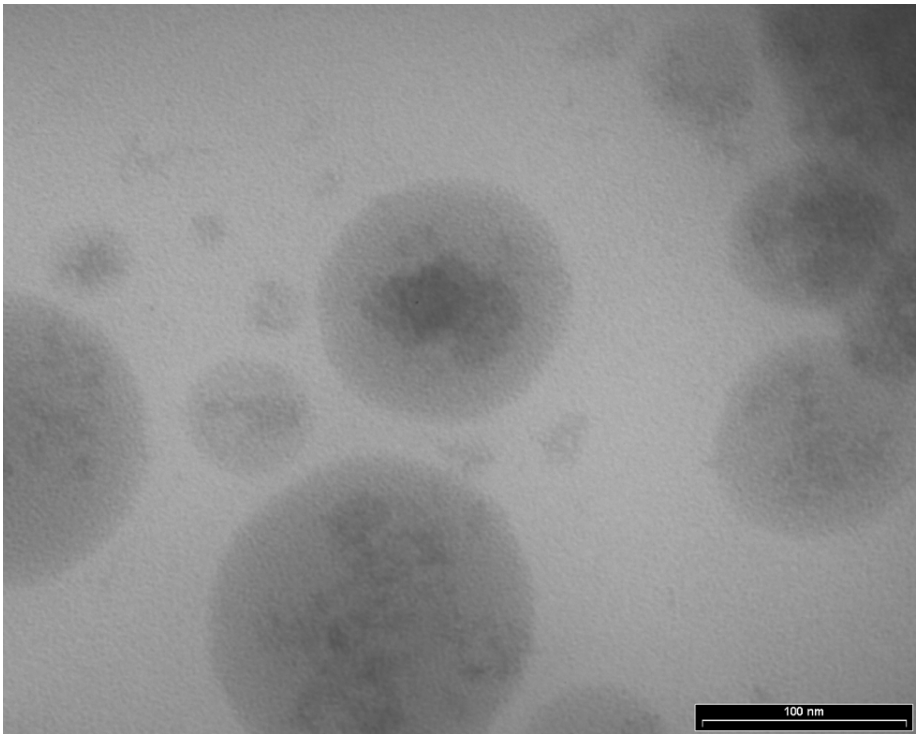

Figure 26: TEM image of 30 mg/mL heparin-PEG and 0.5 mM $GdCl_3$.

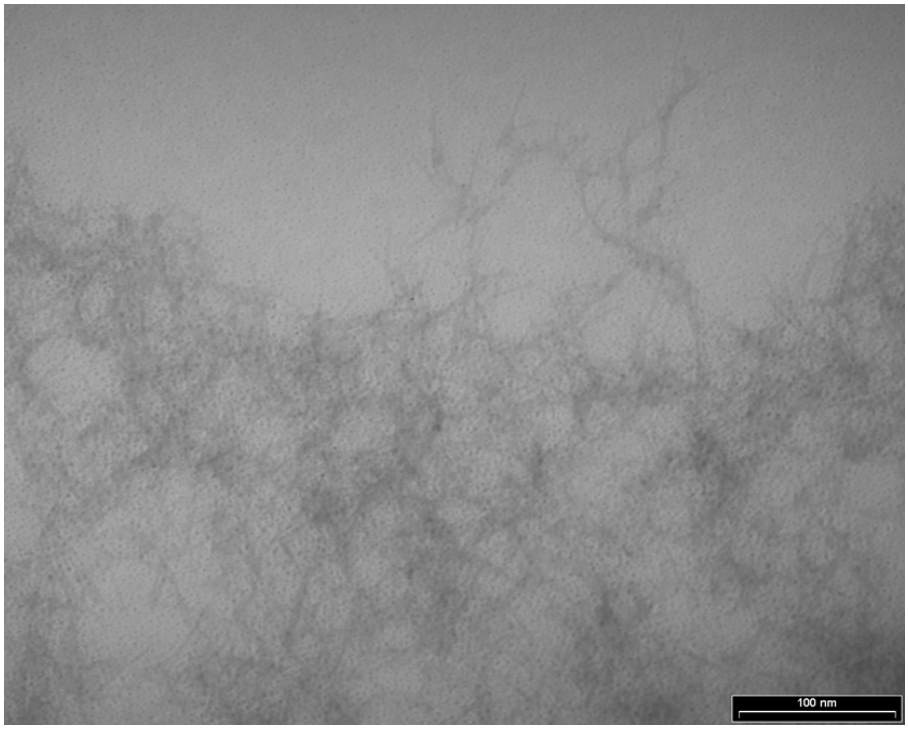

Figure 27: TEM images of 30 mg/mL heparin-PEG and 2.5 mM $GdPO_4$.

When the polymer was mixed with $GdCl_3$ and applied to a TEM grid, the drying resulted in the precipitation of the salt inside the polymer structures. This indicates an interaction of gadolinium with the polymer in solution, but no superstructures form that were measurable by DLS. The addition of phosphate to the polymer-gadolinium solution results in the formation of an insoluble $GdPO_4$ salt, that is stabilized and kept in solution by the polymer. However, the polymer could not be seen anymore on the dried TEM grid. DLS measurements were not performed on this solution

SEM/EDX studies

Scanning electron microscopy is a technique where a high energy beam is focused onto the surface of a sample and signals from the interaction of the incident electrons with the sample's surface are detected. The type of signals gathered in SEM can include secondary electrons, back scattered electrons and characteristic X-rays.
The X-ray emission can also be used in energy dispersive X-ray microanalysis (EDX), which is an analytical technique for elemental analysis. The beam in the SEM excites an electron in an inner shell of an atom, promoting its ejection and resulting in an electron hole within the atom's electronic structure. An electron from an outer shell drops into the hole and the energy difference is released as an X-ray beam with an energy that is characteristic for the two shells' energy difference. Atoms with more than one shell can have several transitions and will result in several bands in the EDX spectra. The "Moseley plot of characteristic X-rays" matches the detected X-ray radiation energies with the corresponding atoms (Figure 28).

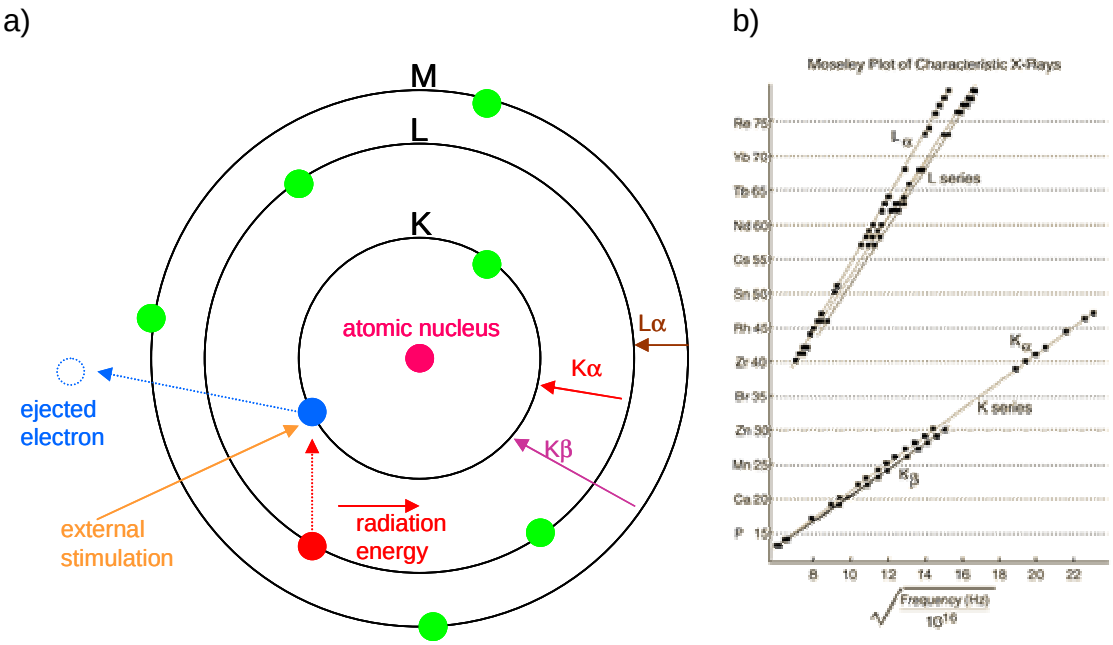

Figure 28: a) Electron transitions to lower shells result in the release of X-ray radiation with a characteristic energy. b) Moseley plot of characteristic X-rays[88].

To gain information if heparin-PEG and gadolinium interact with each other, we acquired SEM images to see what shape the gadolinium phosphate superstructures have in the presence of the polymer. We also measured with EDX if the gadolinium phosphate aggregates are separated from the polymer or if they form a co-aggregate. The images were done on dry samples of heparin-PEG mixed with $GdCl_3$ and NaH_2PO_4 (Figure 29) and as a control, we aquired images and spectra of pure heparin-PEG (prepared by nitrous acid degradation followed by reductive amination, Figure 30), and pure $GdPO_4$ (Figure 31).
The original solutions contained 30 mg/mL heparin-PEG and 10 mM $GdPO_4$ and were dialized against pure water to remove NaCl.
Ca. 0.2 mL of the samples were dropped on the sample holder plate and dried over night. After silver-sputtering, SEM pictures and EDX measurements were performed.

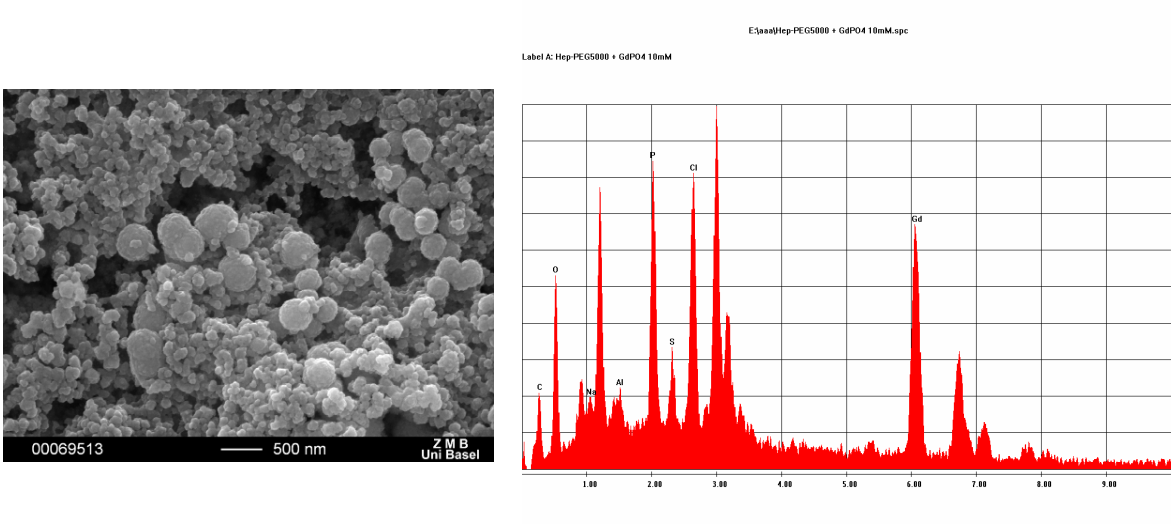

Figure 29: SEM image and EDX spectrum of heparin-PEG (30 mg/mL) + $GdPO_4$ (10mM).
Scale bar (SEM): 500 nm

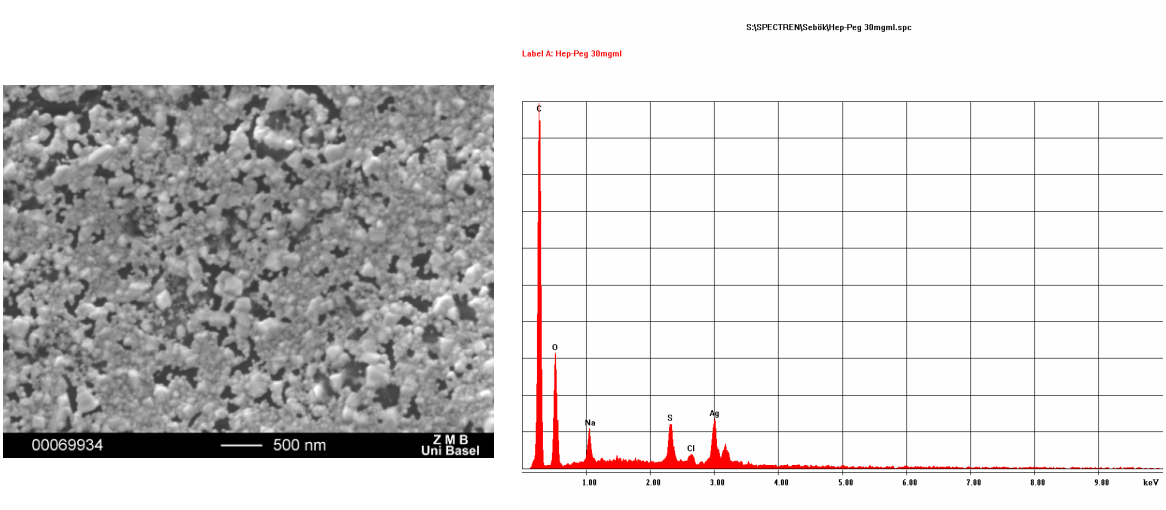

Figure 30: SEM image and EDX spectra of Heparin-PEG (30 mg/mL)
Scale bar (SEM): 500 nm

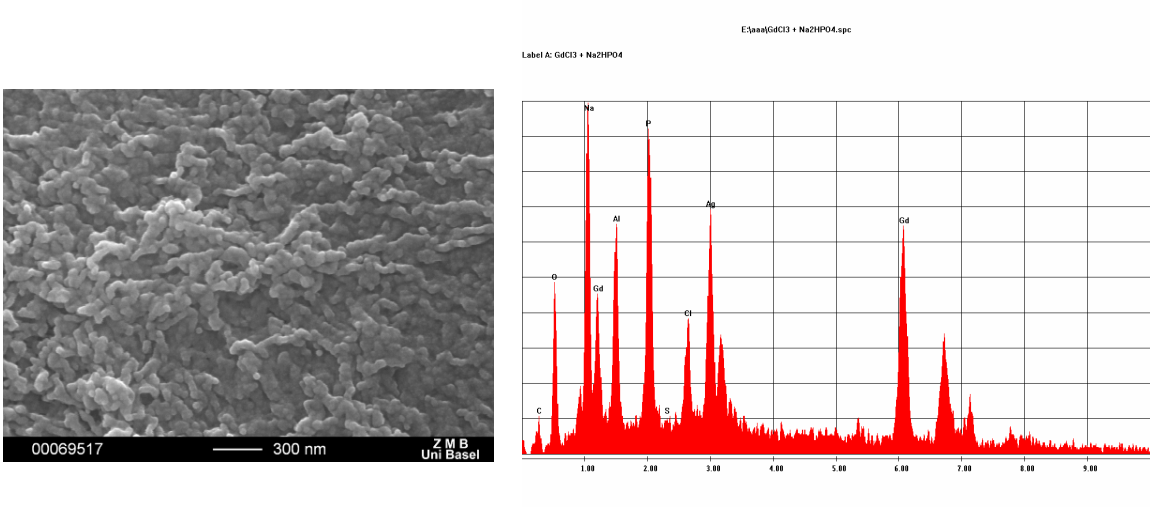

Figure 31: SEM image and EDX spectra of $GdPO_4$ (10 mM)
Scale bar (SEM): 300 nm

It can be observed in the SEM images, that spherical aggregates are present in the mixed solution, whereas they are non-existent in the pure salt or the pure polymeric solution. The EDX measurement in Figure 29 indicates, that the polymer and the salt are not separated, because they were both detected at the same spot. In the control experiment with pure polymer, the SEM image shows a polymer layer that breaks upon electromagnetic radiation, the elements in the polymer were detected by EDX. The gadolinium phosphate control experiment reveals that the salt precipitates in a different, less defined shape than in the presence of the polymer. The EDX spectra shows, that no polymer is present, as no sulphur peak is visible.
These results lead to further investigations of the interaction between gadolinium and heparin-PEG and the stabilization of gadolinium phosphate aggregates by the copolymer. Furthermore, we made a step towards understanding the applicability of stabilized Gd^{3+} and $GdPO_4$ particles for medical imaging. To further investigate the stability and eligibility of such particles, EPR studies were performed.

EPR studies

EPR is a very powerful method for studying magnetic properties and crystal-field symmetry of species containing unpaired electrons, such as lanthanide(III) complexes[89]. For technical details and theory, see methods chapter 6.

In order to establish the complexation ability of the heparin-PEG copolymer to metals, we first used copper as a probe material, due to its capability to coordinate quickly to almost all kinds of organic ligands. It is an ideal metal to investigate interactions with various ligands, since it can adopt a large variety of geometries (e.g. square-planar, tetrahedral, pyramidal, trigonal bipyramidal etc.), to which its spin Hamiltonian is very sensitive.

We mixed heparin-PEG with a solution of copper triflate ($Cu(OTf)_2$) and immediately measured the spectrum at 125 K (Figure 32, line a). The simulation of this spectrum indicated an approximately axial symmetry of the first coordination sphere around the metal, with the gyromagnetic tensor ***g***: 2.079; 2.083; 2.395, and the hyperfine tensor ***A***: 10; 10; 125 Gauss (G). The tensor of the linewidth, considered Gaussian, is Γ: 37; 38; 40 G.

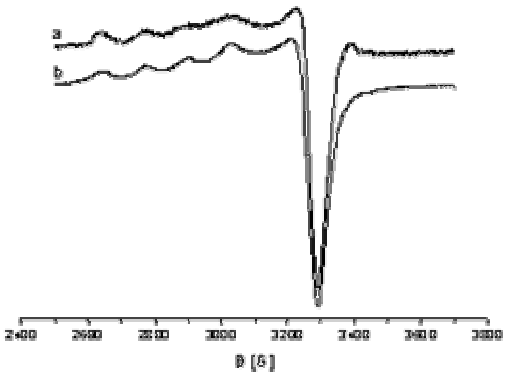

Figure 32: EPR spectrum of Cu(II) paramagnetic species formed between the copper ions and heparin-PEG block copolymer. a) experimental spectrum, b) simulated spectrum

The values of the gyromagnetic tensor are specific for oxygen atoms in the first coordination sphere of copper. The axial symmetry of both gyromagnetic and hyperfine tensors is characteristic for a tetragonal geometry around the metal.

As shown in Figure 32, the presence of the polymer leads to a paramagnetic copper(II), with >90% of Cu(II) being present in a tetragonal symmetry, with four oxygens in the first coordination sphere, which could derive from either PEG or heparin, since both blocks have such potential binding sites.

Knowing that the polymer binds to copper, we measured spectra of $GdCl_3$ solutions and $GdCl_3$ mixed with the copolymer to see how the overall shape of the spectra changes (Figure 33).

The EPR spectrum of $GdCl_3$ has the characteristic quasi-isotropic lineshape, with a gyromagnetic effective factor of 1.982. This changes when the polymer is added to the $GdCl_3$ solution, indicating, that Gd^{3+} is bound to the polymer. The pattern which appears at g_{eff} : 2.480 and 5.889, together with the normal signal at 1.984 shows that the symmetry becomes lower when the metal is bound to the polymer.

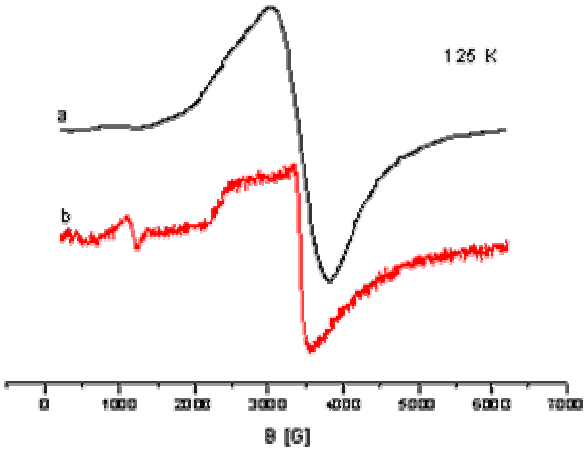

Figure 33: EPR spectra of a) $GdCl_3$ and b) Gd^{III} mixed with heparin-PEG

To see if significant spin-spin interactions are present in Gd^{III}, an EPR spectrum was measured as the function of temperature (Figure 34). The intensity of the high field signal decreases when the temparature increases from 110K to room temperature. This corresponds to a normal Curie behavior, specific to paramagnetic species. Thus, the spin-spin interactions can be considered small enough in the case of Gd^{III}.

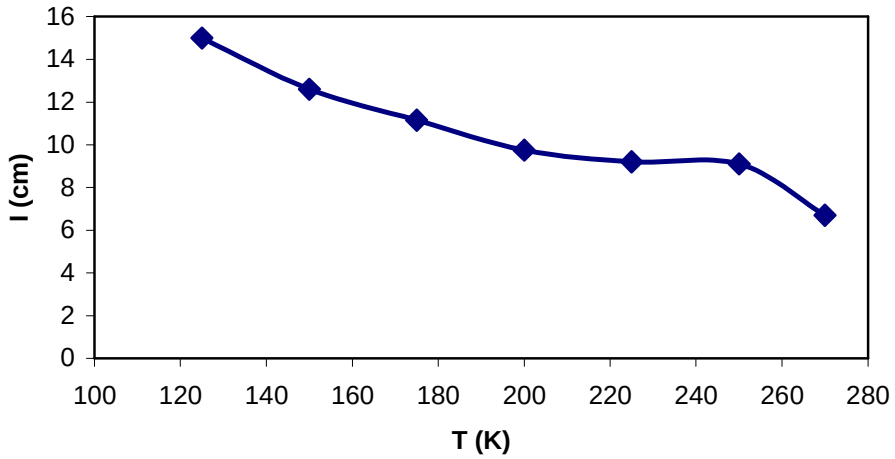

Figure 34: Intensity of EPR high field signal of heparin-PEG as the funcion of temperature.

The transverse electronic relaxation rates, $1/T_{2e}$, were calculated from the dependence of the peak-to-peak EPR linewidths, ΔH_{pp}, as the function of temperature[87] (Figure 35).

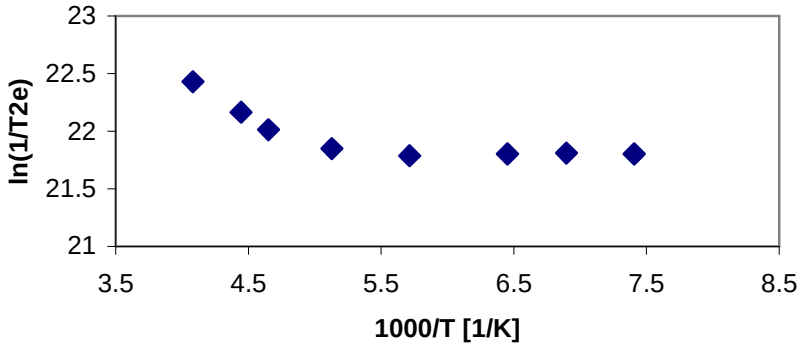

Figure 35: Temperature dependence of the transverse electronic relaxation rates of heparin-PEG mixed with gadolinium

Due to the fact that there is no reliable theory of electron spin relaxation in macromolecular Gd^{III} systems, a detailed analysis of Gd^{III}-Gd^{III} distances is not possible, as is the case of low molecular weight Gd^{III} complexes[90]. The experimental electron spin-spin relaxation rates measured here are higher than those for low molecular weight Gd^{III} complexes. Therefore, besides the transient zero-field splitting mechanism[91], the contribution from intramolecular Gd-Gd

interactions has to be taken into account. We suppose that the dipole-dipole contributions even if they are small, influence the electron spin relaxation rates and are modulated by the global rotational motion of the polymer system.
EPR results prove that gadolinium interacts with oxygen atoms, but as both blocks of the polymer contain oxygen atoms, it is impossible to show where exactly the binding takes place. However, due to the opposing charges, we assume that the interaction is more likely to happen between the Gd and heparin. Further indications that gadolinium is bound to the heparin block of the copolymer are presented in the MRI section below.

MRI studies

We used the bis-hydrophilic heparin-PEG copolymer as a matrix for gadolinium ions and gadolinium phosphate particles. The hydrophilic character of the block-copolymers ensures retention of water molecules in proximity of the paramagnetic core giving high relaxivity. When Gd^{3+} is present freely in the body, it interacts with phosphate and is cytotoxic. It also accumulates in the bone tissue. Phosphate addition results in formation of small gadolinium-phosphate particles with a solubility constant of 10^{-25} mol^2/L^2, meaning, that they are virtually insoluble[92] in aqueous solution. This reduces the toxicity.
These $GdPO_4$ bearing copolymers can be produced by mixing $GdCl_3$ with a solution of or the block copolymers, followed by an addition of PO_4^{3-}.
We assume that when Gd^{3+} ions are mixed with an anionic block-copolymer, they form a network through electrostatic interactions, which is maintained in solution and shielded by the uncharged block at the water-polymer interface. When phosphate is added to this solution, gadolinium phosphate particles grow until they reach the dimension of the core of the polymer-shielded aggregate, around a few nm.
To further explore the possibilities to form such coated gadolinium phosphate particles, we also used a polycation, polylysine, bound to PEG and mixed it first with PO_4^{3-} before addition of $GdCl_3$.
When PO_4^{3-} ions are mixed with a cationic block-copolymer, they form a similar network, with the uncharged blocks at the interface. Addition of Gd^{3+} to polylysine-PEG results in the fomation of assumedly crystalline particles, that are arranged in a star shape (Figure 36). The organization is probably deriving from the interaction with the polymer. We wanted to see if the gadolinium phosphate particles remain stable also when they are produced in a different way.

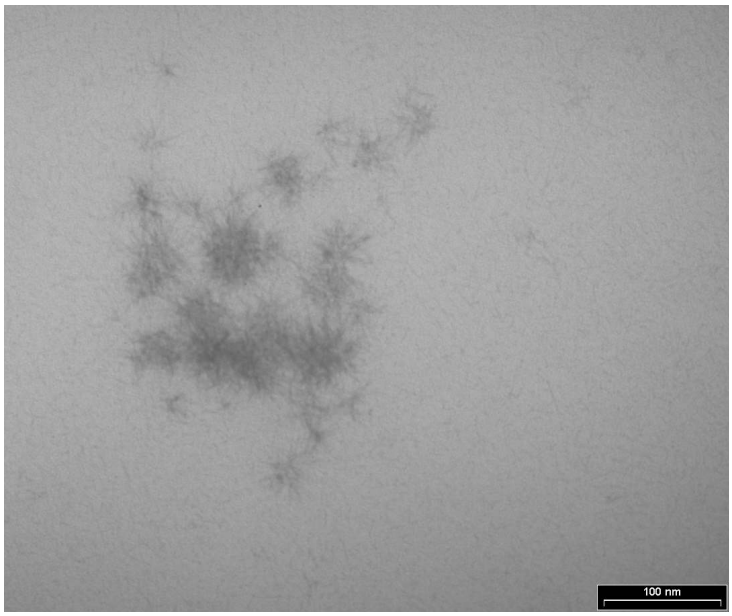

Figure 36: TEM image of gadolinium phosphate particles stabilized by polylysine-PEG

Those aggregates, produced by either method, remain in solution due to the hydrophilic uncharged block. Depending on the concentration, the solutions remain stable in aqueous solution for at least 2 weeks without phase separation.
We will not discuss the polylysine-PEG block copolymer in detail, because it seems to be less promising for medical use, due to polylysine's cytotoxicity. We will discuss the results obtained by MRI measurements to demonstrate the feasibility of gadolinium phosphate aggregates with a polycation-PEG copolymer.

We prepared different concentrations (0.1 mM to 1 mM) and concentration ratios (1:1, 1:2 and 1:5) of $GdCl_3$/$GdPO_4$ and heparin-PEG (and PEG-polylysine, respectively) and measured as a control solutions of $GdCl_3$ without the polymer, the pure polymer and also pure water. As expected, the polymer and the pure water showed no enhancement of the relaxivity and therefore those samples will not be further mentioned anymore.
As further control experiments, we did the same measurements with simply PEG and heparin. For clarity, the different measurements are schematically represented in Figure 37. All measured samples are listed in Table 3.

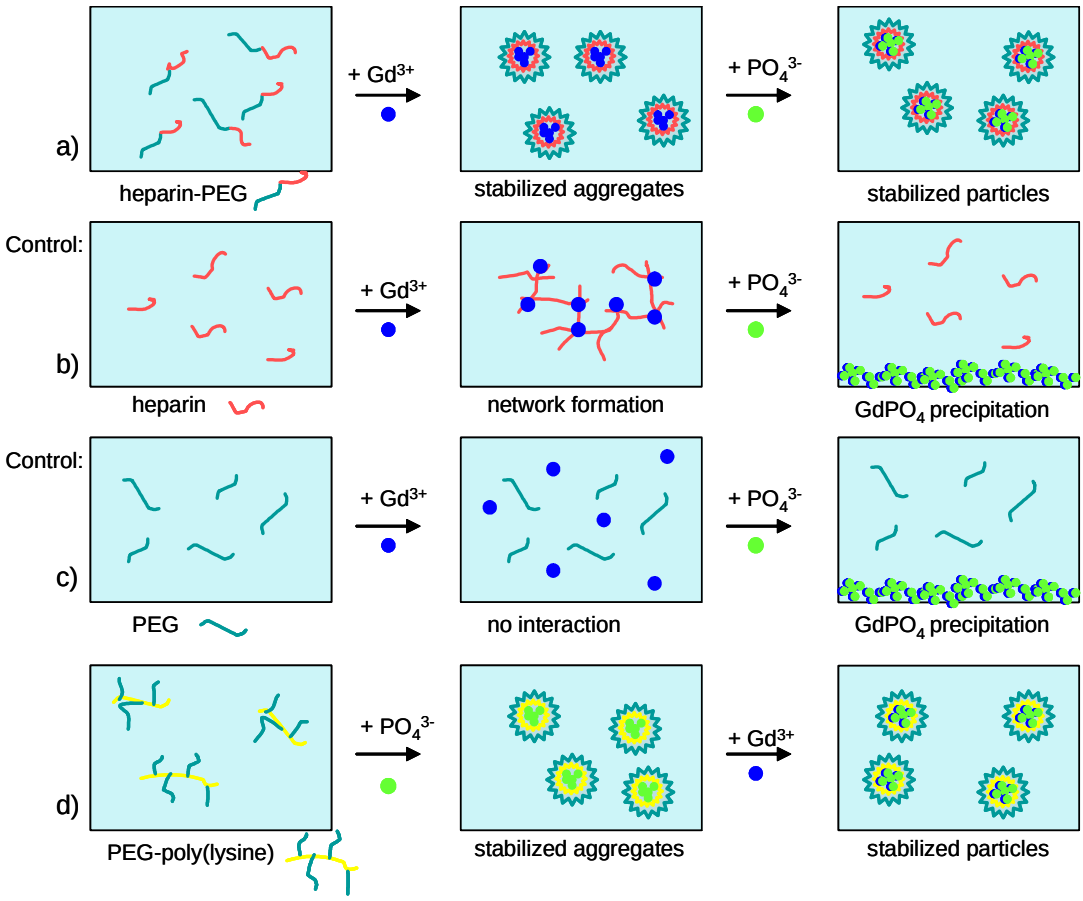

Figure 37: Schematic representation of the sample preparations for MRI measurements. The solutions were mixed with $GdCl_3$, the relaxivity was measured, then Na_2HPO_4 was added and the relaxivity was measured again. a) heparin-PEG solution, the added salts are stabilized by the copolymer. b) heparin forms a network with Gd^{3+}, which is destroyed upon addition of phosphate. The salt precipitates. c) PEG does not interact with Gd^{3+}, addition of phosphate results in immediate precipitiation of the salt. d) PEG-polylysin stabilizes phosphate, addition of gadolinium leads to stabilized salt particles.

Eppendorf test tubes filled with aqueous solutions (concentrations of 0.01, 0.1, 0.2, 0.3, 0.4, 0.5, 1 mM) of heparin-PEG complexed with $GdCl_3$ and $GdPO_4$ with multiple concentration ratios between polymer and Gd^{3+} and $GdPO_4$ salt (5:1, 2:1, 1:1) were scanned on a 1.5T imaging scanner, in order to evaluate the R_1 and R_2 relaxation rates.

By measuring the relaxivities at different concentrations (Figure 38 shows the relaxivities R1 of mixtures of heparin-PEG/Gd^{3+} and heparin-PEG/$GdPO_4$) and plotting them against the concentration, we can calculate $R_{1,0}$ and $R_{2,0}$ from the intercept of the linear regression and the concentration independent relaxivities r_1 and r_2 from the slope.

$$R_{1,2} = R_{1,2_0} + r_{1,2}C$$

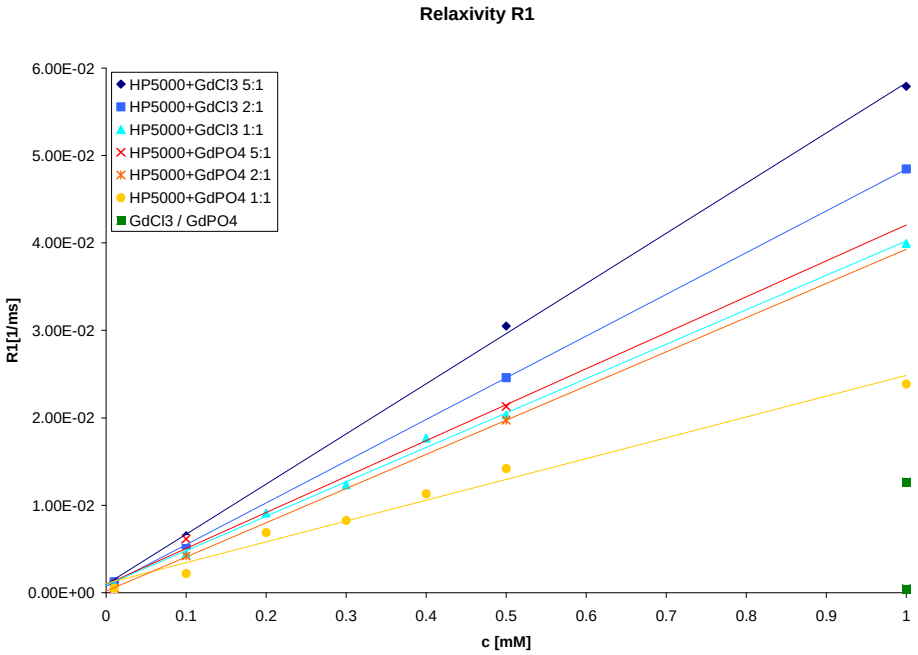

Figure 38: The relaxivities of heparin-PEG/Gd^{3+} and heparin-PEG/$GdPO_4$ mixtures at different concentrations are in a linear relation to each other.

These concentration-independent relaxivities can be used to compare different systems. As a control, we also measured pure Gd^{3+} (relatively low contrast) and $GdPO_4$ (immediate precipitation and loss of contrast). This control experiment emphasizes the need for stabilizing agents for gadolinium species, such as our copolymer.

In Figure 39, we compared our systems to other CA's, Magnevist®, Gadovist® and MultiHance® being commercially available CA's[93] and new CA's, investigated by other research groups[51].

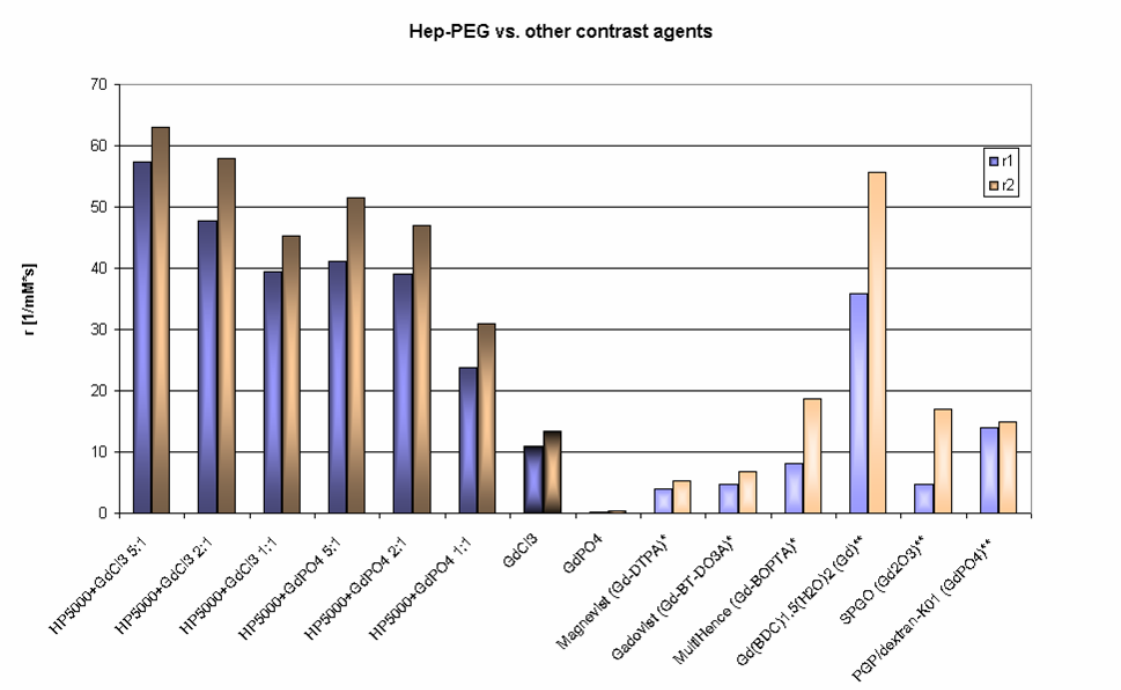

Figure 39: Relaxivities r_1 and r_2 of heparin-PEG and $Gd^{3+}/GdPO_4$ at different ratios compared to other CA's. [*:ref [93]; **: ref [51]]

The relaxivities seem to depend on the ratio between the polymer and the metal. This can be explained by the fact, that if the amount of polymer is not sufficient to bind all metal ions, the unbound ions will only contribute slightly to the relaxivity, as they are small and their rotation freedom is not limited. It is also noticeable that the relaxivities drop upon addition of phosphate. One reason is that the unbound ions will precipitate and not contribute at all anymore. The other reason could be that aggregates form and the gadolinium atoms inside of the particles are not anymore accessible for the exchange with water molecules. Thus, the gadolinium concentration theoretically drops.

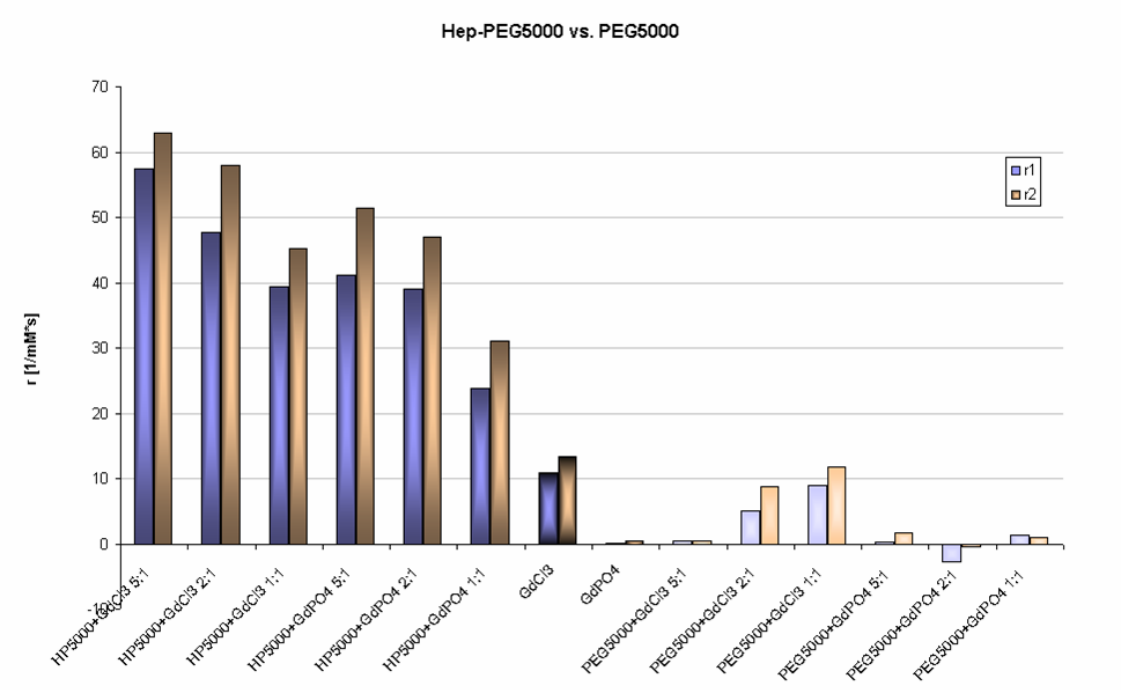

Figure 40: Relaxivities r_1 and r_2 of heparin-PEG and $Gd^{3+}/GdPO_4$ compared to PEG and $Gd^{3+}/GdPO_4$.

The measurements were also compared to mixtures of gadolinium and its phosphate salt with pure PEG (MW: 5000 Da) (Figure 40). The results show that mixing PEG with Gd^{3+} leads to only minor relaxivity change compared to free Gd^{3+}. The 5:1 mixture of PEG with $GdCl_3$ results in almost complete loss of the relaxivity and seems to be an outlier, because no precipitation was observed. The results after the addition of phosphate are not reproducible due to the fact that $GdPO_4$ salt was precipitating and the relaxivities were not in a linear relation (Figure 41).

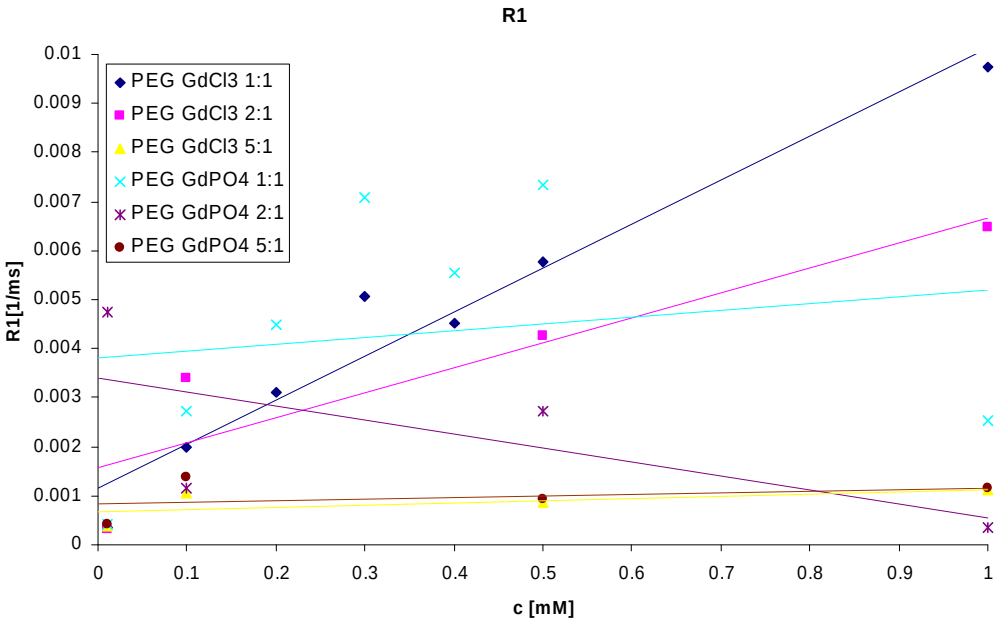

Figure 41: The relaxivities of PEG/Gd^{3+} differ only insignificantly from free Gd^{3+}. PEG/$GdPO_4$ mixtures are not in a linear relation to each other due to precipitation.

When PEG is mixed with a metal ion, there are no negative charges to interact electrostatically, therefore no macromolecular aggregates form with the ion and the mobility is not restricted. This leads to no increase in relaxivity compared to free gadolinium ions.

The change of relaxivity was also measured with mixtures of heparin and Gd/$GdPO_4$ and compared to the results with the heparin-PEG copolymer (Figure 42). The r_2 were extremely high for mixtures of heparin and gadolinium ions, up to 140/mM*s (for clarity, the scale is only shown up to 100/mM*s). The negative charges on heparin lead probably to the formation of a loose network, limiting the mobility of gadolinium ions to a very high extent (cf. Figure 37 b). That is the reason why the relaxivity increased so much when the gadolinium ion is mixed with heparin. But since the network is not stabilized by surrounding PEG blocks, the addition of phosphate leads to the formation of big gadolinium phosphate aggregates. Their growth is not limited by the formation of polymer-gadolinium compartments, therefore the salt precipitates. The relaxivity drops dramatically.

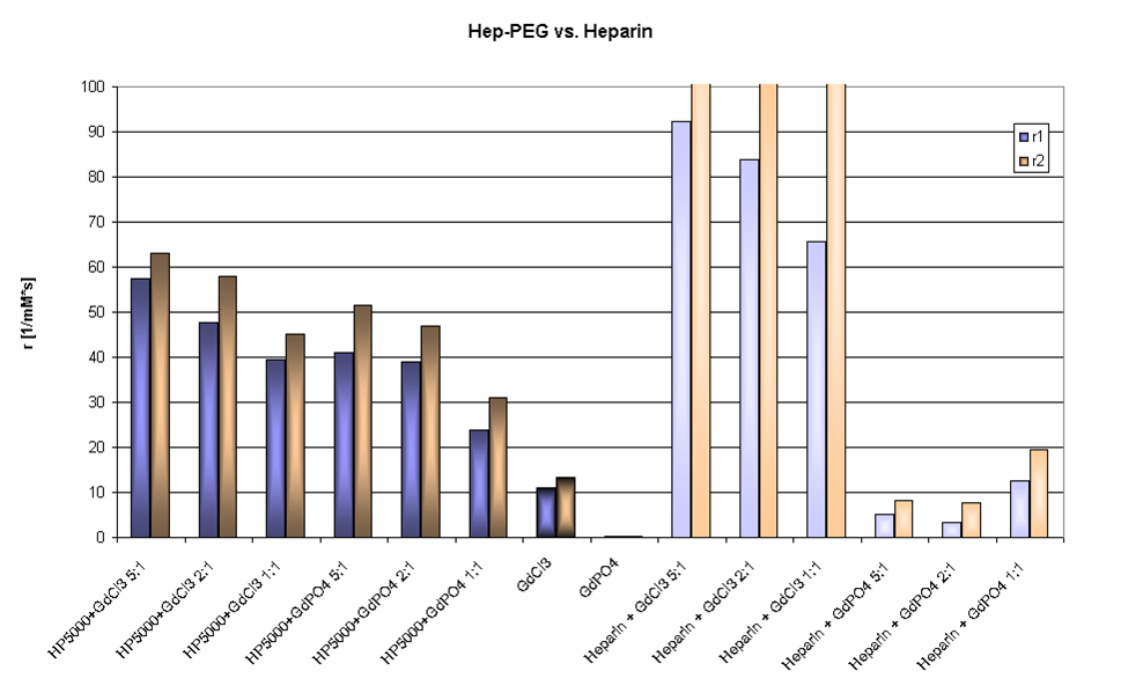

Figure 42: Relaxivities r_1 and r_2 of heparin-PEG and $Gd^{3+}/GdPO_4$ at different ratios compared to heparin.

These results showed that we produced a system with an excellent relaxivity compared to commercially available CA's. This enhances the signal-to-noise ratio, allowing enhancement of the spatial resolution and gives the opportunity to decrease the concentration of gadolinium and thus make the system less harmful for human use. The toxicity can be further lowered by the addition of phosphate, because it forms an insoluble salt with gadolinium.
The control measurements with heparin and PEG supported the assumption that a copolymer with one negatively charged block and a neutral block are necessary to form a stabilizing aggregate and keep the salt in solution. We also confirmed by the measurements with pure heparin that the interaction of gadolinium and oxygen takes place with the negatively charged oxygen atoms on heparin and PEG does not or negligibly interact with the metal ions.

Gadolinium phosphate nanoparticles were also prepared by formation of phosphate-polymer superstructures and then mixing with gadolinium. Obviously, we needed a polycation to interact with the negatively charged phosphate. We chose poly-L-lysine (MW: 20'000-30'000 Da) grafted with PEG (MW: 5000 Da)

blocks. Ca. 60% of the amino groups of poly-L-lysine are occupied by PEG (Figure 43).

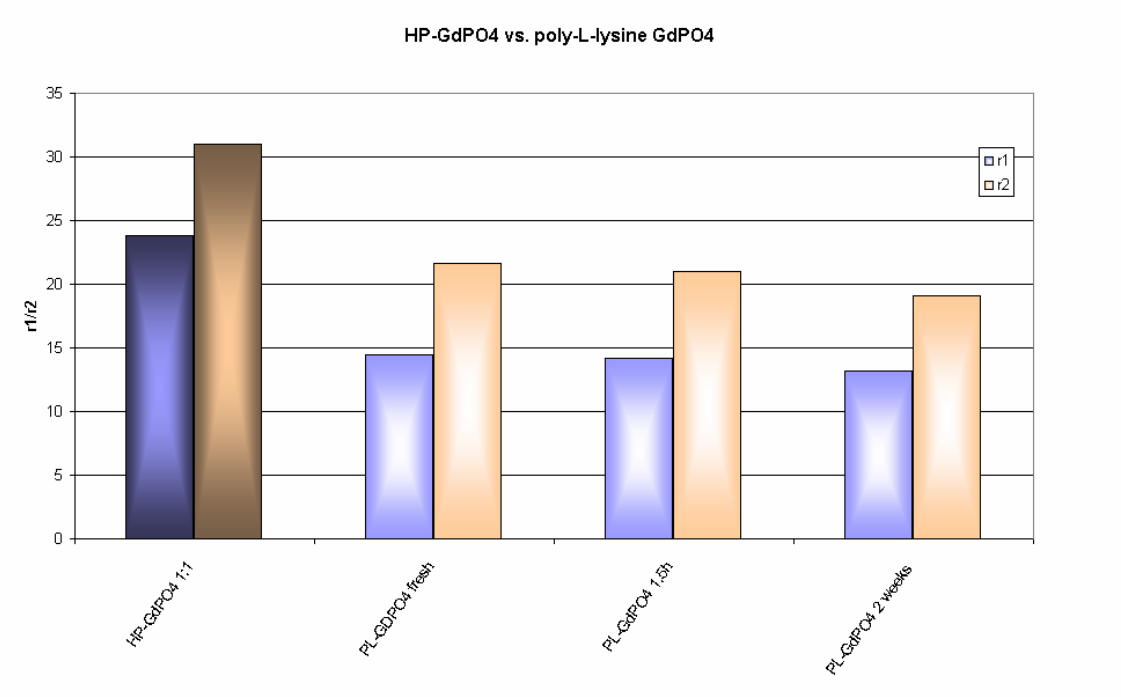

Figure 43: $GdPO_4$ aggregates stabilized by poly-L-lysine compared to $GdPO_4$ in heparin-PEG. The relaxivities remain stable for 2 weeks.

Stable particles did form, although the relaxivities are lower than with the heparin-PEG copolymer.

Those polymer-$GdPO_4$ aggregates, produced by either method, remain stable in solution for up to 2 weeks without phase separation.

Thorough stability studies were performed with different concentrations / ratios of polymer-gadolinium. Each sample was measured immediately after preparation, then again after 1.5h and again after 2 weeks. Some of the samples showed an immediate phase separation, visible by eye; some of them only after some time.

In Table 3, we compared the stabilities of all samples and concentrations depending on how much time passed between preparation and measurement.

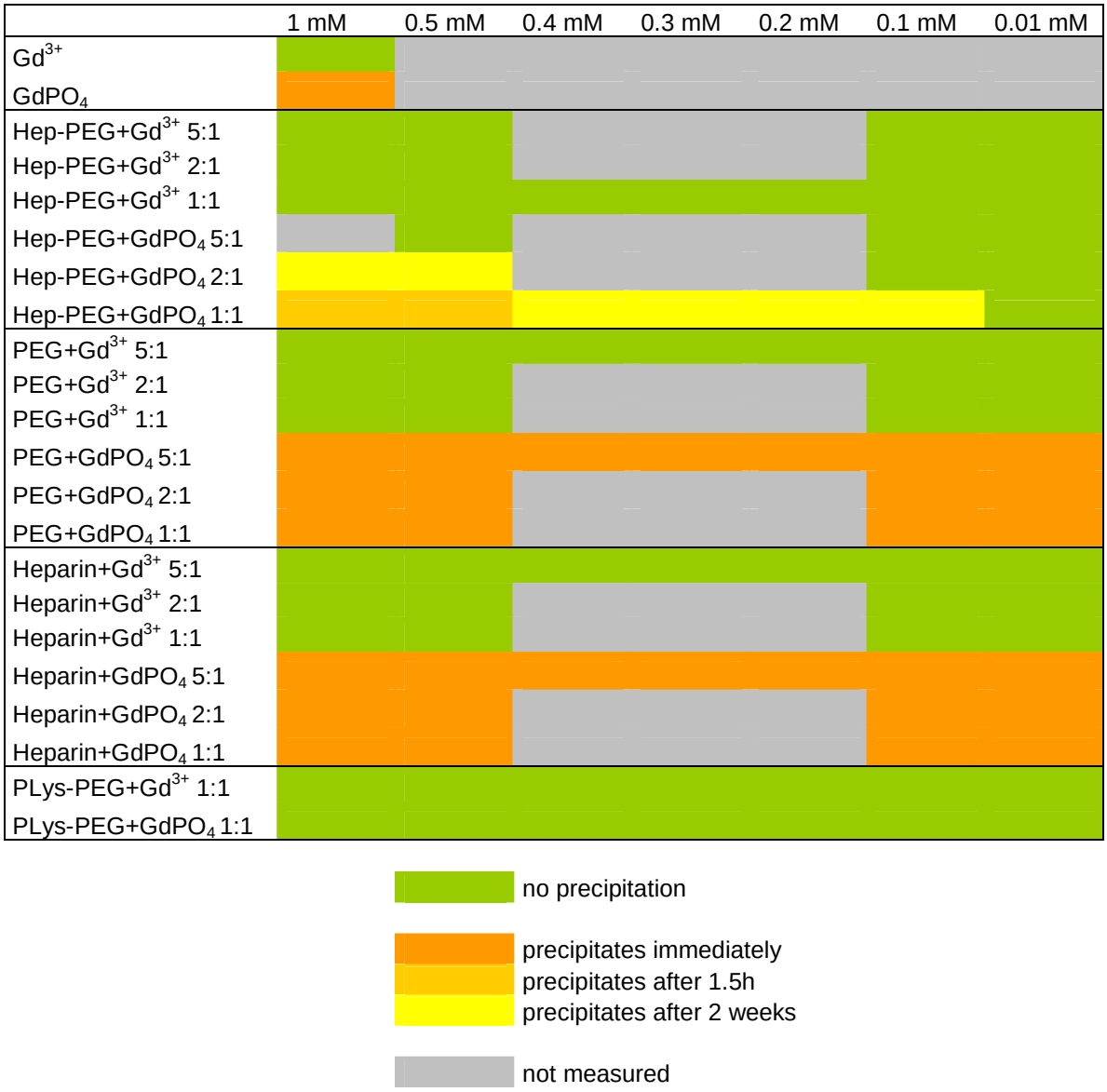

Table 3: Stability studies on all measured polymers with gadolinium ions and gadolinium phosphate. All samples were measured three times: freshly prepared, after 1.5 h and after 2 weeks.

The samples with copolymer – heparin-PEG and PEGpoly(lysine) – remained in solution (green) even after addition of phosphate, however, the stability is not given at higher concentrations. Furthermore the ratio between copolymer and salt seems to play a role for solubility.

Pure PEG and pure heparin are not able to keep the salt in solution. All samples precipitated immediately after preparation.

3.4 Glycopeptide

Another class investigated in this thesis was a combination of a short helical peptide with a sugar moiety. The initial idea was to combine heparin with a truncated derivative of gramicidin A, the peptide W-(DL-W)$_3$ *(TRUNK).* The β-sheet like folding motif combined with the presence of a D-amino acid (D-leucin) results in the channel structure as illustrated in Figure 44.

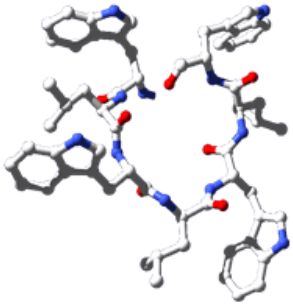

Figure 44: *TRUNK*, view along the helical axis of the peptide. The channel has an inner diameter of ca. 6.6 Å.[55]

At the same time we wanted to find simple and reproducible reaction conditions to couple a sugar to a peptide.
As heparin turned out to be difficult to handle and would have been too long a hydrophilic block for the peptide, we decided to take the two main building blocks of GAGs, the monosaccharides D-glucuronic acid and D-glucosamine (Figure 45) as carbohydrate coupling models.

a) b)

Figure 45: a) D-glucuronic acid and b) D-glucosamine

The peptide was chosen because of its known self-assembling properties as shown by Dittrich et al.[59] with oligo-lysine as a hydrophilic block. We were interested, how the self-assembly changes if the hydrophilic block is an

uncharged saccharide and wanted to find new ways to couple sugars to a peptide.

3.4.1 Coupling D-glucuronic acid (GluAc) to the *TRUNK*

TRUNK-GluAc was synthesized by Fmoc SPPS on Rink Amide AM resin in DMF using HCTU as a coupling agent and DIPEA as a base (Figure 46). GluAc was dissolved in formamide and coupled the same way. Cleavage from the resin and removal of the protecting groups was carried out with 95% TFA, Triethylsilane (TES) as scavenger and H_2O. The residual crude product was dried over night in a desiccator.

.

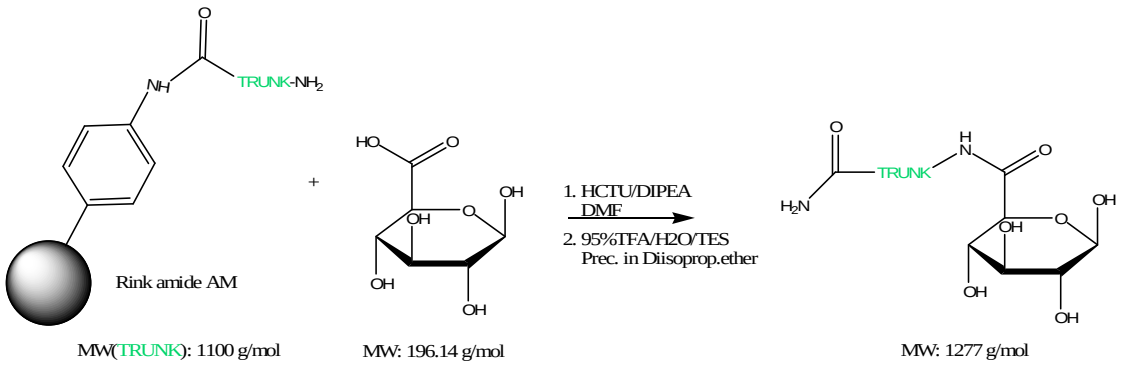

Figure 46: Scheme of the SPPS coupling reaction of the sugar to W-(DL-W)$_3$ (*TRUNK*)

The glycopeptide was purified and analyzed by HPLC on reverse phase columns (Figure 47), collected and then identified by MALDI-TOF (Figure 48).

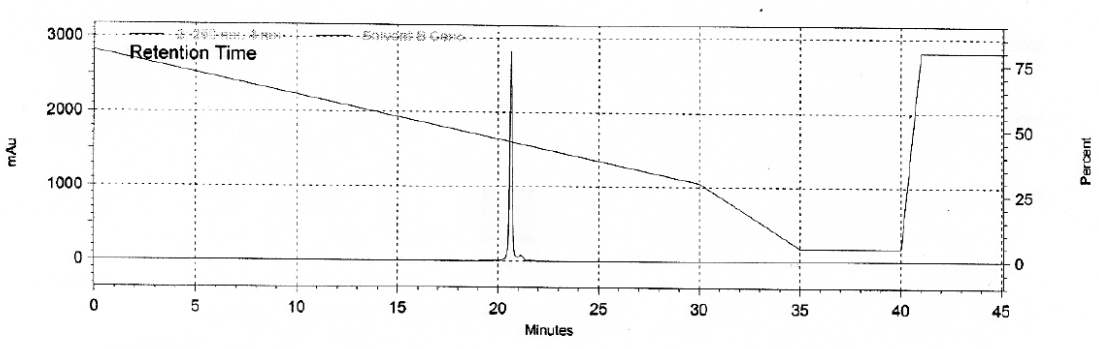

Figure 47: Analytic HPLC run with the 96% pure product peak

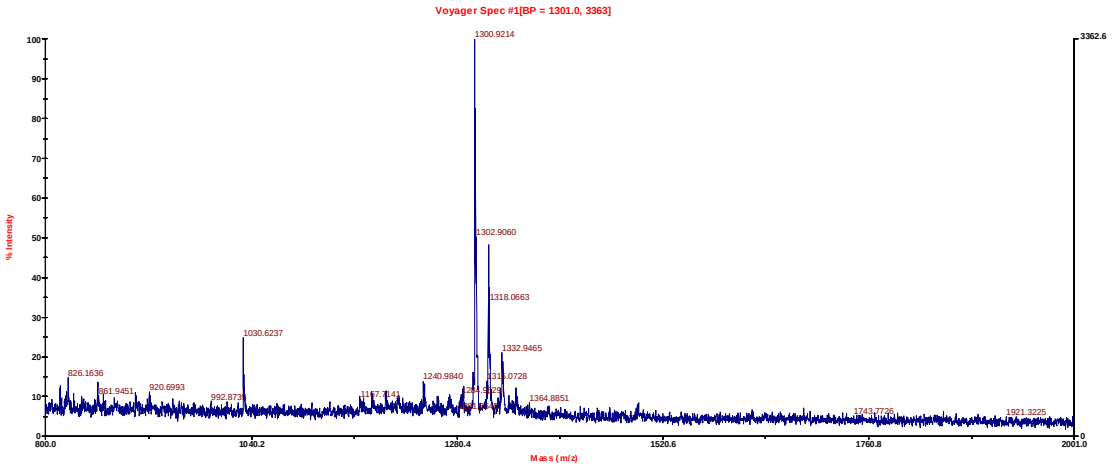

Figure 48: MALDI-TOF diagram of *TRUNK*-GluAc after purification. 1300 Da correspond to the sodium salt of the molecule ion

The analytical HPLC diagram shows, that we obtained the product in a purity of 95%. The correct product mass was detected by MALDI-TOF. The *TRUNK* has a molar mass of 1079.26 g/mol and the d-glucuronic acid 194.14 g/mol. With sodium as counter ion the molar mass corresponds to 1296.26 g/mol. Protonation of the tryptophane amino acids adds up to 1300.26 g/mol, which is what we measured by MALDI-TOF.

Membrane self-assembly

Glucuronic acid was chosen as the hydrophilic part because of the possibility to couple the acid functional group to the peptide by the same synthetic pathway as the peptide itself on solid phase. This simple and effective synthesis strategy leads to high yields. Moreover, the uncharged head group avoids unfavourable electrostatic repulsion when superstructures form.
However, dialysis of an ethanolic solution of the glycopeptide against pure water led to formation of particles, which aggregate and finally precipitate. DLS measurements still revealed a hydrodynamic radius around 250 nm and polydispersities around 1, but lacking a concentration specification, the fits could not be reliably accomplished.
LSM images were taken by excitation of the tryptophane at λ = 280 nm. The uniformly round particles could be very clearly seen by eye, but due to Brownian motion, no sharp picture could be taken (Figure 49).

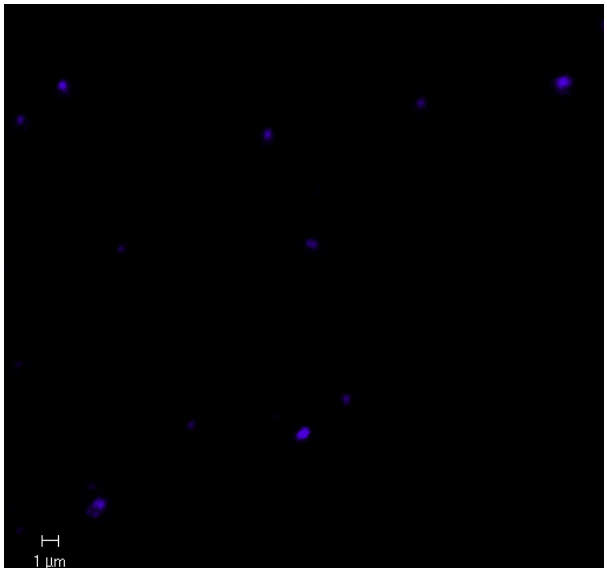

Figure 49: LSM image of a glycopeptide solution prepared by dialysis against pure water

In order to avoid the precipitation of the particles we used 10% EtOH in water as the solvent. Nevertheless, after a few days we observed a slight sedimentation. From DLS measurements, a hydrodynamic radius of 176 nm was calculated.
The particles were observed by LSM, their size corresponded to the size measured by DLS, but similar to the samples in water, no sharp images could be acquired (Figure 50).

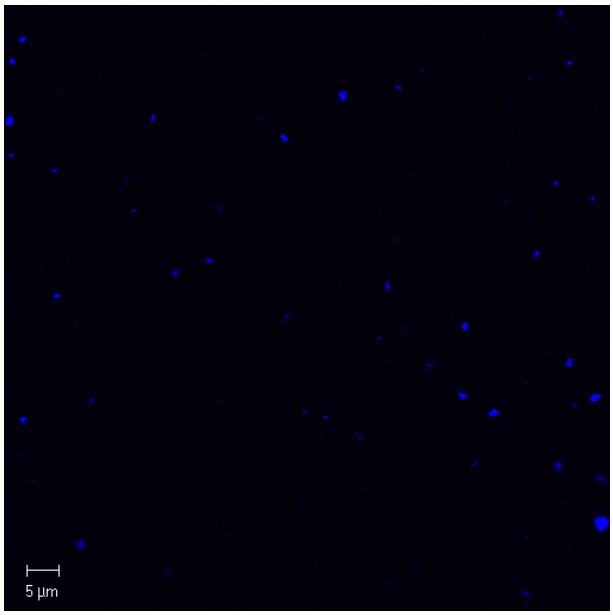

Figure 50: LSM image of a glycopeptide solution in 10% EtOH

To further investigate a suitable solvent for the particles, where sedimentation doesn't take place, we dialyzed against 20% EtOH. The solution remained opalescent with no sedimentation even after one week. The particles have a radius of 137 nm according to DLS. LSM imaging (Figure 51) supports those results, although the concentration of the particles seemed to be lower than with pure water or 10% EtOH as solvent. This could be explained by the fact, that more molecules stay in solution as the ethanol concentration is increased.

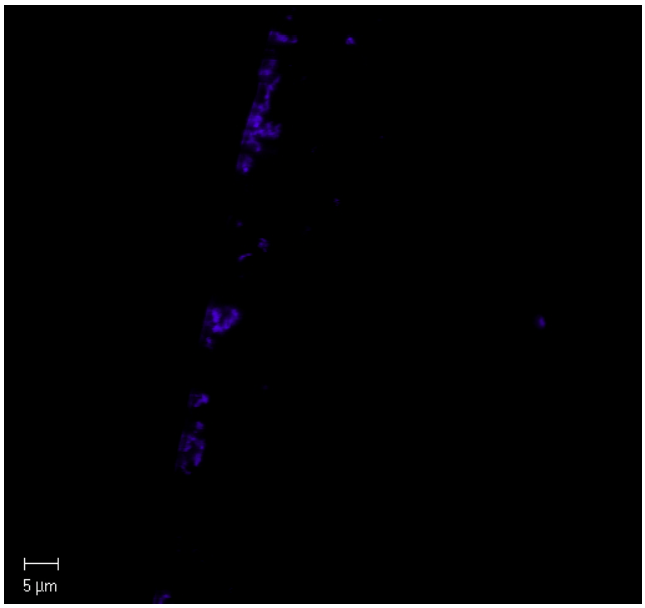

Figure 51: LSM image of a glycopeptide solution in 20% EtOH

Since the LSM images in all solutions remained diffuse and the resolution was not high enough to see details, we did TEM imaging.
The solutions in pure water (Figure 52) revealed aggregates in the size range that was measured by DLS. It was surprising that in the edges of the particles were not smooth. A reason could be that in pure water crystallization is initiated that influences the shape. Contrariwise, this could also be a drying effect.

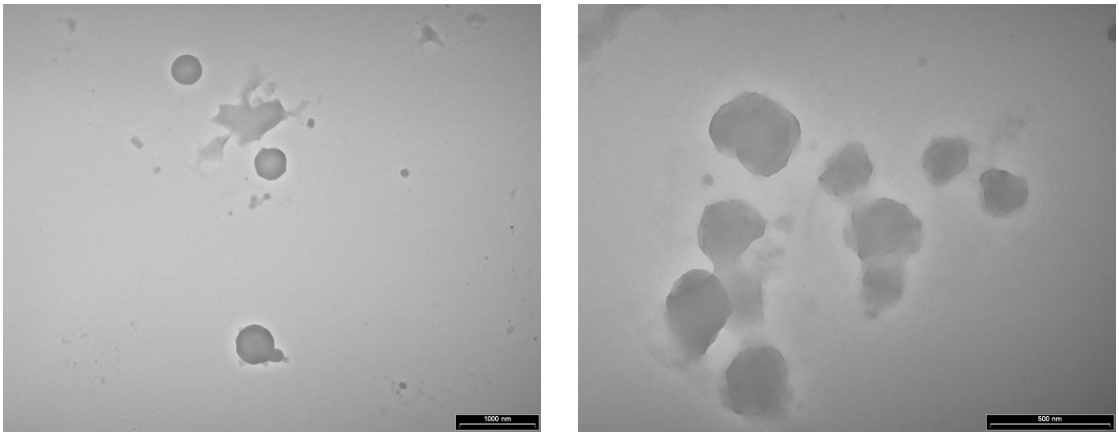

Figure 52: TEM images of a glycopeptide solution prepared by dialysis against pure water

In a solution of 10% EtOH (Figure 53), the particles are spherical and after some time they aggregate. In the TEM image, they seem to aggregate and form a network. A polymer film that contracts upon drying could explain this phenomenon. The size of the particles corresponds to the size that was measured by DLS.

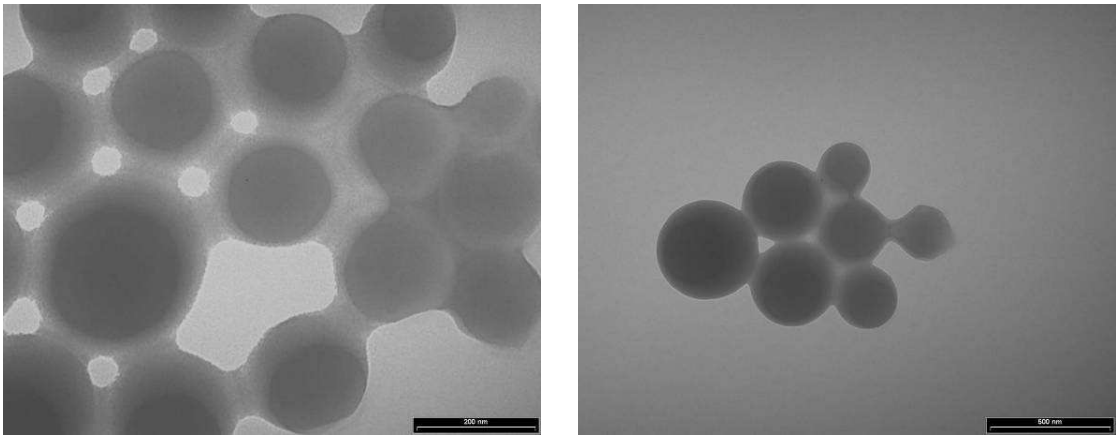

Figure 53: TEM images of a glycopeptide solution in 10% EtOH

In the TEM pictures from a solution of 20% ethanol, the shapes become blurry and aggregate (Figure 54). It can be speculated, that the high amount of ethanol leads to the formation of loose particles that aggregate in an undefined shape upon drying.

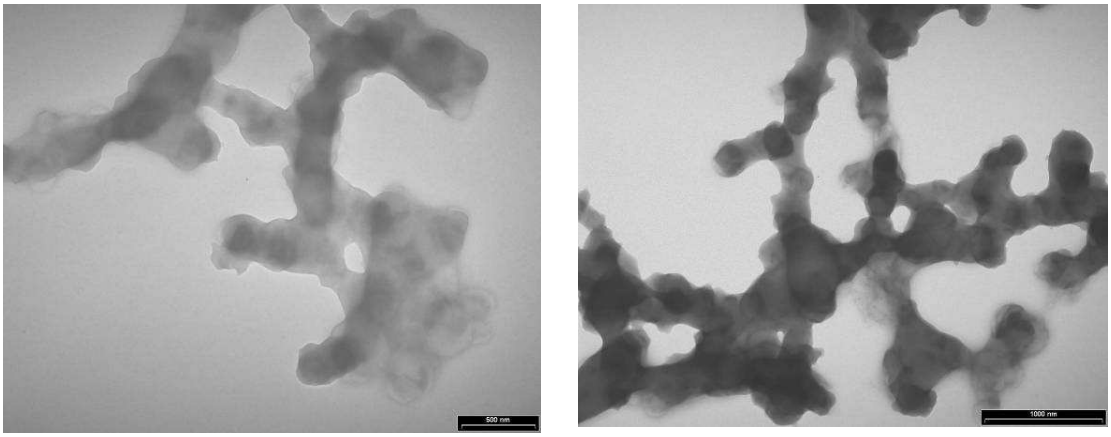

Figure 54: TEM images of a glycopeptide solution in 20% EtOH

We also attempted atomic force microscopy (AFM, Figure 55) and cryo-TEM (Figure 56) with the solution in 10% EtOH to get further insights into the nature of the superstructures.

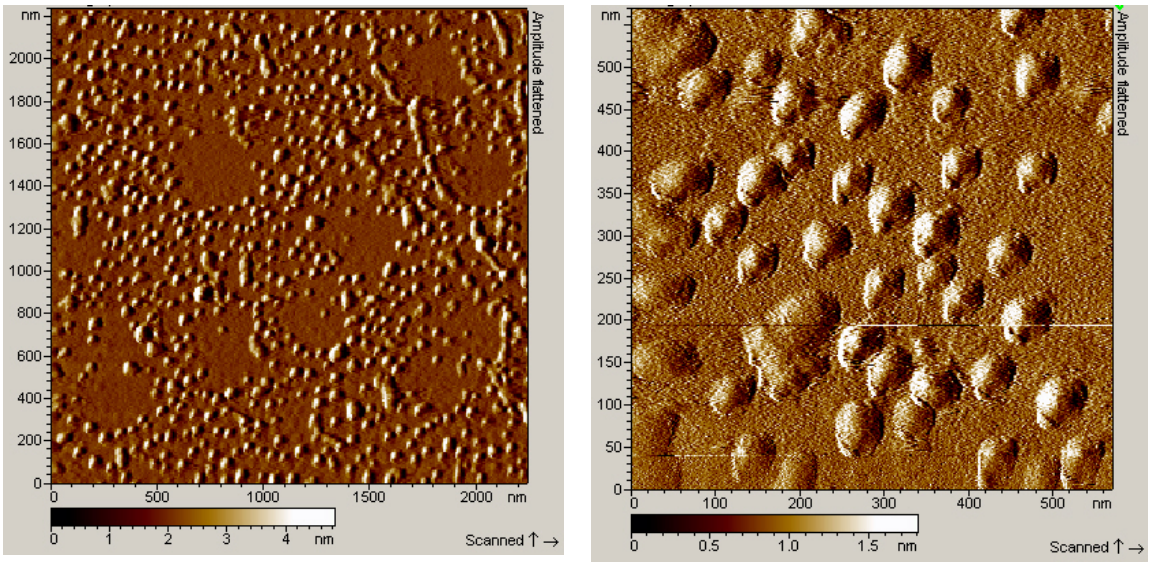

Figure 55: AFM images of a glycopeptide solution prepared in 10% EtOH

We found small spheres on a graphite surface by AFM, which did not correspond to the size of the aggregates we measured before by DLS and TEM. They were considerably smaller. We conjectured that a mono- or multilayer of glycopeptide formed on the surface by hydrophobic interaction of the peptide with the graphite surface. The particles are then assumed to be packed in the layer.

The particle radius could be calculated with the height and the diameter of the segment of those spheres. The radius (r) of a sphere can be calculated from the segment's height (h) and its diameter (a):

$$r = (a^2 + 4h^2) / 8h$$

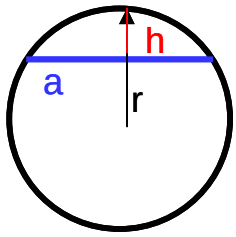

The diameters (a) of the segments range between 50 nm and 60 nm, their heights between 1.8 and 2.5 nm. Taking two mean values: 55 nm for the diameter and 2.2 nm for the height, we obtain a particle radius of 173 nm, which corresponds well with the data measured by DLS (R_h = 176 nm).Cryo-TEM images showed structures which could be interpreted as the particles (Figure 56). The network that we saw in the TEM images was also observed in the cryo-TEM images; however the sizes are slightly smaller. Furthermore, the differentiation from water-crystals is not ensured, therefore the interpretations have to be handled with care. The large feature in the background is the supporting carbon film.

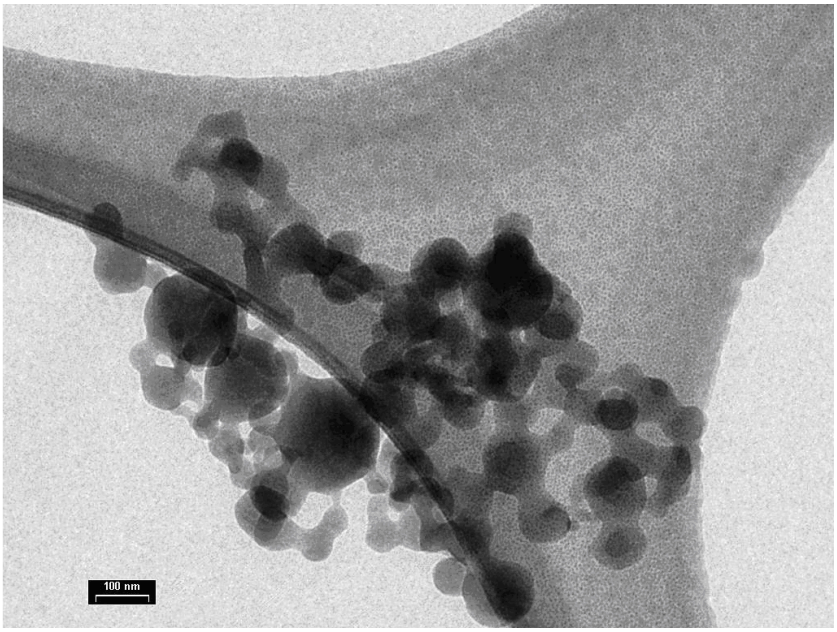

Figure 56: Cryo-TEM image of a glycopeptide solution prepared by dialysis against 10% EtOH.

In summary, we developed a simple and effective glycopeptide synthesis method by coupling D-glucuronic acid to the N-terminus of the *TRUNK* on solid phase. The glycopeptide self-assembles when dialyzed against pure water and solutions of 10% EtOH and 20% EtOH. In pure water, the particles form, but most of them immediately aggregate and precipitate. By increasing the amount of EtOH in the solvent, the aggregation can be prevented. However, since the glycopeptide is soluble in EtOH, there is a limitation of the ethanol ratio. The nature of the superstructures could not be definitely determined, but there are indications that we did not obtain vesicular structures. The particles could be of compound micellar structure or particles formed by glycopeptide multilayers.

3.4.2 Coupling D-glucosamine to the *TRUNK* (W-(DL-W)$_3$) via carboxylate

The first attempt to couple the monosaccharide D-glucosamine to the *TRUNK* was done in solution by synthesizing the peptide by Fmoc solid-phase synthesis (SPPS) on 2-chloro trityl chloride, which results in a carboxylate functionality at the C-terminus upon cleavage. The SPPS was carried out in DMF, with HCTU and coupling agent and DIPEA as base.
After cleavage from the resin with 0.5%TFA in DCM and evaporation of the solvent, the peptide was dissolved in DMF and D-glucosamine in formamide was added. Addition of HCTU and DIPEA was supposed to result in the formation of an amide bond between the amino functionality of the sugar and the carboxylate of the peptide. The product was characterized by MALDI-TOF (Figure 57) and analytical HPLC.

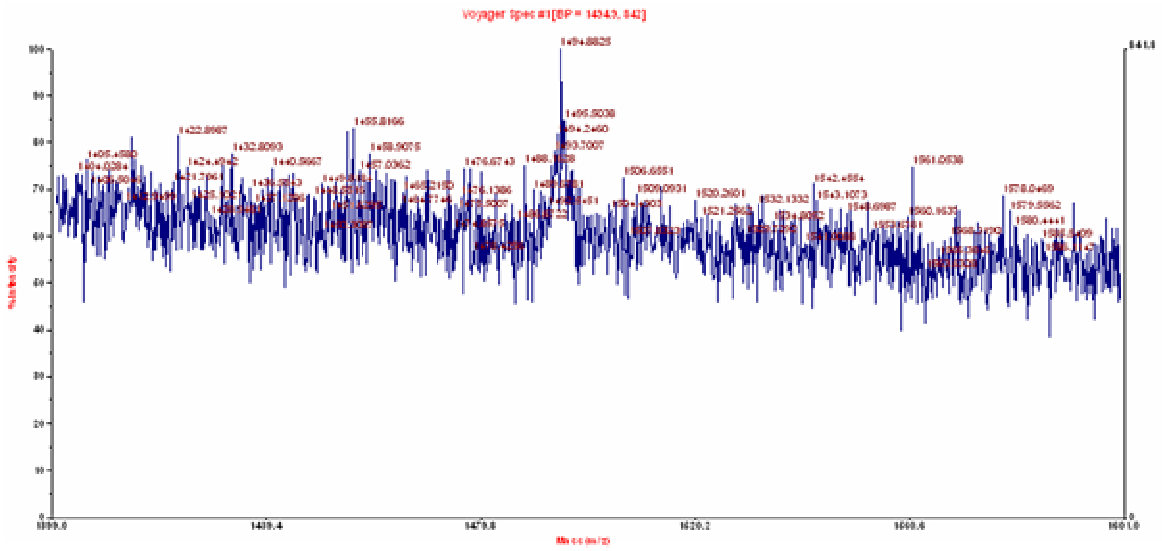

Figure 57: The product with a molar mass of 1495 Da could be identified by MALDI-TOF-MS.

The product with a molar mass of 1495 could be detected by MALDI-TOF-MS, but the amount was too low to be detected in HPLC. Therefore we tried another synthesis strategy to couple D-glucosamine.

3.4.3 Coupling D-glucosamine to the *TRUNK* via reductive amination

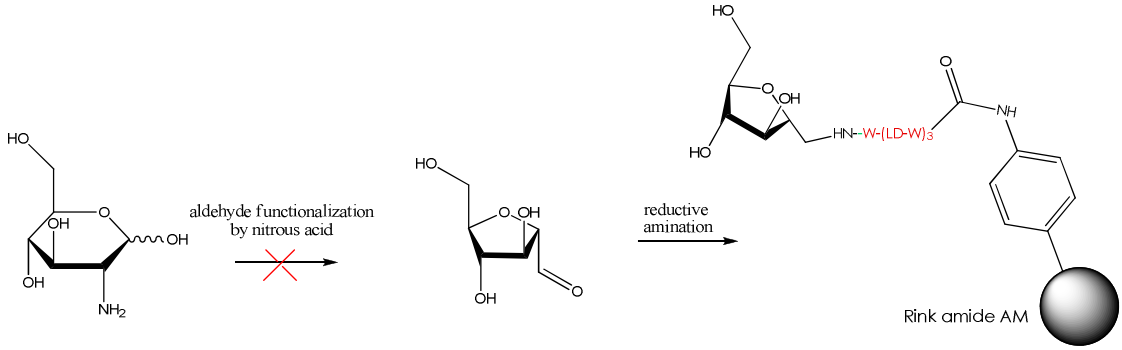

Figure 58: Formation of an aldehyde end-function on D-glucosamine with nitrous acid.

As a first step, D-glucosamine was supposed to be functionalized to result in an aldehyde, which then could be coupled to carboxylate via reductive amination (Figure 58).
The reaction of D-glucosamine with nitrous acid seemed to work, because we could observe the formation of nitrogen bubbles. But after drying the product, we

found a brown-black residue, which according to IR did not contain aldehyde functions.
We assumed that the low pH, which dropped further by evaporation of the water could result in a side reaction, hence we raised the pH back to 7 before removal of the water. The yellow residue turned out not to be an aldehyde again.
An explanation for the failure of this approach is probably that the aldehyde attacks the amine group of unreacted D-glucosamine nucleophylically. In this process a Schiff's base forms, resulting in a "disaccharide".
To avoid this reaction, we used an acetylated D-glucosamine to protect the amino groups.
In heparin, most of the glucosamine moieties are also acetylated; therefore we assumed that the aldehyde formation should still be possible. The reaction with N-acetly-D-glucosamine () was carried out in the same way as the one with D-glucosamine, but no bubbles formed. IR spectroscopy revealed that no reaction took place.

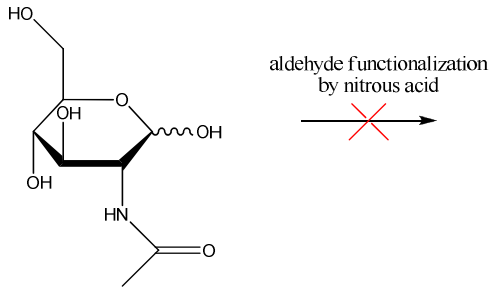

Figure 59: N-acetyl-D-glucosamine did not react to the aldehyde.

Since we did not manage to produce a stable aldehyde-functionalized D-glucosamine, we tried the reductive amination with pure D-glucosamine. As sugars in solution are in equilibrium of the α- and β- anomeric forms and the transition is an open conformation with an aldehyde functionality, we hoped, that this would be enough to react with the N-terminus of the *TRUNK.*
The *TRUNK* was synthesized by Fmoc SPPS on Rink Amide AM resin.
After the last coupling step, the N-terminal tryptophane was deprotected and a solution of D-glucosamine in water was added with a small amount of sodium cyanoborohydride. After cleavage from the resin and purification, the residue was analyzed by MALDI-TOF-MS and analytical HPLC. No product could be detected.

4 CONCLUSIONS

Heparin was coupled to hydrophobic and hydrophilic blocks by different synthesis approaches. Because of the strongly polar character of heparin, it is only soluble in very polar solvents such as water and formamide. This restricts the choice of hydrophobic blocks and the analysis methods.
Coupling of heparin to PDMS could be achieved, but the purification and quantification still remain improvable. DCC/DMAP coupling turned out to be a simple one-pot-reaction with retention of heparin's anticoagulant activity, as was proven by antifactor Xa activity test in citrate plasma. Binding to ATIII was observed and stoichiometry suggests a heparin/PDMS ratio close to 1:1.
The insertion of this glycopolymer into the membrane of polymeric vesicles formed by PEG-PPS was successfully achieved. Fluorescently labelled protamine salmine A1, a small, positively charged peptide with a high binding affinity to heparin was used to visualize the interaction with heparin-coated vesicles by confocal microscopy. FCS/FCCS measurements confirmed the interactions of heparin within the superstructures.

Coupling of heparin to the hydrophilic PEG block was achieved by nitrous acid degradation, where a major part of the bioactive pentasaccharide moiety gets segmented and heparin looses most of its anticoagulant activity. The activity loss could be measured by antifactor Xa activity test.
Nevertheless, the bis-hydrophilic compound was investigated in terms of its self-assembly behavior and interaction of the negatively charged heparin functional groups with the positively charged Gd^{3+} ion. TEM images showed that the copolymer forms highly dynamic superstructures, which after interaction with gadolinium ions, seem to become more organized. The copolymer influences the shape of $GdPO_4$ particles, resulting in spherical aggregates, as could be observed by SEM imaging.
EPR measurements showed that gadolinium was stably bound to oxygen atoms of the polymer, suggesting that aggregates with heparin and gadolinium in the core and PEG exposed to the surface had been formed.
We made a new type of MRI contrast agent based on block-copolymer stabilized Gd^{3+} or $GdPO_4$ particles. In vitro MRI measurements showed that the polymer-gadolinium aggregates enhance the proton relaxivity to a very high extent. The relaxivities are much higher than for commercially available CA's, therefore the

amount of gadolinium can be decreased, making the system less harmful for human use. Heparin's activity loss upon degradation further enhances the potential of those aggregates as CA because blood coagulation activity would be an undesirable side effect for the use as a CA.
Addition of phosphate leads to small salt aggregates which remain dispersed due to the stabilization by the heparin-PEG polymer and further lower the toxicity of gadolinium ions. Control experiments with heparin and PEG support the assumption that the copolymer with one charged block and a neutral block are necessary to stabilize the salt particles in solution.

Saccharides were also studied as building blocks for glycopeptides.
Two new methods were investigated to couple D-glucosamine to the *TRUNK* (W-(DL-W)$_3$). The first one involved coupling in solution by obtaining a carboxylic acid function on the *TRUNK* after cleavage from chlortrityl chloride. Then, D-glucosamine was coupled with HCTU. The resulting product was detectable but not sufficient to be purified.
As a second trial we attempted to functionalize the sugar to obtain an aldehyde end-functionality and then couple it via reductive amination to the N-terminus of the *TRUNK*, but the aldehyde functionalized sugar reacted with the educt to form a Schiff's base resulting in a disaccharide. We tried to avoid this side-reaction with an acetylate-protected D-glucosamine. This attempt resulted in no product. Therefore we did the reaction with non-functionalized D-glucosamine, but no coupling took place.

As the second monosaccharide, we chose glucuronic acid (GluAc), to be coupled to the *TRUNK*. The amphiphilic glycopeptide (W-DL)$_3$-W-GluAc was synthesized and purified. The coupling was accomplished by the formation of an amide bond between the carboxylic acid group of D-glucuronic acid and the N-terminus of the peptide on solid phase with HCTU as coupling agent and DIPEA as the base.
The glycopeptide was investigated in terms of its self-assembly behavior and was found to form spherical structures after dialysis from EtOH. The superstructures aggregated and precipitated in pure water. Ethanol-in-water solutions of 10% and 20% as solvents prevented precipitation. TEM, cryo-TEM and LSM images supported the formation of spherical aggregates; their sizes were confirmed by DLS.

In summary, we combined saccharides with synthetic and peptidic blocks to produce new materials. We explored new synthesis and characterization routes, studied the self-assembly and investigated potential applications of those substances.

5 OUTLOOK

Even though the synthesis of heparin-based block copolymers was successfully achieved, the characterization and especially the purification turned out to be difficult and can be further improved. The variation of the hydrophobic block in the case of the amphiphiles can simplify those factors. For example, if a hydrophobic block is chosen, which is soluble in a co-solvent (mixture) with the hydrophilic block, a wider range of applicable purification and characterization methods would be accessible.
Instead of heparin, a wide range of other polysaccharides can be introduced as hydrophilic blocks and investigated in terms of their properties, especially in terms of bioactivity.

For the MRI measurements, different polyelectrolytes coupled to PEG can be investigated to stabilize gadolinium. It will also be investigated if the gadolinium phosphate aggregates are crystalline or amorphous to understand what the nature of the aggregates is. In the perspective of applicability for medical imaging, in vitro and in vivo toxicity experiments, adsorption and elimination studies followed by clinical research assays are essential.

After prosperous development of a new glycopeptide synthesis and its characterization, further elucidation of their aggregation behavior is key information in terms of their applicability as e.g. vaccine. The folding motif and di- or multimerization in water of glycopeptides and peptides based on gramicidin and its derivatives is the topic of ongoing investigations. This information would deliver conclusions about the still inexplicit superstructure formation behavior.
Further on, a variation of the coupled sugar and its length would lead to new materials with interesting self-assembly properties.

6. METHODS

6.1 Syntheses

6.1.1 Heparin coupled to PDMS by degradation and reductive amination

200 mg Heparin (MW: 5000Da, 40 μmol) was dissolved in 60 mL H_2O in a 100 mL round flask at RT, followed by addition of 2 mg $NaNO_3$. The pH was adjusted to 2.7 using 1M HCl and the solution was stirred for 24h at RT.
Then NaOH was added until pH 7 was reached.
Upon ultrafiltration (cut-off 1000 Da), followed by lyophilization on a Heto Maxi Dry Lyo, heparin-aldehyde was obtained.
40 mg (8 μmol) heparin-aldehyde was dissolved in 25 ml 0.15M NaCl solution.
20 mg (4 μmol) PDMS-$(C_3H_6\text{-}NH_2)_2$ (MW=5000Da) was dissolved in 25 mL EtOH. After mixing the two solutions, pH was adjusted to 3.5
20 mg (0.32 μmol) of cyanoborohydride was added and the solution was stirred at 50℃. After 24h, the solution was ultrafiltrated (cut-off 10'000 Da). Lyophilization led to 37 mg heparin-PDMS (2.5 μmol).

6.1.2 Heparin coupled to PDMS by iodine method

200 mg heparin (40 μmol) was dissolved in 1mL H_2O and passed through a Dowex 50X8 (H^+) column. After lyophilization, 200 mg I_2, dissolved in 100 mL 20% MeOH was added.
The reaction mixture was stirred over night at room temperature.
The solution was filtered through a paper filter to get rid of undissolved iodine and lyophilized for 5h to reduce the volume.
Then the solution was poured into 200 mL 20% EtOH containing 8g (4% (w/v)) KOH and the solution was subjected to ultrafiltration (cut-off 3000 Da). Upon freeze-drying of the ultrafiltered solution, oxidized heparin was obtained. The product was dissolved in 2 mL water and passed through a Dowex 50X8 (H^+) column. Upon freeze-drying the eluate, lactone-heparin was obtained.
100 mg lactone-heparin was dissolved in 5 mL DMF.

50 mg NH_2-PDMS-NH_2 was dissolved in $CHCl_3$ and added to the lactone-heparin solution. 0.1 mL tri-*n*-butyl amine was added to the reaction mixture and stirred for 8h at 80℃.
The reaction mixture was dried and washed with hexane. The residue thus obtained was dissolved in water and passed through a Dowex 50X8 (H^+) column. The eluate upon ultrafiltration (cut-off 10'000 Da) and lyophilization resulted in the heparin-PDMS-heparin (4.9 mg (0.33 μmol)).
Characterization: NMR spectroscopy in a 1:1 mixture of D_2O and acetone-C_6 suggested the coexistence of PDMS and a residue of the sugar. It could not be evaluated if the product still contained heparin, its decomposition product or other impurities.

6.1.3 Synthesis of heparin-PDMS by DCC/DMAP method

Heparin-PDMS was synthesized using dicyclohexyl carbodiimide (DCC) as coupling agent and 4-dimethylaminopyridine (DMAP) as a base. The amine group of diaminopropyl functionalized poly(dimethyl siloxane) (PDMS-(C_3H_6-NH_2)$_2$) forms a peptide bond to the carboxylic acid moieties of iduronic acid moieties of heparin. 0.5 g heparin were dissolved in 50 mL formamide and 0.25 g PDMS-(C3H6-NH2)2 (0.5 eq), were dissolved in 50 mL DMF. DCC (1 eq) and DMAP (1 eq) were added to the heparin solution followed by stirring for 10 min and addition of the PDMS-(C_3H_6-NH_2)$_2$ solution. The reaction mixture was stirred at 50℃ for 12h under nitrogen atmosphere. To remov e unreacted heparin, the solution was diluted with water and set to ultrafiltration, cutoff 10'000 Da. After ultrafiltration, the product was washed with cyclohexane and dried in vacuo.

6.1.4 Fluorescence labeling of protamine

To bind the succinimidyl ester group of OG488 to an amine group of protamine the following reaction was used according to the coupling reaction described by Invitrogen, *Amine reactive probes*, 2005. 5.2 mg of protamine (1eq) was dissolved in 0.5 mL of a 0.1M sodium bicarbonate buffer (pH 8.4). 0.5 mg OG488 (0.83 eq) dissolved in 50 μL DMF were added while stirring. After vortexing, the reaction was incubated for 4 hours at room temperature under continuous stirring. The product was purified by HPLC chromatography, using a LiChrosopher 100, RP-18e (5μm), 250-4.6 column. The product was

characterized by MALDI-TOF (PerSeptive Biosystems Voyager-DE Pro, Biospectrometry).

6.1.5 Hydrogenation of PB-NH_2 to PEE-NH_2

Amino end functionalized poly(butadiene) PB-NH_2 (MW: 2000 Da) was synthesized and kindly donated by the group of Prof. Axel Müller (Universität Bayreuth) [81].
4.2 g of PB-NH_2 were dissolved in 100 mL cyclohexane. 0.5 g Pd catalyst on carbonate were prepared in a glass vial and activated under H_2-atmosphere in the autoclave at 100 bar, 70°C for 4h. After cooling down to RT, the pressure chamber was opened and the PB-NH_2 solution added to the catalyst. The reaction mixture was set under H_2 atmosphere at 100 bar 100°C for 12h. Then, the reaction mixture was filtered through Millipore syringe filters, cutoff 0.45µm and dried in vacuo.
Yield: 1 g PEE-NH_2

6.1.6 Coupling heparin to PEE

46 mg heparin was dissolved in 10 mL H_2O. 100 mg PEE was dissolved in 20 mL THF. The two solutions were mixed and 10 mg $NaBH_3$ was added. The pH was adjusted to 3.5 with HCl and the reaction mixture was stirred under argon atmosphere at 50°C for 8h, then purified with preparative RP-HPLC.
Yield: ca. 5 mg heparin-PEE

6.1.7 Preparation of heparin-PEG with triazine method

125 mg Heparin (0.25mmol, ~1mmol carboxylic acid) was mixed with previously washed Dowex H^+ to obtain the acid. Then it was dissolved in 10 mL H_2O, followed by addition of acetonitrile. The mixture was stirred for 2 h. 110 µl (1mmol) 4-methylmorpholine was added, cooled to 0°C and stirred shortly.
90mg (0.5mmol) CDMT, resp. 45 mg (0.25mmol) CMDT was added and the reaction mixture was stirred for 1h at RT.
125 mg (1mmol) amino-PEG50000 was dissolved in 6 mL H_2O and added to the reaction mixture, followed by stirring for 20h at RT.

For purification, the product was ultrafiltrated (cut-off 10'000 Da), until no conductivity was measurable in the outflow.

6.1.8 Synthesis of heparin-PEG by degradation and reductive amination

Nitrous acid degradation

200 mg heparin (MW: 5000Da, 40 μmol) was dissolved in 60 mL H_2O in a 100 mL round flask at RT, followed by addition of 2 mg $NaNO_3$. The pH was adjusted to 2.7 using 1M HCl and the solution was stirred for 24h at RT.
Then NaOH was added until pH 7 was reached.
Upon ultrafiltration (cut-off 1000 Da), followed by lyophilization, heparin-aldehyde was obtained.

Coupling with PEG(5000)-NH_2 by reductive amination

20 mg (4 μmol) heparin-aldehyde was dissolved in 100 mL 0.15M NaCl solution.
100 mg (20 μmol) PEG-NH_2 (MW=5000Da) was dissolved in benzene and freeze-dried (3x), then added to the heparin-aldehyde. PH was adjusted to 3.5 using 1M HCl.
10 mg (0.16 μmol) of cyanoborohydride was added, and the solution was stirred for 48h at 50℃.
After cooling, the solution was ultrafiltrated (cut-off 5000 Da) with H_2O. Lyophilization led to 100 mg heparin-PEG (2.1 μmol).

6.1.9 Coupling D-glucosamine to the TRUNK via carboxylate

The *TRUNK* was synthesized by Fmoc SPPS on chlortrityl chloride resin. The synthesis was carried out with the same procedure as described in chapter 6.1.12, except the deprotection step of the resin could be omitted, because chlortrityl chloride is free of protecting groups. The *TRUNK* was cleaved from the resin with the addition of 0.5% TFA in DCM (5 mL) and shaking for 2 h.
After purification in ice-cold isopropyl ether, the reaction mixture was dissolved in DMF. 4 equivalents D-glucosamine were dissolved in formamide and added to the DMF solution together with HCTU (1 eq) and 0.5 mL DIPEA and shaken for

24 h. Then the reaction mixture was poured into ice cold isopropyl ether and dried. The residue was analyzed by MALDI-TOF-MS and analytical HPLC:
The product could be detected by MALDI-TOF-MS, but the amount was too low to be detectable by HPLC.

6.1.10 Preparation of D-glucosamine-aldehyde

1 g of D-glucosamine (4.64 mol) was solved in 50 mL water. Then 300 mg sodium nitrite was added. HCl was added drop wise, until the pH was set to 2.7. The formation of bubbles shows that nitrogen gas developed, which is an indication that the reaction started. The solution was gently stirred for 24 h.
After evaporation of water we found a brown-black residue, which could not be detected as aldehyde by IR.
As a second attempt, we raised the pH back to 7 before removal of the water. The yellow residue turned out not to be an aldehyde again.
To avoid the formation of a Schiff's base right after the formation of the aldehyde with amino-groups of still unreacted D-glucosamine molecules, we used an acetylated D-glucosamine to protect the amino groups. The reaction was carried out in the same way, but no bubbles formed. IR spectroscopy revealed that no reaction took place. For the coupling reaction we took plain D-glucosamine.

6.1.11 Coupling D-glucosamine-aldehyde to the TRUNK via reductive amination

After the last coupling step of the *TRUNK* synthesis by Fmoc SPPS on Rink Amide AM, the N-terminal tryptophane was deprotected with 20% piperidin, washed with DMF and isopropanol and dried.
4 equivalents of D-glucosamine in water were added to the resin with a small amount (tip of a spatula) of sodium cyanoborohydride. The reaction solution was shaken for 2 h and washed 3 times with water.
For the cleavage from the resin, a solution of 4.75 mL TFA, 0.125 mL H_2O and 0.125 mL TES were added to the Rink Amide and shaken for 2 h. Then the reaction mixture was poured into 40 mL of ice cold isopropyl ether and centrifuged. The residue was collected and analyzed by MALDI-TOF-MS and analytical HPLC.
No product could be detected.

6.1.12 Synthesis of TRUNK –GluAc by SPPS

The glycopeptide was synthesized with a batch synthesizer (Syro 1 MultiSynTech Workstation) on solid phase using Fmoc protection group synthesis. Rink Amide AM resin (loading 0.7mmol/g) was used as solid phase and all reactions were carried out in DMF as reaction solvent. The synthesis was performed in a 10 mL syringe filled with 200 mg resin. The Fmoc protected amino acids were dissolved in DMF (0.5 M) and glucuronic acid was dissolved in formamide (0.5M) prior to the synthesis. The reaction was carried out according to the protocol in Table 4.
The Fmoc protection group was cleaved twice for each coupling step using 40% piperidin in DMF. HCTU was used as coupling agent and DIPEA, dissolved in NMP, as a base. The coupling reaction was executed with 4 equivalents (eq) of amino acid, 4 eq of glucuronic acid, 4 eq of HCTU and 12 eq DIPEA relative to the resin loading. After each coupling step, the terminal amino group was capped by acetylation with a solution of 4 eq acetic anhydride and 5 eq of DIPEA in DMF. The product was alternatingly washed three times with DMF respectively isopropanol and subsequently dried over night.

Step	Reagent/Solvent	Repetitions	Time	Description
1	40% Piperidin/DMF	1	5 min	Fmoc deprotection
2	40% Piperidin/DMF	1	10 min	Fmoc deprotection
3	DMF, 4eq Fmoc protected AA/glucuronic acid	5	1 min	Wash
4	4 eq HCTU, 12 eq DIPEA	1	60 min	Coupling
5	DMF	2	1 min	Wash
6	4 eq HCTU, 12 eq DIPEA	1	20 min	End capping
7	DMF	3	1 min	Wash

Table 4: Reaction protocol for the Fmoc SPPS of the glycopeptide

Cleavage from Resin

Glycopeptide cleavage from the resin and removal of protection groups was done with 95% TFA, 2.5% triethylsilane and 2.5% H_2O. The ice cooled cleavage mixture was added to the resin and agitated during 120 min. Subsequently, the cleavage mixture was precipitated in 40 mL ice cooled diisopropylether and

centrifuged for 20 min at 9000 rpm. The supernatant was decanted and the precipitated glycopeptide redispersed in another 40 mL of diisopropylether. After another centrifugation (20 min, 9000 rpm) the residual crude product was dried over night in a desiccator.

Preparative Purification (Reverse Phase HPLC)

All HPLC purifications were carried out on a Shimadzu Prominence 20A HPLC-System.
In the following, buffer A denotes 0.1% TFA in bidistilled H_2O, buffer B stands for acetonitrile (ACN).
The glycopeptide was purified on a Shimadzu Prominence HPLC. The glycopeptide crude material was dissolved in 2 mL DMF, diluted with H_2O (0.1% TFA) to a final volume of 20 mL, then ACN was added until the glycopeptide was completely dissolved. The solution was filtered through a 0.45 μm PTFE syringe filter. The solution was pumped into a RP-18e (5 μm), 250-10 column at a flow rate of 3 mL/min by a sample pump. After 5 minutes of column equilibration on 20% buffer B the gradient to 95% buffer B was applied.
The product was fractionated when the absorption exceeded 200 mAU at 280 nm and the collected fractions were analyzed qualitatively for mass by MALDI-TOF MS and quantitatively for purity by analytical HPLC. Fractions with more than 50 area% product peak were combined and diluted 1:1 with 2% AcOH in H_2O and reapplied to the preparative RP-HPLC column, this time with 2% AcOH in the aqueous solvent A. The fractionation conditions in the second run and the analysis of the collected fractions were performed according to the first purification run; fractions with more than 95% product peak were combined.

Product Characterization

Purity analysis and quantification of the sample was determined by analytical HPLC (RP-18e(5μm), 250-4.6) and calculated by the ration of product peak integral to the overall integral of the elution diagram.

Elimination of Counter Ions

TFA^- - counter ions were eliminated by the second preparative RP-HPLC step carried out with 2% acetic acid in the aqueous phase. AcO^- in turn, as a counter

ion of the cationic peptides, was eliminated by repeated addition of ammonia prior to lyophilisation according to the following protocol.

1. Addition of ammonia to pH 11 and lyophilization on a Heto Maxi Dry Lyo
2. Dissolution in 40 mL 30% ACN in bidistilled water, addition of ammonia to pH 11 and lyophilization
3. Repetition of step 2
4. Dissolution in 40 mL 30% ACN in bidistilled H_2O and lyophilization
5. 2 repetitions of step 4

6.2 Characterization methods

6.2.1 Light scattering

Dynamic light scattering (DLS) and static light scattering (SLS) measurements give the opportunity to evaluate if the aggregates were vesicles. When an incident beam of electromagnetic radiation interacts with a molecule and changes its direction without loosing energy, elastic scattering takes place.
Particles in solution are in constant random movement due to thermal collisions (Brownian motion). This results in fluctuations in the scattered intensity, which is measured in the case of dynamic light scattering. DLS renders information about the dynamics of a system, such as translational diffusion coefficient (D_{app}) from which the hydrodynamic radius (R_h) of spheres can be calculated using the Stokes-Einstein equation:

$$R_h = k_B T/6\pi\eta D_0$$

k_B = Botzmann constant
T = absolute temperature
η = solvent viscosity
D_0 = diffusion coefficient at infinite dilution, obtained by extrapolation to zero concentration

In SLS, the excess intensity of the solution containing the particles is compared to the scattered intensity of the pure solvent. The photons collected by the

detector are averaged over a certain time. SLS provides information about weight average molecular weights and radii of gyration.
Dynamic light scattering was performed using an ALV DLS/SLS-5022 F compact goniometer system (ALV-Laser Vertriebs GmbH, Langen/D) equipped with an ALD/CGS-8F goniometer, an ALV-5000-EPP multiple tau digital Correlator, ALV Correlator software 3.0 and a 1145P-3083 HeNe-laser (JDS Uniphase, Manteca/CA, 22mW, 622nm) at scattering angles between 30° and 150°. Quartz cuvettes were obtained from Hellma (Hellma, Müllheim/D).
Prior to measurement, aqueous solutions were extruded through a 0.8µm Millipore filter to remove impurities. Measurements were typically performed with five dilutions per sample and at angular steps of 10° between 30° and 150°.

6.2.2 Transmission electron mictroscopy (TEM)

TEM images were taken on a Philipps EM 400 (Philips Electronics, Eindhoven/NL) operated at 80 kV equipped with a Megaview III charge-coupled device camera (CCD) and controlled with Morgagni 268D control and image acquisition software.
2 µL sample was absorbed on a glow discharged, parlodion coated, 300 mesh copper grid and incubated for 5 min, before the droplet was blotted away.

6.2.3 MALDI-TOF-MS

MALDI-TOF-MS (matrix assisted laser desorption ionization – time of flight – mass spectroscopy) was accomplished on a PerSeptive Biosystems Voyager-DE Pro (Biospectrometry) spectrometer; 0.8 µl of sample solution (c ~ 1 mg/mL) was applied to a gold sample plate and mixed with 0.8 µl of matrix solution (1 mg/mL α-cyano-4-hydrocinnamic acid (dissolved in a 1:1 mixture of ACN and H_2O (0.1% TFA)). Spectra were taken in reflector mode with positive polarity and a manual acquisition control. The grid voltage was set to 75%. 400 to 600 laser shots were averaged.

6.2.4 Antifactor Xa activity test

The antifactor Xa activity tests were carried out on a coagulation analyzer STA-R from Stago.
Human blood was centrifuged for 10 min at 6000 g to sediment thrombocytes. The plasma overstand was used as solvent and antithrombin III source. The highest measurable concentration of LMWH for the antifactor Xa activity test is 1.5 IU LMWH, which corresponds to ca. 15 µg/mL. To obtain solutions of 15 µg/mL, stock solutions were prepared in water. For the coupled heparin samples, the assumed actual heparin concentration was calculated. 1.5 µl of each was added to 1 mL plasma.
The samples were heated to 37℃ and vortexed. 50 µl plasma solution was pipetted, then 125 µl chromogenic substrate (S-2222: N-benzoyl-L-isoleucyl-L-glutamyl-glycyl-L-arginine-p-nitroaniline hydrochloride and its methyl ester, conc. 2 mg/mL) were added. The mixture was incubated at 37℃ for 4 min. After transfer to the measuring block, 125 µl factor Xa solution (2 mg/mL) was added and absorbance of p-nitroanilin was measured after 20 s and 60 s.
Factor Xa decouples p-nitroanilin from the tripeptide, which then absorbs at a wavelength of 405 nm. Upon inhibition of Xa, the increase of the detachment of p-nitroanilin slows down, meaning that the absorbance increase slows down with time. Comparing the absorbances with heparin calibration curves, the amount of active heparin and heparin derivatives in solution could be determined.

6.2.5 Gel electrophoresis

1g agarose was dissolved in100 ml 0.04 M barium acetate. The pH was adjusted to 5.8 with acetic acid and the solution was heated in the microwave oven until agarose had dissolved. Then the solution was poured into a holder, an eight hole comb was placed inside and cooled down to RT.
Solutions of approx. 0.5 mg/ml were placed into the holes together with loading buffer.
As running buffer 0.05 M 1,2-diaminopropane (1.853g/500 ml), pH 9 adjusted with acetic acid, was used.
The current was set to 50 mA for 150 min. Then the gel was set into a 0.2% cetylpyridium chloride and shaken over night. After rinsing with water, the gel was placed into a fridge box with 100 mL 0.2% toluidine blue solution in buffer (500

mL EtOH, 490 mL H_2O, 10 mL acetic acid) [37]. The same buffer – without toluidin blue - was used to destain until the sample stains were visible.

6.2.6 Fourier transform infrared spectroscopy

FT-IR spectra were acquired on a Shimadzu FTIR8400S spectrometer by placing a small amount (tip of a spatula) dry sample on the sapphire holder of the spectrometer.

6.2.7 NMR

NMR spectra were acquired on a Varian Unity 400 NMR spectrometer; the spectrometer was operated at 400 MHz with a sweep width of 8278.146 Hz and 22° pulse width of 2.96 µs. For water soluble compounds, D_2O was used as solvent; in case of heparin-containing amphiphiles D_2O was mixed with acetone-D_6 in a 1:1 ratio. In case of hydrophobic substances, $CDCl_3$ was used as solvent. Quantification was carried out by using a chemical shift table from Mulloy et al.[94]

I	H^1	5.22
I	H^2	4.35
I	H^3	4.20
I	H^4	4.10
I	H^5	4.81
A	H^1	5.39
A	H^2	3.29
A	H^3	3.67
A	H^4	3.77
A	H^5	4.03
A	H^6 pro-(*S*)	4.39
A	H^6 pro-(*R*)	4.27
A	NH	7.82

Table 5: ^{1}H chemical shifts in ppm. I = iduronate residue; A = glucosamine residue

The anomeric protons at the iduronate and the glucosamine residue (I=5.22, A=5.39) were taken as indications to find heparin and to quantify the sugars. They were chosen because they don't overlap with other signals.

6.2.8 Fluorescence Imaging by Confocal Microscopy

Confocal laser scanning microscopy (LSM) images were taken with a ZEISS LSM 510 META with FCS ConfoCor 2 confocal microscope, equipped with a 100x water immersion objective. An argon laser (488 nm) was used to excite OG 488 and a HeNe laser (633 nm) to excite BODIPY. To detect the fluorescence emission of OG 488 a band-pass 530-600 nm was inserted and to detect the BODIPY a low-pass > 650 nm was used.

6.2.9 FCS/FCCS measurement

Fluorescence correlation spectroscopy (FCS) and fluorescence cross correlation spectroscopy (FCCS) measurements were accomplished on a ZEISS LSM 510 META/Confocor2 microscope equipped with different laser lines. The filter sets for λ = 488 nm and 633 nm were chosen to excite the OG488 and BODIPY 633 labelled samples.

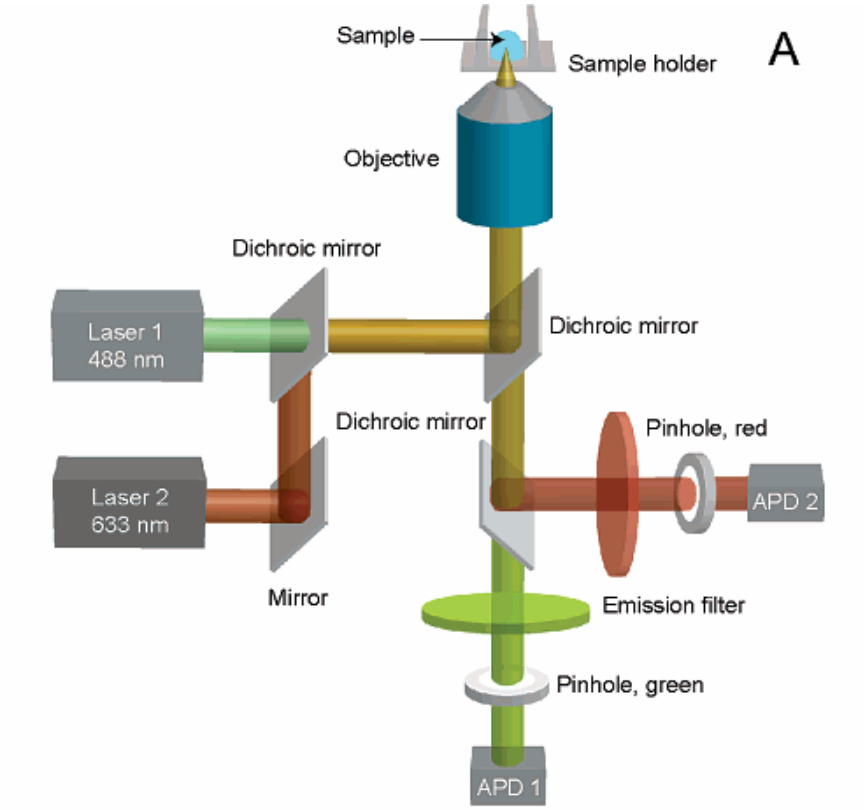

Figure 60: Schematic diagram of the beam path of the dual-laser cross-correlation setup [95]

FCS is measured in a volume smaller than ¼ femtoliter. The number of detected molecules fluctuates due to thermodynamic fluctuations, similar to DLS. But in contrary to scattered light, the measured intensity reflects the varying number of excited molecules. The measured signal can be described as constant mean intensity < I > and a fluctuating contribution δ I (t). These fluctuations δ I (t) carry the information we are interested in. From comparing the signal with each other (FCS) or with another signal (FCCS), a correlation function can be calculated:

$$G(\tau) = 1 + \frac{\langle \delta I(t) \delta I(t+\tau) \rangle}{\langle I \rangle^2}$$

The thus obtained function can be fitted to a biophysical model, being - for the simplest case - a single dilute species:

$$G(\tau) = \frac{1}{N} \cdot \frac{1}{\left(1 + \frac{\tau}{\tau_D}\right)} \cdot \frac{1}{\sqrt{1 + \frac{\tau}{\omega^2 \cdot \tau_D}}}$$

N = number of molecules
τd = diffusion time of molecule
ω = ωz/ ωxy, aspect ratio of det. volume

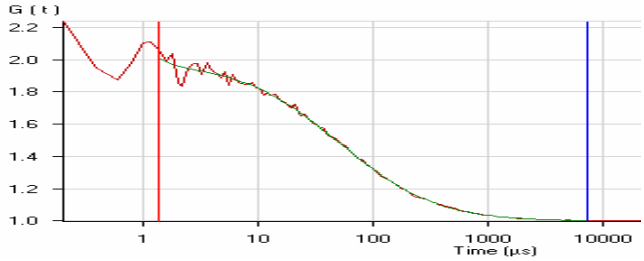

The resulting fitted curve gives the information about the concentration and the diffusion time of the molecules or particles in the sample and thus their size.

6.2.10 EPR measurements

The basic physical concept of EPR is analogous to NMR, but instead of nuclei spins, electron spins are excited.

The electron's magnetic moment aligns itself either parallel or antiparallel to an external magnetic field, with a specific energy for each alignment. The energy levels split proportionally to the magnetic field's strength.
An unpaired electron can change between the two energy levels by either absorbing or emitting electromagnetic radiation. Due to Maxwell-Boltzmann distribution, there are more electrons in the lower state, therefore there will be a total net absorption, which is measured. EPR spectra are usually presented as first derivatives of the absorbance.
If an atom with an unpaired electron has a nuclear spin, this electron will be affected by the nucleus' magnetic moment. This leads to the splitting of the EPR resonance signal, and is called hyperfine coupling, comparable to J-coupling in NMR.

Electron paramagnetic resonance (EPR) spectra were recorded with a CW Bruker ElexSys500 X-band CW spectrometer, equipped with a helium temperature control system (ER4112HV), to which the wave-guide resonance cavity was attached. Microwave power was adjusted at levels below the saturation condition: for copper this was at 2 mW for high field measurements and at 10 mW for low field measurements, while for Gd this was at 6mW. The modulation frequency was 100 kHz and the modulation amplitude was 0.5 mT; other spectral parameters were adjusted for each spectrum individually. 15 spectra were acquired to optimize the signal-to-noise ratio, and 3^{rd}-order polynomial averaging was used for subsequent noise reduction.
Cu samples were measured at 125K and 77K, while Gd samples were measured in a temperature interval of 270K - 125K. The intensity of each spectrum was calculated via double integral of D1EPR. Gaussian line shapes were considered with the line-width adjusted for each spectrum.
The spectral parameters were obtained with the SIMFONIA software package (Bruker Instruments Inc., Manning Park, Billerica, MA), where co-axial g and hyperfine tensors were assumed. The *g*-values were referenced to diphenylpicryhydrazyl (DPPH) (g = 2.0036) as an external standard.

6.2.11 MRI measurements

Eppendorff test tubes filled with aqueous solutions (concentrations of 0.01, 0.1, 0.2, 0.3, 0.4, 0.5, 1 mMol) of heparin-PEG complexed with $GdCl_3$ and $GdPO_4$ with multiple concentration ratios between polymer and Gd^{3+} or $GdPO_4$ salt (5:1,

2:1, 1:1) were scanned on a human whole-body 1.5T imaging scanner (Avanto, Siemens Medical Solutions, Erlangen, Germany) in order to evaluate the R_1 and R_2 relaxation rates. The samples were set into a holder for Eppendorff vials. For R_1 evaluation, conventional 2D spin echo sequences with multiple TR values of 100, 200, 300, 400, 500, 750, 1000, 2000 ms, a TE of 11 ms, a resolution of 0.47x0.47x5 mm3, matrix size 256x104, slice thickness of 5 mm and a bandwidth of 130Hz/px were used; for R_2 measurements a multi-contrast 2D spin echo sequence with same resolution, TR 4000ms and 32 contrast with echo spacing of 18ms was acquired.

Image processing and parameter fitting

The images were exported to a computer and evaluated using Matlab (The Mathworks, Natick, MA). The extrapolation of the relaxation rates was obtained through nonlinear least-squares fitting of the mean signal over ROIs placed in the tubes. The fitting function for the R_1 estimation was the standard T_1-weighted spin echo function:

$$S = \alpha\left(1 - 2e^{-R_1(TR-TE/2)} + e^{-R_1 TR}\right),$$

the fitting function for R_2 estimation was a monoexponential function:

$$S = \alpha e^{-R_2 TE}$$

The linear regression coefficient of relaxation rates at different concentrations was calculated in order to obtain the contrast agent relaxivity.

6.2.12 SEM/EDX

SEM images were acquired on a Philips XL 30 ESEM (Philips Electron Optics, The Netherlands) scanning electron microscope, equipped with a dedicated gaseous secondary electron detector (GSED) that allows true secondary electron imaging at full SEM resolution in gas or water vapor. An embedded module allows energy dispersive X-ray microanalysis (EDX).

6.3 Sample preparations

6.3.1 PEG-PPS GUV's with heparin-PDMS for fluorescence imaging

11.8 mg PEG-PPS were dissolved in 1.5 mL chloroform (2.73 mM) and 1.8 mg of heparin-PDMS was dissolved in 0.5 mL water (0.36 mM). Three emulsions with different heparin-PDMS to PEG-PPS ratios were prepared (Table 6). As a control experiment a sample with pure 0.46 mM PEG-PPS solution was prepared (table, sample 4). 1 μL of 6.7 mM BODIPY (6.7 nmole) dissolved in DMSO was added to all solutions. Accordingly the solutions were vortexed for some seconds and then stirred for 3 hours. To form immobilized giant vesicles with diameters between 10-100 μm, glass fibers were coated with a thin polymer film by dipping them into the polymer solutions[76]. The fibers were dried in a vacuum drier for 20 hours (RT, 1 mbar). For imaging the dry fibers were resolved in 0.5 mL water. To verify the binding 3 μL of 2 mM labeled protamine (6 nmole) were added.

Sample	VP-P (μL)	VH-P (μL)	nP-P (nmole)	VP-P (nmole)	nP-P /nH-P
1	50	50	137	18	7
2	150	40	410	14	30
3	100	10	273	3.6	76
4	300	-	137	-	-

Table 6: Ratios between PEG-PPS (P-P) and heparin-PDMS (H-P)

6.3.2 Preparation of PEG-PPS samples with heparin-PDMS for fluorescence imaging and FCS/FCCS

PEG-b-PPS polymer, dissolved in chloroform, was mixed with heparin-PDMS in water at different ratios. The solutions were shaken until an emulsion formed. Thin glass fibers were dipped into the solution and dried over night in an oven. The glass fibers were rehydrated with water containing BODOIPY 630. For FCS and FCCS measurements, the samples were dried without glass fibers and rehydrated. After dissolution, the samples were filtered six times through a 0.2 μm Millipore filter before the measurements.

6.3.3 Preparation of glycopeptide aggregates

The glycopeptide was dissolved in 2 mL EtOH at concentrations of 0.5 to 2 mg/mL. Subsequently, the mixture was dialyzed (CE 1000 Da cutoff) three times against 1 L of bidistilled H_2O.

6.3.4 Dynamic Light Scattering (DLS) of the glycopeptide

An ethanol solution of the glycopeptide was filtered through a 0.8µl Millipore filter and dialyzed against 20%EtOH in H_2O, 10% EtOH in H_2O, and pure H_2O. The solutions were subjected to DLS using an ALV/CGS-8F platform based goniometer system equipped with an ALV/-5000/E correlator and an argon-ion laser with a wavelength of 633 nm (35 mW). Correlation functions were fitted by the cumulant function. Concentration dependencies and multiple scattering effects were minimized by extrapolation of the concentration and the angle to 0.

7 REFERENCES

1. Simopoulos, A. P., Essential fatty acids in health and chronic disease. *American Journal of Clinical Nutrition* **1999,** 70, (3, Suppl.), 560S-569S.
2. Regen, S. L., Lipid-lipid recognition in fluid bilayers: solving the cholesterol mystery. *Current Opinion in Chemical Biology* **2002,** 6, (6), 729-735.
3. Curatolo, W., Glycolipid function. *Biochimica et Biophysica Acta, Reviews on Biomembranes* **1987,** 906, (2), 137-60.
4. Napoli, A.; Sebok, D.; Senti, A.; Meier, W., Block copolymer vesicles. *Block Copolymers in Nanoscience* **2006**, 39-71.
5. Tanford, C., The hydrophobic effect and the organization of living matter. *Science***1978,** 200, (4345), 1012-18.
6. Israelachvili, J. N.; Mitchell, D. J.; Ninham, B. W., Theory of self-assembly of lipid bilayers and vesicles. *Biochim Biophys Acta* **1977,** 470, (2), 185-201.
7. Staudinger, H., Polymerization. *Ber. Dtsch. Chem. Ges. B* **1920,** 53B, 1073-85.
8. Muelhaupt, R., Herman Staudinger and the origin of macromolecular chemistry. *Angew. Chem., Int. Ed.* **2004,** 43, (9), 1054-1063.
9. Hajduk, D. A.; Kossuth, M. B.; Hillmyer, M. A.; Bates, F. S., Complex Phase Behavior in Aqueous Solutions of Poly(ethylene oxide)-Poly(ethylethylene) Block Copolymers. *J. Phys. Chem. B* **1998,** 102, (22), 4269-4276.
10. Won, Y.-Y.; Davis, H. T.; Bates, F. S., Giant wormlike rubber micelles. *Science (Washington, D. C.)* **1999,** 283, (5404), 960-963.
11. Jain, S.; Bates, F. S., On the Origins of Morphological Complexity in Block Copolymer Surfactants. *Science (Washington, DC, United States)* **2003,** 300, (5618), 460-464.
12. Kita-Tokarczyk, K.; Grumelard, J.; Haefele, T.; Meier, W., Block copolymer vesicles-using concepts from polymer chemistry to mimic biomembranes. *Polymer* **2005,** 46, (11), 3540-3563.
13. van Hest, J. C. M.; Delnoye, D. A. P.; Baars, M. W. P. L.; van Genderen, M. H. P.; Meijer, E. W., Polystyrene-Dendrimer Amphiphilic Block-Copolymers with a Generation-Dependent Aggregation. *Science* **1995,** 268, (5217), 1592-1595.
14. Zhang, L. F.; Eisenberg, A., Multiple Morphologies of Crew-Cut Aggregates of Polystyrene-B-Poly(Acrylic Acid) Block-Copolymers. *Science* **1995,** 268, (5218), 1728-1731.
15. Mecke, A.; Dittrich, C.; Meier, W., Biomimetic membranes designed from amphiphilic block copolymers. *Soft Matter* **2006,** 2, (9), 751-759.
16. Discher, B. M.; Bermudez, H.; Hammer, D. A.; Discher, D. E.; Won, Y. Y.; Bates, F. S., Cross-linked polymersome membranes: Vesicles with broadly adjustable properties. *Journal of Physical Chemistry B* **2002,** 106, (11), 2848-2854.

17. Nardin, C.; Hirt, T.; Leukel, J.; Meier, W., Polymerized ABA Triblock Copolymer Vesicles. *Langmuir* **2000,** 16, (3), 1035-1041.
18. Ahmed, F.; Discher, D. E., Self-porating polymersomes of PEG-PLA and PEG-PCL: hydrolysis-triggered controlled release vesicles. *Journal of Controlled Release* **2004,** 96, (1), 37-53.
19. Meng, F. H.; Hiemstra, C.; Engbers, G. H. M.; Feijen, J., Biodegradable polymersomes. *Macromolecules* **2003,** 36, (9), 3004-3006.
20. Napoli, A.; Boerakker, M. J.; Tirelli, N.; Nolte, R. J. M.; Sommerdijk, N. A. J. M.; Hubbell, J. A., Glucose-oxidase based self-destructing polymeric vesicles. *Langmuir* **2004,** 20, (9), 3487-3491.
21. Napoli, A.; Valentini, M.; Tirelli, N.; Muller, M.; Hubbell, J. A., Oxidation-responsive polymeric vesicles. *Nature Materials* **2004,** 3, (3), 183-189.
22. Tong, X.; Wang, G.; Soldera, A.; Zhao, Y., How Can Azobenzene Block Copolymer Vesicles Be Dissociated and Reformed by Light? *J. Phys. Chem. B* **2005,** 109, (43), 20281-20287.
23. Nardin, C.; Thoeni, S.; Widmer, J.; Winterhalter, M.; Meier, W., Nanoreactors based on (polymerized) ABA-triblock copolymer vesicles. *Chem. Commun. (Cambridge)* **2000**, (15), 1433-1434.
24. Graff, A.; Winterhalter, M.; Meier, W., Nanoreactors from Polymer-Stabilized Liposomes. *Langmuir* **2001,** 17, (3), 919-923.
25. Graff, A.; Sauer, M.; Van Gelder, P.; Meier, W., Virus-assisted loading of polymer nanocontainer. *Proc. Natl. Acad. Sci. U. S. A.* **2002,** 99, (8), 5064-5068.
26. Kumar, M.; Grzelakowski, M.; Zilles, J.; Clark, M.; Meier, W., Highly permeable polymeric membranes based on the incorporation of the functional water channel protein Aquaporin Z. *Proc. Natl. Acad. Sci. U. S. A.* **2007,** 104, (52), 20719-20724.
27. Sauer, M.; Haefele, T.; Graff, A.; Nardin, C.; Meier, W., Ion-carrier controlled precipitation of calcium phosphate in giant ABA triblock copolymer vesicles. *Chemical Communications (Cambridge, United Kingdom)* **2001**, (23), 2452-2453.
28. Broz, P.; Benito, S. M.; Saw, C.; Burger, P.; Heider, H.; Pfisterer, M.; Marsch, S.; Meier, W.; Hunziker, P., Cell targeting by a generic receptor-targeted polymer nanocontainer platform. *Journal of Controlled Release* **2005,** 102, (2), 475-488.
29. Warren, L., *Bound Carbohydrates in Nature*. ed.; 1994; 'Vol.' p 126 pp.
30. Hill, K.; Rhode, O., Sugar-based surfactants for consumer products and technical applications. *Fett/Lipid* **1999,** 101, (1), 25-33.
31. Trowbridge, J. M.; Gallo, R. L., Dermatan sulfate: new functions from an old glycosaminoglycan. *Glycobiology* **2002,** 12, (9), 117R-125R.
32. Hoffman, J.; Larm, O.; Scholander, E., A new method for covalent coupling of heparin and other glycosaminoglycans to substances containing primary amino groups. *Carbohydrate research* **1983,** 117, 328-31.
33. Mahoney, D. J.; Whittle, J. D.; Milner, C. M.; Clark, S. J.; Mulloy, B.; Buttle, D. J.; Jones, G. C.; Day, A. J.; Short, R. D., A method for the non-covalent

immobilization of heparin to surfaces. *Analytical Biochemistry* **2004,** 330, (1), 123-129.
34. Cremers, H. F. M.; Kwon, G.; Bae, Y. H.; Kim, S. W.; Verrijk, R.; Noteborn, H. P. J. M.; Feijen, J., Preparation and characterization of albumin-heparin microspheres. *Biomaterials* **1994,** 15, (1), 38-48.
35. Chung, H. J.; Kim, H. K.; Yoon, J. J.; Park, T. G., Heparin Immobilized Porous PLGA Microspheres for Angiogenic Growth Factor Delivery. *Pharmaceutical Research* **2006,** 23, (8), 1835-1841.
36. Bergman, K.; Elvingson, C.; Hilborn, J.; Svensk, G.; Bowden, T., Hyaluronic Acid Derivatives Prepared in Aqueous Media by Triazine-Activated Amidation. *Biomacromolecules* **2007,** 8, (7), 2190-2195.
37. Smith, P. K.; Mallia, A. K.; Hermanson, G. T., Colorimetric method for the assay of heparin content in immobilized heparin preparations. *Analytical Biochemistry* **1980,** 109, (2), 466-73.
38. Jin, L.; Abrahams, J. P.; Skinner, R.; Petitou, M.; Pike, R. N.; Carrell, R. W., The anticoagulant activation of antithrombin by heparin. *Proc Natl Acad Sci U S A* **1997,** 94, (26), 14683-8.
39. Rosenberg, R. D.; Lam, L., Correlation between structure and function of heparin. *Proc. Natl. Acad. Sci. U. S. A.* **1979,** 76, (3), 1218-22.
40. Lindahl, U.; Backstrom, G.; Hook, M.; Thunberg, L.; Fransson, L. A.; Linker, A., Structure of the antithrombin-binding site in heparin. *Proc Natl Acad Sci U S A* **1979,** 76, (7), 3198-202.
41. Andersson, L. O.; Barrowcliffe, T. W.; Holmer, E.; Johnson, E. A.; Soederstroem, G., Molecular weight dependency of the heparin potentiated inhibition of thrombin and activated factor X. Effect of heparin neutralization in plasma. *Thrombosis Research* **1979,** 15, (3-4), 531-41.
42. Rosenberg, R. D.; Jordan, R. E.; Favreau, L. V.; Lam, L. H., Highly active heparin species with multiple binding sites for antithrombin. *Biochemical and Biophysical Research Communications* **1979,** 86, (4), 1319-24.
43. Jordan, R. E.; Favreau, L. V.; Braswell, E. H.; Rosenberg, R. D., Heparin with two binding sites for antithrombin or PF4. *Journal of Biological Chemistry* **1982,** 257, (1), 400-6.
44. Danielsson, A.; Raub, E.; Lindahl, U.; Bjork, I., Role of ternary complexes, in which heparin binds both antithrombin and proteinase, in the acceleration of the reactions between antithrombin and thrombin or factor Xa. *J Biol Chem* **1986,** 261, (33), 15467-73.
45. Schmitz-Huebner, U.; van de Loo, J. C. W., *Low molecular weight heparin*. ed.; 1986; 'Vol.' p.
46. Hirsh, J., Low-molecular-weight heparin a review of the results of recent studies of the treatment of venous thromboembolism and unstable angina. *Circulation* **1998,** 98, (15), 1575-1582.
47. Broze, G. J., Jr., Tissue factor pathway inhibitor and the revised theory of coagulation. *Annu Rev Med* **1995,** 46, 103-12.
48. Bjoerk, I.; Lindahl, U., Mechanism of the anticoagulant action of heparin. *Mol. Cell. Biochem.* **1982,** 48, (3), 161-82.

49. Torchilin, V. P., PEG-based micelles as carriers of contrast agents for different imaging modalities. *Advanced Drug Delivery Reviews* **2002,** 54, (2), 235-252.
50. Runge, V. M.; Carollo, B. R.; Wolf, C. R.; Nelson, K. L.; Gelblum, D. Y., Gd DTPA: a review of clinical indications in central nervous system magnetic resonance imaging. *Radiographics* **1989,** 9, (5), 929-58.
51. Hifumi, H.; Yamaoka, S.; Tanimoto, A.; Citterio, D.; Suzuki, K., Gadolinium-Based Hybrid Nanoparticles as a Positive MR Contrast Agent. *Journal of the American Chemical Society* **2006,** 128, (47), 15090-15091.
52. Laurent, S.; Vander Elst, L.; Thirifays, C.; Muller, R. N., Paramagnetic Liposomes: Inner versus Outer Membrane Relaxivity of DPPC Liposomes Incorporating Lipophilic Gadolinium Complexes. *Langmuir*, ACS ASAP.
53. Ranney, D. F. Metal-ion chelates with acidic saccharides and glycosaminoglycans, and methods of enhancing MRI imaging. 9514491, 19950601, 1995.
54. Schlaad, H.; Antonietti, M., Block copolymers with amino acid sequences: Molecular chimeras of polypeptides and synthetic polymers. *Eur. Phys. J. E* **2003,** 10, (1), 17-23.
55. Dittrich, C. Controlled Self-Assembly of Short β-helical Peptides. University of Basel, Basel, 2007.
56. Kimura, S.; Kim, D. H.; Sugiyama, J.; Imanishi, Y., Vesicular self-assembly of a helical peptide in water. *Langmuir* **1999,** 15, (13), 4461-4463.
57. Hotchkiss, R. D.; Dubos, R., Chemical properties of bactericidal substances isolated from cultures of a soil bacillus. *J. Biol. Chem.* **1940,** 132, 793-4.
58. Wallace, B. A., Recent advances in the high resolution structures of bacterial channels: gramicidin A. *J. Struct. Biol.* **1998,** 121, (2), 123-141.
59. Dittrich, C.; de Bruyn Ouboter, D.; Meier, W. P., Self-Assembly of Short Peptides to Functional Membranes Based on a Repetitive Sequence of *l*-Trp and *d*-Leu. *submitted*.
60. Davis, B. G., Synthesis of Glycoproteins. *Chemical Reviews (Washington, D. C.)* **2002,** 102, (2), 579-601.
61. Specker, D.; Wittmann, V., Synthesis and application of glycopeptide and glycoprotein mimetics. *Top. Curr. Chem.* **2007,** 267, (Glycopeptides and Glycoproteins), 65-107.
62. Jagannadh, B.; Reddy, M. S.; Rao, C. L.; Prabhakar, A.; Jagadeesh, B.; Chandrasekhar, S., Self-assembly of cyclic homo- and hetero-b-peptides with cis- furanoid sugar amino acid and b-hGly as building blocks. *Chemical Communications (Cambridge, United Kingdom)* **2006**, (46), 4847-4849.
63. Pratt, M. R.; Bertozzi, C. R., Synthetic glycopeptides and glycoproteins as tools for biology. *Chemical Society Reviews* **2005,** 34, (1), 58-68.
64. Ramiah, V.; Matahwa, H.; Weber, W.; McLeary, J. B.; Sanderson, R. D., CMC and phase separation studies of RAFT mediated amphiphilic diblock glycopolymers with methyl acrylate and styrene. *Macromolecular Symposia* **2007,** 255, (Polymers for Advanced Applications), 70-80.

65. Haase, C.; Seitz, O., Chemical synthesis of glycopeptides. *Top. Curr. Chem.* **2007,** 267, (Glycopeptides and Glycoproteins), 1-36.
66. Warren, J. D.; Geng, X.; Danishefsky, S. J., Synthetic glycopeptide-based vaccines. *Top. Curr. Chem.* **2007,** 267, (Glycopeptides and Glycoproteins), 109-141.
67. Fekete, G., Turbidimetric estimation of heparin with protamine. *Naturwissenschaften* **1956,** 43, 279-80.
68. Olander, B.; Wirsen, A.; Albertsson, A.-C., Silicone elastomer surface functionalized with primary amines and subsequently coupled with heparin. *Biomacromolecules* **2003,** 4, (1), 145-8.
69. Matsuda, T.; Magoshi, T., Terminally Alkylated Heparin. 1. Antithrombogenic Surface Modifier. *Biomacromolecules* **2001,** 2, (4), 1169-1177.
70. Jee, K. S.; Park, H. D.; Park, K. D.; Kim, Y. H.; Shin, J.-W., Heparin Conjugated Polylactide as a Blood Compatible Material. *Biomacromolecules* **2004,** 5, (5), 1877-1881.
71. Napoli, A.; Tirelli, N.; Kilcher, G.; Hubbell, J. A., New Synthetic Methodologies for Amphiphilic Multiblock Copolymers of Ethylene Glycol and Propylene Sulfide. *Macromolecules* **2001,** 34, (26), 8913-8917.
72. Ramamurthy, N.; Baliga, N.; Wakefield, T. W.; Andrews, P. C.; Yang, V. C.; Meyerhoff, M. E., Determination of low-molecular-weight heparins and their binding to protamine and a protamine analog using polyion-sensitive membrane electrodes. *Anal. Biochem.* **1999,** 266, (1), 116-124.
73. Chang, L.-C.; Lee, H.-F.; Chung, M.-J.; Yang, V. C., PEG-Modified Protamine with Improved Pharmacological/Pharmaceutical Properties as a Potential Protamine Substitute: Synthesis and in Vitro Evaluation. *Bioconjugate Chemistry* **2005,** 16, (1), 147-155.
74. Sautiere, P.; Briand, G.; Gusse, M.; Chevaillier, P., Primary structure of a protamine isolated from the sperm nuclei of the dog-fish Scylliorhinus caniculus. *European Journal of Biochemistry* **1981,** 119, (2), 251-5.
75. Capila, I.; VanderNoot, V. A.; Mealy, T. R.; Seaton, B. A.; Linhardt, R. J., Interaction of heparin with annexin V. *FEBS Letters* **1999,** 446, (2,3), 327-330.
76. Napoli, A.; Bermudez, H.; Hubbell, J. A., Interfacial Reactivity of Block Copolymers: Understanding the Amphiphile-to-Hydrophile Transition. *Langmuir* **2005,** 21, (20), 9149-9153.
77. Rigler, R.; Mets, U.; Widengren, J.; Kask, P., Fluorescence correlation spectroscopy with high count rate and low background: Analysis of translational diffusion. *European Biophysics Journal* **1993,** 22, (3), 169-75.
78. Schwille, P.; Meyer-Almes, F.-J.; Rigler, R., Dual-color fluorescence cross-correlation spectroscopy for multicomponent diffusional analysis in solution. *Biophysical Journal* **1997,** 72, (4), 1878-1886.
79. Rigler, R.; Foldes-Papp, Z.; Meyer-Almes, F.-J.; Sammet, C.; Volcker, M.; Schnetz, A., Fluorescence cross-correlation: A new concept for polymerase chain reaction. *Journal of Biotechnology* **1998,** 63, (2), 97-109.

80. Starchev, K.; Zhang, J.; Buffle, J., Applications of fluorescence correlation spectroscopy-particle size effect. *Journal of Colloid and Interface Science* **1998,** 203, (1), 189-196.
81. Nosov, S.; Schmalz, H.; Mueller, A. H. E., One-pot synthesis of primary amino end-functionalized polymers by reaction of living anionic polybutadienes with nitriles. *Polymer* **2006,** 47, (12), 4245-4250.
82. Ebrahimi-Moshkabad, M.; Winterbottom, J. M., Heterogeneous hydrogenation of polybutadienes in a stirred tank reactor. *IChemE Research Event, A Two-Day Symposium, Newcastle upon Tyne, Apr. 7-8, 1998* **1998**, 1457-1465.
83. Andre, X.; Zhang, M.; Mueller, A. H. E., Thermo- and pH-Responsive micelles of poly(acrylic acid)-block-poly(N,N-diethylacrylamide). *Macromol. Rapid Commun.* **2005,** 26, (7), 558-563.
84. Casse, O.; Shikilnyy, A.; Cölfen, H.; Schlaad, H.; Gräwer, M.; Häussinger, D.; Meier, W.; Taubert, A., Self-assembly of the non-ionic, double-hydrophilic diblock copolymer poly(ethylene oxide)-block-poly(2-methyl-2-oxazoline) in dilute aqueous solution. ***submitted***.
85. Faul, C. F. J.; Antonietti, M., Ionic self-assembly: Facile synthesis of supramolecular materials. *Adv. Mater. (Weinheim, Ger.)* **2003,** 15, (9), 673-683.
86. Kaminski, Z. J., 2-Chloro-4,6-disubstituted-1,3,5-triazines. A novel group of condensing reagents. *Tetrahedron Lett.***1985,** 26, (24), 2901-4.
87. Nicolle, G. M.; Toth, E.; Schmitt-Willich, H.; Raduchel, B.; Merbach, A. E., The impact of rigidity and water exchange on the relaxivity of a dendritic MRI contrast agent. *Chemistry--A European Journal* **2002,** 8, (5), 1040-1048.
88. Moseley, H., Atomic models and X-ray spectra. *Nature (London, United Kingdom)* **1914,** 92, 554.
89. Szyczewski, A.; Lis, S.; Krzystek, J.; Staninski, K.; Klonkowski, A.; Kruczynski, Z.; Pietraszkiewicz, M., Gadolinium(III) cryptates investigated by multifrequency EPR. *Journal of Alloys and Compounds* **2008,** 451, (1-2), 182-185.
90. Powell, D. H.; Ni Dhubhghaill, O. M.; Pubanz, D.; Helm, L.; Lebedev, Y. S.; Schlaepfer, W.; Merbach, A. E., High-pressure NMR kinetics. Part 74. Structural and Dynamic Parameters Obtained from 17O NMR, EPR, and NMRD Studies of Monomeric and Dimeric Gd3+ Complexes of Interest in Magnetic Resonance Imaging: An Integrated and Theoretically Self-Consistent Approach. *Journal of the American Chemical Society* **1996,** 118, (39), 9333-9346.
91. Powell, D. H.; Merbach, A. E.; Gonzalez, G.; Bruecher, E.; Micskei, K.; Ottaviani, M. F.; Koehler, K.; von Zelewsky, A.; Grinberg, O. Y.; Lebedev, Y. S., Magnetic-field-dependent electronic relaxation of gadolinium(3+) in aqueous solutions of the complexes [Gd(H2O)8]3+, [Gd(propane-1,3-diamine-N,N,N',N'-tetraacetate)(H2O)2]-, and Gd(N,N'-bis[(N-methylcarbamoyl)methyl]-3-azapentane-1,5-diamine-3,N,N'-

triacetate)(H2O)] of interest in magnetic-resonance imaging. *Helvetica Chimica Acta* **1993,** 76, (5), 2129-46.

92. Firsching, F. H.; Brune, S. N., Solubility products of the trivalent rare-earth phosphates. *Journal of Chemical and Engineering Data* **1991,** 36, (1), 93-5.
93. Pintaske, J.; Martirosian, P.; Graf, H.; Erb, G.; Lodemann, K.-P.; Claussen Claus, D.; Schick, F., Relaxivity of Gadopentetate Dimeglumine (Magnevist), Gadobutrol (Gadovist), and Gadobenate Dimeglumine (MultiHance) in human blood plasma at 0.2, 1.5, and 3 Tesla. *Invest Radiol* **2006,** 41, (3), 213-21.
94. Mulloy, B.; Forster, M. J.; Jones, C.; Davies, D. B., NMR and molecular-modeling studies of the solution conformation of heparin. *Biochemical Journal* **1993,** 293, (3), 849-58.
95. Rigler, P.; Meier, W., Encapsulation of fluorescent molecules by functionalized polymeric nanocontainers: investigation by confocal fluorescence imaging and fluorescence correlation spectroscopy. *Journal of the American Chemical Society* **2006,** 128, (1), 367-373.
96. Linhardt, R. J., 2003 Claude S. Hudson Award Address in Carbohydrate Chemistry. Heparin: Structure and Activity. *Journal of Medicinal Chemistry* **2003,** 46, (13), 2551-2564.
97. Marcum, J. A., The development of heparin in Toronto. *Journal of the history of medicine and allied sciences* **1997,** 52, (3), 310-37.
98. Taylor, E. M.; Moloney, P. J. Recovery of heparin. 656268, 1951.
99. Rutty, C. J., Miracle Blood Lubricant: Connaught and the Story of Heparin, 1928-1937. *CONNTACT* **1996,** 9, (4).

8 ANNEX

8.1 Abbreviations

ACN	acetonitrile
AFM	atomic force microscopy
ATIII	antithrombin III
BODIPY	dipyrromethene boron difluoride
CA	contrast agent
CLSM	confocal laser scanning microscopy
CMDT	2-chloro-4,6-dimethoxy-1,3,5-triazine
Da	Dalton
DCC	dicyclohexyl carbodiimide
DCM	dichloro methane
DIPEA	N,N-diisoprpylethylamine
DLS	dynamic light scattering
DMAP	4-dimethylaminopyridine
DMF	dimethyl formamide
DMSO	dimethyl sulfoxide
DNA	deoxyribonucleic acid
EDX	energy dispersive X-ray microanalysis
EPR	electron paramagnetic resonance spectroscopy
EtOH	ethanol
FCS	fluorescence correlation spectroscopy
FCCS	fluorescence cross correlation spectroscopy
FGF	fibroblast growth factor
GAG	glycosaminoglycan
GluAc	D-glucuronic acid
GUV	giant unilamellar vesicles
h	hour(s)
HCTU	O-(6-chlorbenzotriazol-1-yl)-N,N,N’,N’-tetramethyluronium-hexafluorophosphate
HIT	heparin-induced thrombocytopenia
HPLC	high performance liquid chromatography
IR	infrared spectroscopy
ISA	ionic self-assembly
L (DL)	leucine (*D*-leucine)

LamB	Maltoporin
LMWH	low molecular wight heparin
MALDI-TOF-MS	matrix assisted laser desorption absorption-time of flight-mass spectroscopy
M	mol/L
min	minute(s)
MRI	magnetic resonance imaging
NMR	nuclear magnetic resonance spectroscopy
OG	Oregon green
OmpF	E. coli outer membrane porin
OTf	trifluoromethane sulfonate (= triflate)
PDMS	poly(dimethyl siloxane)
PEE	poly(ethyl ethylene)
PEG	poly(ethylene glycol)
PMOXA	poly(methyl oxazoline)
ppm	parts per million
PPS	poly(propylene sulfide)
R_g	radius of gyration
R_h	hydrodynamic radius
RNA	ribonucleic acid
RP	reverse phase
RT	room temperature
SEM	scanning electron microscopy
SLS	static light scattering
SPPS	solid phase peptide synthesis
T_g	glass transition temperature
TEM	transmission electron microscopy
TES	triethylsilane
TFA	trifluoracetic acid
UF	ultra filtration
UFH	unfractionated heparin
UV	ultra violet
W	tryptophane

8.2 Chemicals

- Acetic acid, glacial, 100%, VWR ProLabo 84 528.290
- Acetic anhydride, purum, Synopharm 017700
- Acetone-D_6, Fluka, puriss., 666-52-4
- Acetonitrile, HPLC grade ≥99.9%, Fisher Chemicals A/0626/17
- α-Cyano-4-hydrocinnamic acid (CCA), 97%, Aldrich 14,550-5
- Barium acetate, Fluka, puriss., 534-80-6
- BODIPY® 630-650 methyl bromide (BODIPY), Invitrogen
- 2-Chloro-4,6-dimethoxy-1,3,5-triazine (CDMT), Aldrich 3140-73-6
- Chloroform, Sigma-Aldrich, 98.8%, 67-66-3
- Cyclohexane, Fluka, purum, 110-82-7
- D_2O, Cambridge isotope laboratories Inc. 7789-20-0
- 1,2-Diaminopropane, Fluka, puriss., 78-90-0
- Dichloromethan, rein, Schweizerhall 81830-156
- Dicyclohexylcarbodiimide (DCC), Fluka, puriss., 538-75-0
- 4-dimethylaminopyridine (DMAP), Aldirch, 99%, 1122-58-3
- dimethyl formamide (DMF), Fluka, puriss. 68-12-2
- D-glucuronic acid, 99%, Sigma-Aldrich 6556-12-3
- D-glucosamine, 99%, Sigma-Aldrich 66-84-2
- Diisopropyl ether, puriss. p.a. ≥ 98%, Fluka 38279
- Ethanol, 96% EP, Schweizerhall 82352-102
- Fmoc-D-Leu-OH, ≥98% (HPLC), Novabiochem 04-13-1025
- Fmoc-Trp(Boc)-OH, ≥(HPLC), Novabiochem 04-12-1103
- Formamide, puriss, Fluka 75-12-7
- $GdCl_3$ * 6 H_2O provided by Novartis
- hexane, Fluka, puriss., 110-54-3
- Low molecular weight heparin (LMWH) Na+ salt, Sigma-Aldirch 9041-08-1
- 4-Methyl-morpholine (NMM), Fluka, 109-02-4
- 1-Methyl-2-pyrrolidinone (NMP), ≥99.5% (GC), Fluka 69116
- N-acetyl-D-glucosamine 99%, Sigma Aldrich 7512-17-6
- N,N-Diisoprpylethylamine (DIPEA), 99%, Aldrich D12,580-6
- N,N-Dimethylformamide (DMF), purum, ≥ 99.9% (GC), JT. Baker 7032
- (O-(6-Chlorbenzotriazol-1-yl)-N,N,N',N'-tetramethyluronium-hexafluorophophate) (HCTU), 99.7%, Iris Biotech GmbH 330645879

- Oregon green® 488 dye, carboxylic acid, succinimidyl ester (OG488), Invitrogen, 198139-51-4
- Pd CO3, Fluka, puriss., Fluka, 10%
- Poly(dimethylsiloxane) aminopropyl terminated (PDMS-(C3H6-NH2)2), ABCR 106214-84-0
- Poly-L-lysine MW 20’000-30’000 Da, Fluka 81333
- Piperidine, purum, ≥ 96% (GC), Fluka 80642
- Pyridin, ReagentPlus, ≥99.0% (GC), Fluka 320498
- Rink Amide AM resin (200-400 mesh), Novabiochem 01-64-0038
- sodium cyanoborohydride $NaBH_3CN$, Fluka 25895-60-7
- sodium phosphate Na_2HPO_4, Sigma-Aldrich, 99%, 7558-79-4
- Toluidine blue, Fluka, 6586-04-5
- Triethylsilane (TES), 97%, Fluka 90550
- Trifluoroacetic acid (TFA), ≥ 98%, Fluka 91700

8.3 History of heparin

Heparin was discovered in 1916 at Johns Hopkins University by John McLean, a second-year medicine student in William H. Howell's laboratory. He was isolating phosphatides from heart and liver tissues using organic solvents, and noticed anticoagulant activity of his extracts. He misnamed the active compound hepar (liver) phosphatide, until Howell recognized that the compound had no phosphate but was a polysaccharide and renamed it heparin[96]. During the 1920s, Howell kept investigating heparin and isolated the polysaccharide by extraction with water.

In the early twentieth century, hirudin from leech salivary glands was the most widely used anticoagulant, mainly for indirect blood transfusion, but purification of this inhibitor was expensive and the substance was unsafe for patients. Heparin, being an endogenous mammalian substance, represented a promising coagulation regulator. Howell convinced the pharmaceutical company Hynson, Westcott and Dunning to bring heparin on the market commercially, but as no efforts for further development of the isolation protocol was made, the commercial profit remained unsatisfactory[97].

It only got practically applied from the early 1930, when a team led by Dr. Charles H. Best (1899-1978) at Connaught developed a method to establish a supply that was pure, plentiful, inexpensive and safe for human use.

Connaught, the Department of Physiology at Toronto University, is well known from its involvement in insulin development, but less is known about its role on heparin's history. Until 1928, heparin was only available from dog liver in small amounts. Furthermore, it was expensive and toxic.

Figure 61: Dr. Charles Best

After encouraging early work, Dr. Gordon Murray (1896-1976), a prominent surgeon at Toronto General Hospital, joined Best's team to conduct experimental surgery using heparin. The first choice for a cheaper heparin source was beef liver, readily available at slaughterhouses, but as the pet food industry began to grow, the prices were rising and another source had to be found. Beef lung and intestines turned out to be also good resources of heparin, the latter cheaper and more plentiful as there was no use for it as pet food. The extraction of

heparin proved to be rather unpleasant considering that the method involved letting these tissues “autolyze”, or spoil, before preparation. The next challenge was to study the still mysterious chemistry of heparin. Between 1933 and 1936, purification and crystallization of heparin into a standardized dry form that could be administered in a salt solution was achieved. After insulin, heparin became the second product from Connaught to be recognized as an international biological standard.

Meanwhile in Sweden, Sune Bergstrom, winner of the Nobel Prize for research on prostaglandins, started to investigate the structure of heparin and correctly identified glucosamine as a sugar component, while working as a student with Eric Jorpes in Sweden. Jorpes and later Arthur Charles established that heparin contained a high content of sulfo-groups. In 1950 Jorpes also determined that the glucosamine residue in heparin was primarily N-sulfonated. Melville L. Wolfrom initially identified the uronic acid residue as D-glucuronic acid in 1946. But it was not until 1962, that L-iduronic acid was found and 1968 until it was identified as major uronic acid residue in heparin.

At Connaught in the 1930’s, Murray conducted experimental surgery with various animals using this new potent heparin product. After discovering that heparin definitely cleared up internal blood clots, and also seemed useful for many other dangerous operations where blood coagulated quickly, the next step was to try heparin on human patients under less predictable conditions, which was done first in May 1935 and continued by hundreds of complex surgical cases during which Connaught's heparin played an essential and often dramatic life-saving role.

By 1937 it was proven that Connaught's heparin was a safe, easily available and effective blood anticoagulant. Best's heparin team had opened the door to organ transplantations and open heart surgery, as well as the development of an artificial kidney, pioneered by Murray. Connaught continued to prepare heparin and worked to increase its potency and reduce the price. By 1951, Drs. Edith Taylor and Peter Moloney were successful and received a patent for their improved methods of heparin production[98]. Ironically, this work made heparin more easily produced elsewhere. Thus, by the early 1950s, Connaught had stopped producing this crucial life-saving product that it had pioneered[99].

Despite widely spread medical use of heparin after the second world war, the molecular mechanism by which heparin inhibits blood clotting factors was not determined until the early 1970s, almost thirty years after completion of the work by the Toronto team.